Wintertime measurements of pCO_2 in Arctic Landfast Sea Ice

by

Owen C. Owens

A Thesis submitted to the Faculty of Graduate Studies of

The University of Manitoba

in partial fulfillment of the requirements of the degree of

MASTER OF SCIENCE

Department of Environment & Geography

University of Manitoba

Winnipeg

ABSTRACT

Previous assumptions were that gas is not transferred between the atmosphere and the ocean through sea ice, leaving the frozen Arctic out of global and regional carbon cycle models. Recent work has shown two features of first year sea ice that, when combined, detail a method by which gas exchange can occur through ice. First, carbon fluxes over sea ice surfaces in both directions have been measured. Second, sea ice brine has an elevated capacity over seawater to absorb $CO_{2(g)}$ due to its cold temperature and chemical reactions that promote dissolution of CO_2 and precipitation of carbonates and back.

The purpose of this project was to determine the potential for first year Arctic sea ice to dissolve $CO_{2(g)}$. Sea ice pCO_2 profiles were collected using a new method of remotely sampling gas *in situ* via diffusive membranes placed within growing sea ice. The gas samples were analysed using a GC with a TCD. Gas analysis was complimented by measurements of air and ice temperature, surface PAR, $CO_{2(g)}$ fluxes via the eddy correlation method and ice carbon chemistry. The work was performed on the land-fast Arctic sea ice in Franklin Bay, Canada during the winter and spring as part of the ice fast portion of the Canadian Arctic Shelf Exchange Study (CASES) 2004 project.

Measurements in this experiment indicated that sea ice brine had absorbed up to twenty times the concentration of $CO_{2(g)}$ compared to atmospheric concentrations. Sea ice pCO_2 content appears to be related to ice temperature and is a contributor to ocean-sea ice-atmosphere gas-transfer. The potential temperature relationship is expected as temperature affects sea ice brine absorption capacity and the phase of various solutes in the sea ice. There was also a dramatic diurnal pattern in sea ice pCO_2, with daytime sea ice pCO_2 up to ten times as great as nighttime sea ice pCO_2.

The observed elevation in sea ice pCO_2 coupled with the mobility of the brine points to the role that brine plays in Arctic carbon transport. The gas transport links the Arctic atmosphere and ocean and indicates that a thinning and receding ice cover may not result in creating a negative feedback to the increasing atmospheric $CO_{2(g)}$ concentration.

ACKNOWLEDGEMENTS

We gratefully acknowledge technical and field assistance from Nes Sutherland and Mike Arychuk[2]; Carrie Breneman[3] and the staff and students participating in CASES at University of Manitoba[1]; Alfonso Mucci, Pascal Collin and Constance Guignard[4]; and the officers and crew onboard the CCGS Amundsen.

Research is supported through NSERC (Discovery Grant to T. Papakyriakou[1], and CASES network), Northern Studies and Training and through DFO research funds.

I would like to thank my committee members for their input and comments throughout this process. I would also like to thank all those I came in contact with during this project for anything they may have shared with me.

[1]Centre for Earth Observation Science, University of Manitoba, Winnipeg, MB, R3L 2N2
[2]Institute for Ocean Science, Department of Fisheries and Oceans, Sidney, B.C. V8V 4L1
[3]Dept. of Geography, University of Calgary, Calgary, AB, T2N 1N4
[4]Earth & Planetary Sciences, McGill University, Montreal, QC, H3A 2A7

TABLE OF CONTENTS

ABBREVIATIONS

°C	Degrees Celsius
Alk	Alkalinity
AO	Arctic Oscillation
C	Carbon
Ca^{2+}	Calcium ions
$CaCO_3$	Calcium carbonate or calcite
CASES	Canadian Arctic Shelf Exchange Study
CFCs	Chlorofluorocarbons
CH_4	Methane
Cl^-	Chloride ion
CO_2	Carbon dioxide
CO_3^{2-}	Carbonate ions
DIC	Dissolved inorganic carbon
DO	Dissolved oxygen
DT	Daytime, approximately 8a.m. to 8 p.m.
FYI	First Year Sea Ice
GHG	Greenhouse gasses
H^+	Hydrogen ion
H_2CO_3	Carbonic acid
H_2O_g	Water vapour
HCO^{3-}	Bicarbonate ions
HFCs	hydrofluorocarbons
IPCC	Intergovernmental Panel on Climate Change
k_H	Henry's Law constant
K^+	Potassium ion
mg/kg	Milligrams per kilogram
mg/L	Milligrams per litre
Mg^{2+}	Magnesium ion
MYI	Multi year ice
Na^+	Sodium ion
NAO	North Atlantic Oscillation
N_2O	Nitrous oxide
NT	Nighttime, approximately 8p.m. to 8 a.m.
PAR	Photosynthetically active radiation
pCO_2	Partial pressure of CO_2
PFCs	Perfluorocarbons
ppm	Parts per million
psu	Practical salinity units
SAT	Surface air temperature
SF_6	Sulphur hexafluoride
Si	Silicon
SO_4^{2-}	Sulphate ion
UNEP	United Nations Environment Program

LIST OF TABLES

LIST OF FIGURES

LIST OF EQUATIONS

$$CO_{2(g)} \leftrightarrow CO_{2(aq)} \tag{2.1}$$

$$[CO_{2(aq)}] = K_{CO_2}\, p(CO_2) = 2 \times 10^{-3} \tag{2.2}$$

$$CO_{2(aq)} + H_2O_{(l)} \leftrightarrow H_2CO_{3(aq)} \leftrightarrow H^+ + HCO_3^{-}. \tag{2.3}$$

$$K_{\alpha 1} = \frac{[H^+]\,[HCO_3^-]}{[H_2CO_3]} = 4.45 \times 10^{-7} \tag{2.4}$$

$$HCO_3^{-} \leftrightarrow H^+ + CO_3^{2-}. \tag{2.5}$$

$$K_{\alpha 2} = \frac{[H^+]\,[CO_3^{2-}]}{[HCO_3^-]} = 4.69 \times 10^{-11} \tag{2.6}$$

$$DIC = [CO_2 *] + [HCO^{3-}] + [CO_3^{2-}], \tag{2.7}$$

$$\begin{aligned} A_T = {} & [HCO_3^-]_T + 2[CO_3^{2-}]_T + [B(OH)_4^-]_T + [OH^-]_T \\ & + 2[PO_4^{-3}]_T + [HPO_4^{-2}]_T + [SiO(OH)_3^-]_T \\ & - [H^+]_{sws} - [HSO_4^-] \end{aligned} \tag{2.8}$$

$$k_{H,cp} = k_{cp} \bullet exp\left[-C \bullet \left(\frac{1}{T} - \frac{1}{Tcp}\right)\right] \tag{2.9}$$

$$J = -D\,\frac{\partial \phi}{\partial x} \tag{2.10}$$

$$\frac{\partial \phi}{\partial t} = D\,\frac{\partial^2 \phi}{\partial x^2} \tag{2.11}$$

$$P\,V = n\,R\,T \tag{3.1}$$

$$[CO_2] = m * PA * V^{-1} \quad (3.2)$$

$$A = \alpha zc, \quad (3.3)$$

$$\log_{10} K\downarrow_o - \log_{10} K\downarrow_z = \alpha zc \quad (3.4)$$

$$\log_{10} K\downarrow_z = z\alpha(\log_{10} K\downarrow_o) \quad (3.5)$$

$$K\downarrow_z = e^{(K\downarrow_o - z\alpha)} \quad (3.6)$$

$$FCO_{2D} = t \bullet FCO_{2/s} \quad (3.7)$$

$$FCO_{2P} = P_D \bullet FCO_{2D} \quad (3.8)$$

$$x_i - \bar{x} \quad (3.9)$$

$$\sum_{i=1}^{n} (x_i - \bar{x})^2 \quad (3.10)$$

$$y = -0.0002\ x^2 + 0.0235\ x + 0.1397 \quad (4.1)$$

$$Ca^{2+} + 2HCO_3^- \rightarrow CaCO_{3(s)} + H_2O + CO_{2(aq)} \quad (5.1)$$

$\rightarrow$ cooling

$\leftarrow$ warming

$$CO_{2(ppm,C,0.25mL,S)} - CO_{2(ppm,C,0.25mL,E)} = CO_{2(ppm,Diff,0.25mL)} \quad (B.1)$$

CHAPTER 1: INTRODUCTION TO WESTERN CANADIAN ARCTIC SEA ICE, CLIMATOLOGY, AND CO_2 GAS DYNAMICS

The majority of climate researchers agree the Arctic environment is warming (Intergovernmental Panel on Climate Change (IPCC), 2001; IPCC, 2007). Observed increases in Arctic temperatures (Serreze et al, 2000; IPCC 2001; IPCC, 2007), thinning ice cover (Johannessen et al., 1999; Perovich, 2002; Serreze et al., 2003; Overpeck et al., 2005; Stroeve et al., 2004; Stroeve et al., 2005; IPCC, 2007), and decreased area (Comiso, 2003; Gloersen and Campbell, 1991; Johannessen et al., 1999; Maslanik, and Barry, 1996; Rothrock et al., 1999; Stroeve et al., 2004 and 2005) are correlated to changes in the atmospheric levels of carbon dioxide (CO_2) (Keeling and Whorf, 2004; IPCC, 2007). To better understand these changes, scientists in various disciplines are studying carbon cycles more closely. The ocean and atmosphere are constantly exchanging water and carbon through homeostatic cycles. The combined result of the Earth's carbon cycles is that the oceans are the largest active natural carbon sink (Schlesinger, 1997). Currently, the oceans store $38x10^{18}$g carbon (C) of the total global mass of 10^{23}g C, an amount 51 times greater than the quantity of C contained in the atmosphere (Wanninkof, 1982; Schlesinger 1997). Much remains to be understood about the world's oceans and their potential to remove excess carbon from the atmosphere (IPCC 2001).

Since the world's oceans act as a large CO_2 reservoir and the arctic environment is a crucial part of the carbon cycle, this project provides a method for examining the role of sea ice in the exchange of CO_2 between the atmosphere and the ocean. Until recently, the role of sea ice in CO_2 gas exchange was overlooked (Zubov, 1945). In light of recent work (Kelly and Gosink, 1979; Semiletov et al., 2006), Arctic seawater and sea ice brine have shown increased capacity to absorb and carry CO_2 and carbonates, and we now know that the rate of gas movement through sea ice can be quite high (Kelley and Gosink, 1979).

Global ice coverage ranges from 6.5 million km^2 of the Earth's surface at its summer minimal extent to 14.5 million km^2 at winter maximal extent, or 4.4% and 9.8%, respectively (Walsh and Johnson 1979; Whadams, 1983; Perovich, 2002). It exists as a thin, highly reflective surface that impedes the direct exchange of radiation, heat, and

mass between the atmosphere and polar oceans. Until Gosink (1976) measured gas movement in laboratory grown sea ice, it was assumed that such movement was negligible and that therefore gas exchange through the ocean-sea ice-atmosphere interface (OSA) did not occur (Anderson et al., 1990; Tréguer and Pondaven, 2002). Recent studies suggest that sea ice does allow a carbon exchange between sea ice and surface atmosphere (Papakyriakou et al., 2004; Semelitov et al., 2004; Rysgaard, 2007). Delille et al. (2005) measured elevated pCO_2 over the headspace of brine in an ice sack hole. Collectively these works suggest that we should no longer assume sea ice to be a passive barrier to air-sea CO_2 exchange. Further, sea ice may have the potential to increase the already significant capacity of the ocean to absorb CO_2 (Anderson et al., 2004; Papakyriakou et al., 2004). In addition, brine drainage transports dissolved gases and solutes into the water column (Glud et al., 2002; Papadimitriou et al., 2003), possibly leading to observed supersaturated pCO_2 levels below sea ice (Kelly, 1968; Semiletov et al., 2004).

With global climate models predicting enhanced warming in the polar regions, sea ice will be an indicator and amplifier of natural and anthropogenic climate changes (Serreze et al., 2000; Eicken and Lemke, 2001). Satellite data has allowed us to track changes in sea ice concentration over the past 30 years (Grenfell, 1986; Kattenberg et al. 1996; Flato and Boer, 2002). Decreases in ice coverage range from 0.6% per annum from 1978 to 1994, to 0.8% per annum from 1979-2004 (Gloersen and Campbell, 1991; Chapman, 1993; Rothrock et al., 1999; Cavalieri et al. 2003; Comiso, 2003; Serreze et al. 2003; Stroeve et al. 2005). The implications of decreasing ice cover on the carbon budget of the Arctic Ocean and peripheral seas are uncertain. The laws of gas dissolution state that as a liquid cools the volume of gases it can absorb increases. Therefore, cold high latitude seas are conducive to absorption of CO_2.

Increasing salinity allows a solution to remain liquid at colder temperatures. Although brine makes up a small portion of ice volume (Cox and Weeks, 1983), its impact on sea ice chemistry may be significant by providing access to gases between the upper and lower environments through brine channels. Sinking brine is thought to be effective at removing CO_2 from the atmosphere by carrying $CO_{2(aq)}$ and carbonates away from the surface (Anderson and Jones, 1985; Rysgaard et al., 2007).

The ability of surface seawater to absorb CO_2 depends on seawater temperature, solute content and instability associated with ice production. Two important features of the sea ice environment are that low temperatures may result in a significant change in alkalinity (A_T) and dissolved inorganic CO_2 (DIC) in sea ice compared with surface waters; and research supports that brine, found in first year sea ice (FYI) is rejected into the water column during ice formation, providing high-saline dense water in both shelf and open-ocean areas in seasonal and continuous ice covered seas (Rysgaard et al., 2007; Shcherbina et al., 2003).

Ocean waters that are colder than average are typically zones of deep water formation, effectively removing surface water components (Yool and Fasham 2001; Takahashi et al., 2002; Semiletov et al., 2005; Wetzel et al 2005). The ability of surface seawater, in contact with atmosphere or with the underside of sea ice, to absorb gaseous CO_2 ($CO_{2(g)}$) changes according to the concentration of dissolved $CO_{2(g)}$ already in the surface water. The controlling factors of the seawater CO_2 system are pH, DIC, A_T, the fugacity of CO_2 (fCO_2), and temperature (Broecker, 1974; Millero, 1995). DIC is the sum of the total concentrations of each of the solution components, HCO^{3-}, CO_3^{2-}, H_2CO_3, and CO_2 (UNESCO, 1991); called carbonates. These carbonates make up approximately 2% of seawater dissolved solids and are measured separately as A_T (Dickson, 1981; Almgren et al., 1983; Brewer, 1986). pH and A_T have been used to theoretically show that high DIC can occur in sea ice brine relative to winter surface seawater (Gleitz et al., 1995). Ultimately, the rate of exchange is driven by the air-surface difference in fCO_2, and moderated by the solubility and physics of gas diffusion into the water. fCO_2 is a measure of chemical potential of the gas to change location or state, and related to pCO_2 but adjusted by pressure. A carbonate pump indirectly determines the rate of CO_2 exchange between the ocean and atmosphere (Volk and Hoffert, 1985) by driving carbon between various chemical species.

Using a unique technique for sampling gas within the Arctic sea ice, I examine the role of Arctic FYI in the exchange of CO_2 between the atmosphere and the ocean, in order to improve understanding of the carbon chemistry within the sea ice. These studies provide a point of departure for the hypothesis tested here: that sea ice should play a role

in Arctic carbon dynamics. In this work I explore the role of sea ice through temporal and spatial variation in sea ice pCO_2 and aspects of carbonate chemistry. The conclusion that this can indeed occur is contingent on observation that large amounts of dissolved CO_2 in the ice, specifically the brine, holds significant amounts of dissolved carbon. In Chapter 2, I review sea ice carbonate chemistry, sea ice as a material and pertinent aspects of Arctic oceanography. In Chapter 3, I present field and analytical methods used in this study followed by results presented in Chapter 4. The results are associated with the ice-station phase of the Canadian Arctic Shelf Exchange Study (CASES) which occurred between December 8, 2003 to May 30, 2004 at 70°03'N and 126°18'W (see Chapter 3.1). In Chapter 5, I discuss seasonally evolving pCO_2 across a sea ice cover and identify links among pCO_2, aspects of sea ice thermodynamic state, and measures of the carbonate chemistry of sea ice, upper sea water and atmospheric CO_2 concentrations. In doing so, my work will add to our understanding on the role of sea ice on polar marine carbon dynamics, and will identify aspects of the system that remain poorly understood. Finally, in Chapter 6, I present conclusions relating brine salinity to dissolved CO_2 concentrations.

CHAPTER 2: LITERATURE REVIEW

Literature on ocean carbon exchange rests on the assumption that sea ice does not play a significant role in seawater-atmosphere exchange of CO_2, while recent research has shown that sea ice has the capacity to contain and exchange gas. There is a growing body of research that focuses on the role of brine and brine channels as the potential carriers of CO_2 in the exchange process. In this chapter, I review both of these points. The Arctic ice experiences a broad range of temperatures both across seasons and across different depths at any single point in time. The below freezing conditions that allow for ice coverage to occur also increase the capacity of seawater to absorb gas. Ice brine has a greater CO_2 carrying capacity than seawater as a result of sea ice formation that consequently inputs cold and high salinity water into surface ocean waters. The surface water input from the forming ice has a high density and will sink, thereby increasing the depth of the mixed layer and bringing CO_2 of atmospheric origin downwards (Anderson and Jones, 1985; Delille et al., 2007; Rysgaard, 2007). The new brine-enriched sea water is cold and dense, allowing it to hold more CO_2 than it would in temperate conditions (Killawee et al., 1998).

2.1 Arctic Oceanography: Seawater and Sea Ice

The marine waters of the Canadian Arctic are vast and vary significantly in their physical and biological characteristics. These waters are part of the Arctic Ocean, a large circumpolar body of water which includes the marine areas of Alaska, the Russian Federation, Scandinavia, and Greenland. The Arctic Ocean is approximately 53% continental shelf; the highest percentage of any ocean (Jakobsson, 2002). The remainder of the ocean floor is a deep central basin. The Arctic Ocean is the smallest of the world's oceans with an area of fourteen million square kilometres (Walsh and Johnson 1979; Whadams, 1983; Coble et al., 1987). It typically becomes completely covered by sea ice by February, reaching maximal extent by the end of the winter season. The polar ice cap has two components: multi-year sea ice (MYI) and younger sea ice forms including first year sea ice (FYI). The most northerly part of the Arctic Ocean is covered by multi year sea ice: ice that has survived at least one melt season (Eicken, 2001). MYI averages three

to four meters in thickness, and it is relatively free of salt and other seawater components (Eicken, 1995). Younger sea ice types grow around MYI ice throughout the winter. Once ice becomes established it is termed FYI, some FYI will endure to become MYI depending on factors discussed in section 2.2.1. Ice cover can grow up to two million square kilometres from the central MYI pack, stretching into sub-Arctic Hudson Bay, northern sectors of the Pacific and Atlantic Oceans through the Bering Straight, Davis Straight, and Norwegian Sea (Walsh and Johnson 1979; Whadams, 1983). Landfast ice, in which this portion of the CASES project occurred, is in contact with the shore and does not flow readily with ice further from shore (Hibler, 1989; Kowalik and Proshutinsky, 1994). Sea ice taxonomy is discussed in greater detail in Section 2.2.

The narrow and shallow channels stretching between the Arctic Ocean and the Atlantic (from the Greenland and Norwegian Sea via Davis Strait) and Pacific Ocean (from the Chukchi and Bering Sea via Bering Strait) allow limited surface water exchange in and out of the Arctic Ocean (Aagaard, K and Carmack, EC, 1989; Aagaard et al., 1991; Smethie et al., 1988). The Arctic gyre causes mixing in the shallow waters and forms a stagnant pool of deep, cold water in the central Arctic basin (Aagaard et al., 1985; Rudels and Quadfasel, 1991). The circulation of this secluded body of water is dominated by thermohaline forcing. Thermohaline circulation means that vertical gradients in salinity (halocline) and temperature (thermocline) differences are responsible for bulk seawater flow (Millero, 2000; Sarmiento and Gruber, 2006). Water with higher salinity sinks to the deeper layers of the Ocean (King, 1962; Richardson and McSween, 1989; Duffy et al., 2001).

Fresh water entering the Mackenzie shelf region of the Beaufort Sea originates in the Mackenzie River and provides a large volume of low salinity, high nutrient water to the shallow coastal regions of the circumpolar ocean (Aagaard and Carmack, 1989; Shiklomanov et al., 1999; Lammers et al., 2000). Besides getting about 10% of the Earth's river water via the Mackenzie River (Schlesinger, 1997; Anderson et al., 2004), freshwater is added to the Arctic Ocean by seasonal land melt (Shiklomanov, 1999; Lammers, 2000) and sea ice melting (Section 2.2).

2.2 Arctic First Year Sea Ice Physics and Geochemistry

2.2.1 Formation and Evolution of Sea Ice

The formation of sea ice provides a nutrient rich liquid by removing pure water from Arctic seawater (Backhaus et al., 1997; Rudels et al., 1999). Sea ice melt alters surface seawater nutrient content by introducing low solute water to the ocean. Translucent sea ice extends the dark period to the sea by decreasing solar radiation input. It also provides habitat for flora and fauna. These phenomena are unique to the seasonal ice environments of the Arctic and Antarctic.

Sea ice formation begins when seawater at the surface freezes as a result of air temperature falling below the water's freezing point. In the Arctic Ocean, surface seawater salinity is approximately 34 on the practical salinity scale (pss), this level of saltiness causes the seawater to freeze at approximately –1.86°C (Wegener, A. Institute, 1997; Johnson and Polyakov, 2001). The surface mixed layer is the relatively homogenous upper portion of seawater that can exchange some chemical components freely with air. Meanwhile, it mixes slowly with the water layers beneath it. The layers remain separated due to salinity and temperature differences between the layers and have limited chemical exchange. The upper mixed layer of surface water, up to tens of meters thick, must be chilled to slightly below the freezing point before sea ice formation begins (Aagaard and Carmack, 1989). The fact that colder surface water does not mix with the warmer, deeper water means that only the mixed layer needs to cool in order for an ice cap to form. Microscopic spheres of pure ice crystals form first as ice slush, or frazil ice, in the upper water layers (Eicken, 2000 and 2003). The ice crystals remain near the surface until a layer of soft or slushy ice coalesces. The density of the freezing surface water increases as salt and water segregate as the water freezes, leaving a more saline, and colder, liquid behind. This causes surface water to sink, forcing mixing with the warmer and deeper water that lies immediately below.

Once formed, the ice crystals grow in size and begin adhering to each other, forming frazil ice. The stirring of the frazil ice through several meters of the upper ocean gives it a greasy or grainy appearance. Once the frazil has begun to coalesce at the surface, ice crystals grow downwards into long needles of hexagonal dendrite stars of varying lengths, depending on the force of wave action (Weeks and Ackley, 1986). Assisted by the presence of salts, the sea ice needles allow sea ice to take on a lamellar

structure in the form of vertical ice crystal plates (perpendicular to the freezing surface). This gives rise to the observed fibrous structure and vertical fracture planes of sea ice (Defant, 1961).

Further freezing in calm conditions will consolidate the frazil into thin (<10 cm) sheets of nilas. The advancing ice edge tends to maintain relative calm on encroached cooling seas. Dampened wave action allows thickening of the ice layer, eventually allowing ice chunks and a gradual build up of frazil crystals to form pancake ice via accretion. Pancake ice is composed of round, flat aggregations of grease ice, compressed and compacted together by bumping and grinding against each other under the influence of wind and ocean swells. Pans of ice formed in this way can be measured on the sub-meter to meter scale. Although dampening surface water mixing, rough seas allow pancakes to ride up on each other, quickly doubling the thickness of the ice, which can reach up to 0.5m thick (Weeks, W.F. and S. Ackley, 1986). Ice pancakes come together to form larger pancakes until a solid sheet has formed. Once this initial process has created a solid sheet, freezing of congelation ice underneath takes over as the method of adding thickness to the ice (Weeks and Ackley, 1986). Such downward congelation of sea ice typically adds 60-80% of the total ice pack (Eicken, 2001). The ice continues to grow from the bottom of the surface layer downward as heat is drawn from the layer of seawater directly under the ice upwards to the cooling atmosphere.

The direction of the crystals has an important effect on sea ice salt content (Cobb, 1963). As sea ice growth continues, salt segregation produces lower bulk salinity in the sea ice compared to that in seawater, and consequently, a higher salt content in the surface water than in its lower layers. The process of salt segregation in freezing seawater does not incorporate all the seawater's solutes into the ice structure. Dissolved constituents are, for the most part, expelled as sea ice solidifies (Horne, 1969; Parkinson, et al., 1987). The downward growth of sea ice retains between 10 and 40 % of the seawater salt ions (Weeks and Lofgren 1967; Cox and Weeks, 1983) which remain trapped in the sea ice lamellae. This gives two products, pure ice and the solute dense seawater called brine. Brine is known to reach very high salinities (Cox and Weeks, 1975, 1983; Eide and Martin, 1975; Kasai and Ono, 1984; Wettlaufer et al., 1997), at least as much as 200 pss. Sea ice salinity is inversely proportional to temperature: as

temperatures increase, more ice melts, diluting the brine. Brine remains in liquid form at temperatures as low as –50°C with various solutes precipitating at various discrete temperatures (Figure 2.1; Assur, 1960; Cox and Weeks, 1975; Weeks and Ackley, 1982; Eicken, 1998; Golden et al., 1998, Light et al., 2002). The phase fractions shown in Figure 2.1 were further verified by Richardson and Keller (1966), Richardson (1976) and Melnichenko et al. (1979). Besides brine, gas pockets are also trapped in sea ice due to the formation of ice crystal lattice, though CO_2 retention in them has not been studied in detail (Gavrilo and Gaitskhoki, 1970; Grenfell and Maykut, 1977; Perovich et al., 1998). By summer, FYI will have only 5-10% of the original seawater's salinity (Aagaard and Carmack, 1989).

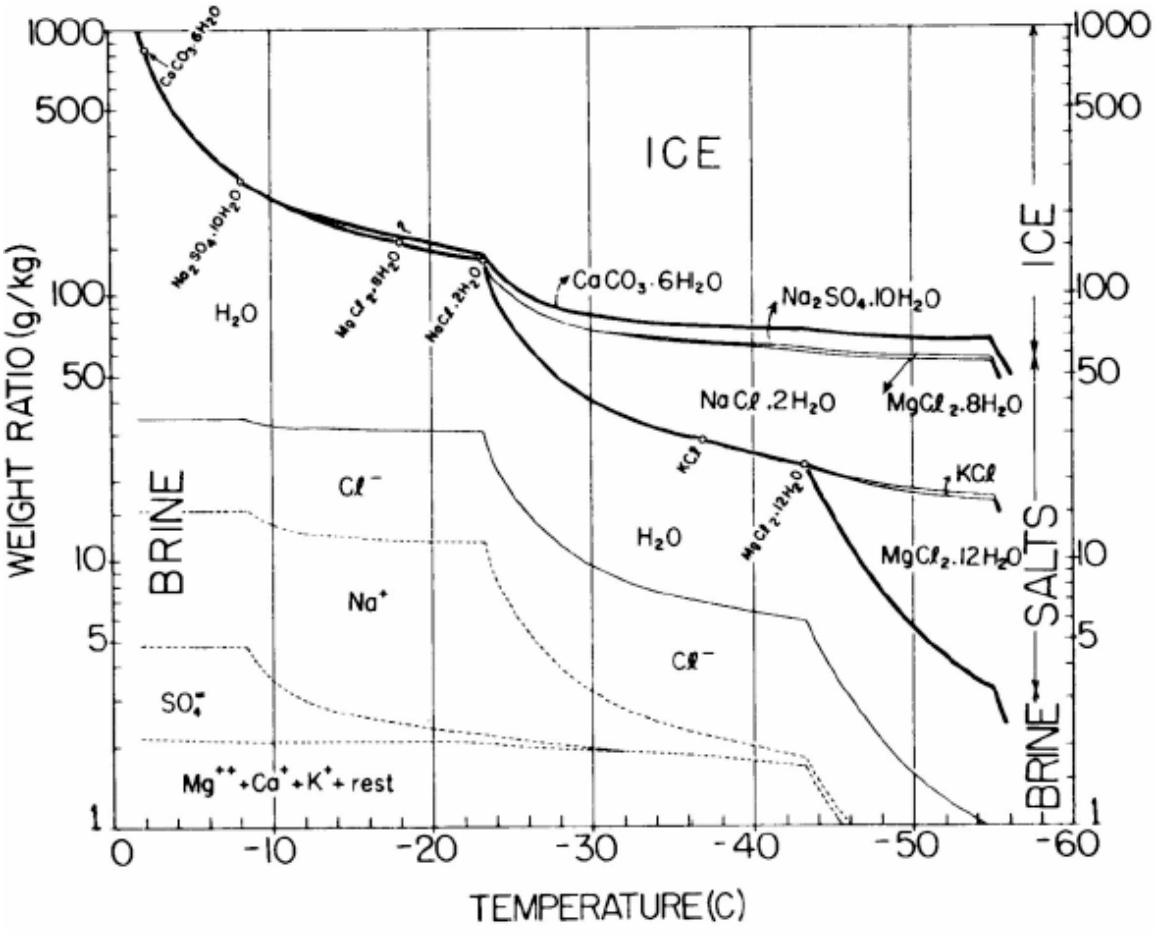

Figure 2.1. Phase composition of sea ice (Assur, 1960).

During the formation and growth of ice, the concentrated and denser brine solution sinks away from the advancing ice front due to the draining water's low

temperature and high salinity (Rysgaard et al., 2007). As a result, more ice grows in fresh seawater than in brine with higher salt concentration because fresh seawater has a warmer freezing point than solute dense brine (Lake and Lewis, 1977; Weeks and Ackley, 1986). Since the salt ions are unable to move as quickly downwards relative to the rate of heat loss, the interstitial layer becomes super-cooled. In contrast, springtime sea ice melt inputs very low saline, almost fresh water into the Arctic Ocean (Section 2.2.2).

Since heat is transferred upwards from the seawater below, and released to the atmosphere when the seawater is warmer than the atmosphere, ice maintains a negative linear temperature gradient from the warm bottom to the cold surface (Perovich and Elder, 2001). Energy balance functions allow ice to grow until the heat conducted into the ice equals the heat conducted out of the ice. On average this balance is achieved at the point at which ice is approximately 2 m thick, but it can thicken to 3 m if it survives as MYI (Parkinson et al., 1987).

2.2.2 Sea Ice Structure and Composition

The lamellar growth pattern of congelation ice resembles in shape the underside of a mushroom cap. It is between these scales of ice that salts remain mobile in ice in the brine. The brine is pushed down these spaces to the seawater in response to temperature gradients and by gravity. These two forces vary in relative strength depending on the ice temperature with the former being the stronger force of the two. As cooling continues and ice grows, the upper ice is chilled further, decreasing the liquid component of the ice. This interior change consolidates the lamellar membranes, lowering the porosity of the ice and producing brine channels and, ultimately, brine pockets (Cox and Weeks, 1983; Parkinson, et al., 1987; Thomas and Dieckmann, 2002b; Thomas and Papadimitriou, 2003).

Although the ice pack appears to only melt during warm periods of melt in spring and summer, microscopically it is always in a state of melting and freezing. The degree of melting is a function of brine salinity, with higher brine salinity values corresponding to colder melting points. Meanwhile, the bulk ice salinity is lower than that of seawater due to the growth processes written above. The melting causes fresh water to be introduced to the brine pockets, decreasing the salinity of the brine contained within, but

only momentarily, as the lower salinity will allow the equivalent amount of water to freeze again. The ice in closer proximity to the warmer seawater below maintains larger brine channels and pockets.

Although much salt is rejected from the ice during formation, desalinization processes further reject it during the summer. New ice has the highest salinity, followed by older FYI, with MYI with the lowest of the three (Parkinson et al., 1987). Gleitz et al. (1995) speculate that brine exchange may not affect the upper layers of sea ice as they become less permeable and that this may isolate not only the ice surface but also the atmosphere from the sea below. Further brine exchange limitations have been proposed by Kühl et al. (2001) where the brine emerging from the lower sea ice meets the seawater include solute exchange within the diffusive boundary layer is subject to molecular diffusion rate limiting factors along chemical gradients.

The rate of freezing, salinity of the source seawater (Horne, 1969), and the length of time these forces have acted on the ice determine how much salt has been pushed out of the matrix determining bulk ice salinity (Cox and Weeks, 1983; Thomas and Dieckmann, 2002b). Slow ice growth results in lower salt build up, because more time is available for salt to be diffused and be pushed out. Conversely, if the solution is rapidly frozen, then more electrolytes remain trapped in the ice by small brine pockets, giving the ice a higher salinity (Parkinson, et al., 1987; Thomas and Papadimitriou, 2003). The salinity (including carbonates) affects the freezing point of seawater and brine: a high salinity value will lower the freezing point and vice versa (Section 2.2.3). The solute portion of brine also possesses carbonates in various forms which act to buffer to changes in C content and produce biologically usable C from unusable forms. Each of these increases the ability for the CO_2 concentration of the ice to increase and due to their central importance to the thesis will be discussed in later sections.

Diurnal and seasonal temperature changes have a particularly important effect on ice chemistry and the physical structure of ice. Along with gravity, changes in temperature lead to brine migration within the ice (Untersteiner, 1968; Lake and Lewis, 1970; Eide and Martin, 1975; Wakatsuchi and Kawamura, 1987; Aagaard and Carmack, 1989; Eicken, 2003). This migration results in vertical movement of the dissolved constituents of the original seawater. The negative gradient in FYI is steep when the

atmosphere is warm and less steep when the atmosphere is cold because the ice is relatively thin (up to 200 cm). Brine migration continues past the end of the ice pack's growing season well into the melt season. Melting ice becomes more permeable, allowing brine drainage by gravity and flushing from surface melt to continue through the melt season. The highly concentrated and cold brine moves from the ice into the seawater, supercooling the top layer of seawater (Eicken, 1992; Ono and Kasai, 1985; Eicken et al., 2000). This brine input contributes to thermohaline convection in the Arctic Ocean (Yu et al., 2001; Stossel et al., 2002) and the ability of the World's oceans to act as a large CO_2 reservoir discussed further in Section 2.2.3.

Even at the coldest temperatures normally observed within ice, around -40°C, gas pockets and brine both continue to exist (Cox and Weeks, 1983; Gavrilo and Gaitskhoki, 1970). Frozen water forms a non-random crystal lattice leaving gaps or pockets between them (Horne, 1969). Changes in temperature also directly affect the pore microstructure of the ice. Hydrodynamic processes and microstructural controls determine the composition, density and morphology of individual channels.

Temperature, gas partial pressure, and salt concentration changes cause the solubility of atmospheric gases in the brine to change, causing these gases to be expelled from the solution into the inclusion. During sea ice birth and growth processes, these expelled gases form gas pockets in the ice (Gavrilo and Gaitskhoki, 1970). While these can combine with brine pockets, gas pockets can exist independently of brine. Brine plays a role in their formation when travelling downwards leaving behind gas spaces around which ice forms. Air pocket formation can occur during the brine migration process or from freshwater flushing downwards from surface melt ponds.

Ice from fresh water contains fewer gas pockets than the more saline oceans. Young sea ice has higher gas content than old sea ice, pointing to a correlation with salt content. Research has shown that the dissolved gases tend to escape along with the brine (Matsuo and Miyake, 1966). As the ice is forming solute precipitation causes the degassing of the brine through nucleation of gas bubbles. These gas bubbles are subsequently trapped within the ice matrix (Killawee et al., 1998; Mock et al., 2002).

2.2.3 Salinity and Temperature as Determinants of Brine Behaviour

The first brine measurements were made for the purposes of polar navigation to calculate sea ice strength, or its ability to withstand force (Cox and Weeks, 1983). They found that gas content affects the density and resulting strength of sea ice more than salt content. Cox and Weeks (1983) developed chemical equations to determine relative gas and liquid volume fractions as a function of sea ice temperature and salinity. Since temperature is the main driving force for change within ice it follows that variables found in these equations are dependent on it. In addition to partially explaining the relationship between gas, brine content and ice strength (a negative correlation), the equations help break down the sea ice components to extract the relationship of gas/brine transfer between the atmosphere and ocean environments. Lowering temperature of the sea surface and atmosphere is the primary cause of:

- ice formation, growth and melt,
- changing of solute concentrations of liquid within the ice, and
- movement of sea ice components, such as brine, through ice.

Temperature fluctuations are also responsible for the dynamic nature of brine changing ice crystals shape and composition. Seasonal temperature changes drive brine movement and chemical composition state changes, as solutes precipitate and re-dissolve. Temperatures variation determines the chemical and physical structure of ice cover.

Consequently, the chemical make-up of the ice and therefore the gas absorption capacities differ according to the same parameters. Due to drastically changing temperatures, mineral precipitation and CO_2 degassing occur during sea ice formation and growth as ice reaches temperatures where species precipitate (Gitterman, 1937; Papadimitriou et al., 2003). Degassing of freezing water has not been observed in nature (Anderson and Jones, 1985; Gleitz et al., 1995), but laboratory experiments by Gitterman (1937) have noted this phenomenon. The carbonate equilibrium expressions associated with the chemical reactions involved are detailed further in Section 2.3. Papdimitriou (2003) presented indirect evidence for carbonate mineral precipitation and CO_2 degassing in artificial sea ice on the basis of the saturation state calculations of seawater and ice brines. Carbonate mineral precipitation was first detected by Dieckman et al. (2008) when they isolated ikaite ($CaCO_3 \cdot 6H_2O$) in natural sea ice. Requiring specific conditions

to form, ikaite can be found in carbonate rich waters where the formation of calcite is inhibited, below 8ºC.

Why is Dieckman's recent paper significant?Observing this in nature would show the capacity of brine to play a role in atmosphere/ocean gas exchange.

Dissolved inorganic carbonate salts affect absorption of gas in brine in two ways: one, by lowering the freezing point of the liquid, and two, by changing the chemistry of the brine to allow for greater gas absorption (Jones, 1973). Much like seawater salts, 85% of sea ice salts are comprised of two ions, sodium (Na^+) and chloride (Cl^-). The remaining 15% of salts include ions of sulphate (SO_4^{2-}), magnesium (Mg^{2+}), calcium (Ca^{2+}), potassium (K^+) and carbonates (Millero and Laferiere, 2002; Lake and Lewis, 1970). These either precipitate out of the liquid and collect within ice crystals, or remain dissolved in brine. Each of the solutes will precipitate at a unique temperature (Assur, 1960), as shown in the phase diagram (Figure 2.1, 1960). Assur (1960) provides a list of the primary species present in ice brine and shows temperatures at which brine weight ratios decrease through the loss of significant amounts of solutes to precipitates. As solids precipitate out of the brine solution, the ionic composition of the brine changes. About 10% of solutes are dissolved within sea ice brines until the frigid temperature of about –40ºC (Assur, 1960).

Gitterman (1937) was among the first to detect chemical changes in sea ice such as precipitation of minerals (Horne, 1969, Weeks and Ackley 1983). Subsequently, observations in the lab and in the field have been made on the precipitation of salts in sea ice at various temperatures (Assur, 1960; Horne, 1969; Weeks and Ackley, 1986; Marion and Farren, 1999). The progression of precipitating brine salt species begins at seawater freezing point. The solid precipitates primarily include derivatives of Cl^-, CO_3^{2-} or SO_4^{2-} with Ca^{2+}, Na^+, Mg^{2+} or K^+. Each of the ions that precipitate out of the brine solution do so at different temperatures; thus, for example, $CaCO_3$, a major proportion of seawater carbonates, is the first to precipitate (along with some of its derivatives) just below the freezing point of seawater, potentially removing itself from solution (Gitterman, 1937; Richardson, 1976; Lazar et al., 1983; Anderson and Jones, 1985; Marion, 2001;

Papadimitriou et al., 2003). The first non-carbonate to solidify is mirabilite ($Na_2SO_4 \cdot 10H_2O$) at -6.3°C (Marion and Farren, 1999).

Upwards conductive heat transfer from the seawater to the sea ice causes the ice to undergo some degree of melt throughout its life cycle. This has been described as part of the process of brine migration. Ice begins to thin only once the input of energy from the atmosphere to the ocean exceeds the reverse (DeAbre, 1994). As the pack warms in late winter, brine pockets enlarge to compensate for the increasing brine volume fraction. Brine movement accelerates due to higher temperatures. The morphology of the pockets allows them to begin connecting (Weeks and Ackley, 1986). Salinity of brine within brine pockets decreases due to addition of melted sea ice to the brine volume. Sea ice desalination is at its peak during the melt season because of increased porosity of warm sea ice. Salts in the liquid brine and those that had precipitated out of solution, such as $CaCO_3$ and Na_2SO_4, re-enter the liquid solution at various temperatures (Cox and Weeks, 1983). At –8°C, carbonates begin to re-enter solution aggressively. As the sea ice warms to melting point, dissolution of precipitates continues and brine volumes approach maximum, due to melt (Cox and Weeks, 1975). Assur's (1960) figure is once again useful for providing a nearly complete breakdown of dissolved salts in the ice near the melting point.

As ice cools, it expands, creating a higher ice-to-liquid volume ratio. At the same time, the salt concentration of the liquid increases, escalating the ice-to-liquid weight ratio. The brine is forced into discrete pockets that shrink as more of the liquid is frozen and the brine is concentrated (Vant et al., 1986; Weeks and Ackley, 1986). Brine pockets are mobile with predictable migration in ice (Kingery and Goodnow, 1963; Hoekstra et al., 1965; Harrison, 1965). Brine migration is a process of movement whereby a brine pocket advances by melting ice at its warm end: as the warm, bottom end of a brine pocket melts, the colder, top end refreezes, shifting the salts and pockets downwards (Niedrauer and Martin, 1979; Weeks and Ackley, 1986). This allows the brine to maintain the necessary salinity value to remain liquid at the temperature of its surroundings. Alternating dissolution and precipitation maintain the required concentration of brine salts for the current location's temperature (Kingery and Goodnow, 1963; Cox and Weeks, 1975; Wakatsuchi and Kawamura, 1987; Niedrauer

and Martin, 1979). Once ice becomes warm enough to reach a mass melting point in the spring season, brine pockets become large enough to be flushed.

Ice and brine have different specific heat capacities: more energy is required to raise the temperature of one gram of brine by one Kelvin (K) than to raise the temperature of one gram of ice by 1 K. Therefore, during the melting process, ice will warm more slowly than brine. Once heating of the pack reaches a point where bulk melting occurs, any further addition of heat results in surface melting. This process, called surface ablation, causes the ice surface to flood with melt water. The implications of surface melt pond formation are in the energy balance and chemistry of the sea ice. The melt ponds are fresh water pools with low albedo, very different from sea ice, and as a result, their appearance alters the energy balance (Hanesiak et al., 2001;). Water contained in melt ponds has the potential to percolate downwards through the expanded brine channels, flushing out salts and other ice constituents. As a result of the surface melt flushing salts from the surface downward, the mobility of brine is increased (Cox and Weeks, 1975; Eide and Martin, 1975; Niedrauer and Martin, 1979; Wakatsuchi and Kawamura, 1987).

Brine migration in combination with other forms of sea ice salt movement, such as salt segregation, gravity drainage, and brine expulsion induce varying salinity values according to depth within the ice pack. Often, the scenario involves salt depletion in the middle of the ice pack (Malmgren, 1927) as gravity pulls brine downwards while capillary action draws it upwards. Brine migration rates are dependent on temperature. Harrison (1965) noticed that the droplets increase in size and velocity as they approach the ice-liquid interface. In the spring and summer, flushing is the main mechanism of salt removal. Meanwhile, gravity and increased brine mobility and drainage continue to take place, allowing surface snow melt to drain down to the sea through the expanding brine channels (Parkinson, et al., 1987). The percolation of snow melt from melt ponds desalinates MYI and (old) FYI, thus differentiating them from new ice (Parkinson, et al., 1987).

2.2.4 Sea Ice as a Habitat

Besides research into sea ice geochemistry and physics, studies of the ecology of sea ice organisms in the intricate brine channel system have been conducted (Goto et al.,

2000; Thomas and Dieckmann, 2002a). An abundance of organisms has been observed within sea ice cover. Due to the nature of the ice matrix, these sympagic communities are small and very dependent on their environment (Krembs et al., 2002). They are found in brine channels and pockets within the sea ice where liquid water still exists. These highly saline encasements experience depressed freezing points due to chemicals, such as dimethylsulphoniopropionate (DMSP) excreted by the organisms that inhabit the tiny spaces (Trevena et al., 2003). Currently, their accumulated low metabolic rates compared to other organisms in the Arctic sea ice system are considered to exert an insignificant influence on the C system in relation to the sea ice organisms such as ice algae (Arrigo and Thomas, 2004).

2.3 Ocean Carbon Chemistry

The World's oceans act as a large CO_2 reservoir with a storage capacity of 38 x10^{18} g C of the total global mass of 10^{23} g C (Skirrow, 1965; Schlesinger 1997). Seawater allows much more effective absorption of CO_2 than of other anthropogenic gases (e.g., chlorofluorocarbons (CFCs), excess CH_4 emissions). Carbon in the CO_2-carbonate system plays an important role in three principle reactive zones of the oceans: the atmosphere-sea interaction, the chemistry of seawater, and the deposition of marine sediments (Bollin, 1960; Horne, 1969). While the primary source of inorganic C to seawater is dissolved CO_2 (Equation 2.1), it exists in the ocean in three forms: aqueous CO_2 (Equation 2.1), carbonic acid, H_2CO_3 (Equation 2.3), bicarbonate ion, HCO^{3-} (Equation 2.3), and as carbonate ion (CO_3^{2-}) (Equation 2.5) (Garrels and Thompson, 1962; Horne, 1969; Richardson and McSween, 1989; Schlesinger 1997; Sarmiento, 2006).

Exchange processes at the atmosphere and water surface work to maintain equilibrium of **Aqueous CO_2** ($CO_{2(aq)}$), herein referred to as partial pressure of CO_2 (pCO_2[1]), in surface water equal to that of air. The CO_2 flows between the atmosphere and the ocean as in the equation:

[1] The partial pressure of a substance is the gas pressure of that substance when it is in equilibrium with the liquid form. Unlike in a gas mixture, where the addition of a new gas will affect the partial pressure of each gas in the volume, introducing another gas into a gas/liquid mixture does not affect the equilibrium rate at which gas molecules move from the liquid to the gas (or vice versa). This relationship

$$CO_{2(g)} \leftrightarrow CO_{2(aq)} \quad (2.1)$$

The notations *g*, and *aq* refer the state of the species: gaseous and aqueous, respectively. $CO_{2(aq)}$ is non-ionic, and makes up about 1% of the total inorganic C of the global oceans (Horne, 1969). The direction that CO_2 will travel is a function of solubility equilibrium constant (K_{sp}). The reverse of Equation 2.1 represents replacement of CO_2 back into the atmosphere.

Henry's Law defines CO_2 transfer between different solutions, such as air, seawater, or brine. According to Henry's Law, the relationship between partial pressures (*p*) and temperature regulates gas dissolution in liquids. At a constant temperature, the *p* of gases dissolving in a liquid is defined as the pressure which the gas would have if it alone occupied the volume. This value is directly proportional to the *p* of the gas in equilibrium with the particular liquid. The formula for Henry's Law is:

$$p = k_H c \quad (2.2)$$

where c is the concentration of the solute in the solution (in an appropriate unit) and k_H is Henry's Law constant with units atm/(mol fraction), L·atm/mol, etc. Henry's Law constant is solvent and temperature dependent. Note that: L is litres of solution; atm is the *p* of the gaseous solute above the solution (in atmospheres of absolute pressure); mol is the moles of the gaseous solute in the solution; and all at standard temperature and pressure (stp). For instance, in fresh water at 298K, some values for k include: CO_2, k = 29.4 L·atm/mol; O_2, k = 769.2 L·atm/mol; and H_2, k = 1282.1 L·atm/mol; with molarity as the unit of concentration.

The reaction of $CO_{2(aq)}$ with $H_2O_{(l)}$ results in the **bicarbonate ion**, HCO_3^-:

$$CO_{2(aq)} + H_2O_{(l)} \leftrightarrow H_2CO_{3(aq)} \leftrightarrow H^+ + HCO_3^- \quad (2.3)$$

and, the K_{sp} of a chemical equation provides an indication of the ions' ability to dissolve in a liquid and can be determined for any chemical equilibrium between solid and dissolved states of a compound at saturation. For HCO_3^-:

$$K_{\alpha 1} = \frac{[H^+]\,[HCO_3^-]}{[H_2CO_3]} = 4.45 \times 10^{-7} \quad (2.4)$$

---

is described by Henry's law: concentration of dissolved gas is equal partial pressure of gas x Solubility coefficient of the gas.

where brackets represent total concentrations of each of the solution components in mol*kg^{-1}. The equilibrium expression (Eq. 2.2) is Henry's Law equation (@ 25 °C). The K_{sp} of a solution provides an indication of the unit-less measure of its fugacity. In this case, fugacity is a measure of the tendency of a substance to prefer one phase (liquid vs. gas) to another. Fugacity is a measure of chemical potential in the form of 'adjusted pressure.' It directly relates to the tendency of a substance to prefer (or to flee or escape) one phase over another. The phase with the lowest fugacity will thermodynamically be the most favourable because that is a situation that minimizes Gibbs free energy. The bicarbonate ion makes up about 91% of the total inorganic C in the global oceans and has implications on the pH of seawater. pH changes in seawater affect the amount of inorganic C species the seawater can hold and the habitat of seawater organisms. The ionization constant of HCO^{3-} is very small, causing the slightly ionized HCO^{3-} ion to dissociate, forming the H^+ ion and the CO_3^{2-} ion. The **carbonate ion** (CO_3^{2-}) behaves as a base (Brønsted and Lowry, 1923; Horne, 1969) and remains after the removal of the H^+ from the bicarbonate ion.

$$H^+ + HCO_3^- \leftrightarrow 2H^+ + CO_3^{2-}. \qquad (2.5)$$

and,

$$K_{\alpha 2} = \frac{[H^+]\,[CO_3^{2-}]}{[HCO_3^-]} = 4.69 \times 10^{-11} \qquad (2.6)$$

The carbonate ion contributes about 8% of the total inorganic C content in seawater (Horne, 1969; Mehrbach et al., 1973).

The factors in control of surface water CO_2 partial pressure (pCO_2) are surface ocean temperature, salinity, pressure, and dissolved inorganic carbon content (DIC) (Broecker, 1974). Dissolved inorganic carbon is the sum of inorganic carbon species that includes CO_2 (where CO_2 is the concentration of all unionized CO_2, whether present as H_2CO_3 or as CO_2; SOP2, 1997; UNESCO, 1991), bicarbonate (HCO_3^-), and carbonate (CO_3^{2-}): The DIC content of seawater can be defined as:

$$DIC = [CO_2 + H_2CO_3] + [HCO_3^-] + [CO_3^{2-}], \qquad (2.7)$$

DIC and alkalinity values provide insight into the limits of further absorption of CO_2 by the ocean, while temperature and salinity are seawater characteristics that indirectly affect seawater gas-dissolution laws. Equations 2.1, 2.3, 2.5, and 2.7 show how the chemical

species comprising carbonate alkalinity (A_C) (the carbonates), and dissolved inorganic $CO_{2(aq)}$ (as pCO_2) interact as two of the four main controlling parameters of the seawater carbonate system (Millero, 1995). The alkalinity is a measure of the bases in a solution as in Equation 2.8.

$$A_T = [HCO_3^-]_T + 2[CO_3^{2-}]_T + [B(OH)_4^-]_T + [OH^-]_T + 2[PO_4^{-3}]_T + [HPO_4^{-2}]_T + [SiO(OH)_3^-]_T - [H^+]_{sws} - [HSO_4^-] \quad (2.8)$$

As in A_T, the subscript T indicates the total concentration, not just the free concentration, of the species in the solution as measured. In seawater and brine carbonates make up most of the total alkalinity due to dissolution of carbonate rocks and atmospheric CO_2 dissolving into the liquid. A_C is comprised of the first two terms on the right hand side of equation 2.8. Alkalinity indicates the degree of the carbonate composition of a parcel of seawater, and the ocean's ability to neutralize acids, or, act as a buffer to changing pH levels (Dickson, 1981). The bases HCO^{2-} and CO_3^{2-} make up the bulk of alkalinity (identified in Equations 2.3 and 2.5) and the concentration of these bases dissolved in seawater are expressed as micromoles per kilogram (μmol/kg). The role of temperature and salinity will be discussed in Section 3.4.1.

Additional input of inorganic C to seawater already saturated in DIC causes expulsion of CO_2 back to the atmosphere (upwards) or to a different unsaturated layer in the ocean (downwards), depending on equilibrium states of the destinations. Excess CO_2 can remain in the atmosphere, since seawater has limits on gas volume absorption (Brewer et al., 2000). The absorption of CO_2 by surface water creates an acidic solution buffered by the carbonates in the seawater. Change to pH by such chemical additions as import or export of CO_2 is determined by the water's buffering capacity (its ability to absorb acids and/or bases), an important component of pH balance in seawater (Horne, 1967). The release of H^+ ion, described in Equations 2.3 and 2.5, during the formation of carbonate and bicarbonate enable the buffering capacity of the carbonate system. There exists a fundamental difference between the expression of acid-base properties of pH and alkalinity. pH is a measure of the cations in a solution, while alkalinity is the capacity of a water sample to sustain reaction with added acids or act as a neutralizer. (Dickson, 1981; Almgren et al., 1983; Lazar et al., 1983; Brewer et al., 1986; Dickson et al., 2002)

The components that make up seawater alkalinity are a portion of salinity. Salinity has been redefined in the practical salinity scale (pss) as the conductivity ratio of a sea water sample to a standard KCl solution (UNESCO 1981a and 1981b). The assumed proportion of the primary carbonates in seawater, as described in Equations 2.1 to 2.3, is: 1% aqueous CO_2, 8% CO_3^{2-} and 91% HCO_3^- (Almgren et al., 1983; Brewer et al., 1986). In seawater, it has been estimated that roughly 2% of salinity is made up of carbonates. However, this assumption does not hold true across all brine temperatures, such that the specific carbonate proportions of salinity change as sea ice cools and warms. Figure 2.1 illustrates the various temperatures at which brine solutes undergo precipitation. Although there is some similarity in the nucleation temperature for some solutes, such as at –8˚C (SO_4^{2-}, some Na^+, and Cl^-), -24˚C (Na^+, Cl^-), and -43˚C ($MgCl_2$, further Na^+, Cl^-, and SO_4^{2-}), the solutes come out of solution over a range greater than 50˚C. It can be noted, however, that carbonates tend to precipitate out of solution earlier than many of the other solutes. The analysis of precipitation data is important for understanding sea ice brine gas absorption capabilities.

Dissolution of gas in the oceans provides a large sink for anthropogenic CO_2 (Chung et al., 2003), due in part to its high solubility, but above all because of the dissociation of CO_2 into ions and interactions with seawater constituents. Along with gaseous CO_2 dissolution, surface seawater alkalinity is influenced by precipitation and dissolution of calcium carbonate ($CaCO_3$). Referring back to Equation 2.3, we see that the addition of $CO_{2(g)}$ to seawater creates an acidic environment. The buffering effect results when carbonate ions (CO_3^{2-}) interact with calcium (Ca^{2+}) and magnesium (Mg^{2+}) ions to cause the precipitation of salts. Reactions like this tend to buffer changes in atmospheric CO_2. Without the carbonate buffering system, free CO_2 would form large amounts of carbonic acid, decreasing pH of seawater. The buffering capacity of carbonates allows for large quantities of CO_2 to be absorbed by seawater without drastic alterations of pH. Alkalinity of seawater is relatively stable but can change over time; due to biological nitrate consumption and release and $CaCO_3$ sedimentation and dissolution, over days to weeks and over tens to hundreds of thousands of years, respectively, depending on the pH or mineral content and temperature of the seawater.

Therefore, the presence of precipitated carbonates provides a reaction engine for any newly absorbed CO_2.

The formation and destruction of $CaCO_3$ has a strong influence on DIC and A_T. The formation of $CaCO_3$ will cause DIC to decrease due to C uptake into inorganic matter, and A_T to decrease due to uptake by calcium ions [Ca^{2+}] (Rysgaard, 2007; Papadimitriou, 2003; Killawee, 1998). The double charge of the calcium ion causes alkalinity to be altered twice as fast as DIC. In reverse, the dissolution of $CaCO_3$ will increase DIC half as fast as increases in A_T. In the surface water, $CaCO_3$ formation is a factor driving DIC and A_T down. In the deep water below the lysocline (the intersection between calcite saturation and carbonate ion content) high pressure also increases the solubility of gases in liquids, making $CaCO_3$ dissolution strong and driving DIC and A_T up. The increase in pressure increases the concentration of carbonic acid, which dissolves $CaCO_3$.

Takahashi (1961) observed that temperature dependent physical-chemical processes might be more important than photosynthetic process after measuring a peak in pCO_2 of some ocean surface waters during solar noon. Though C has been shown not to be a limiting element in oceanic biological activity (Schlesinger, 1996), changes in seawater carbonate chemistry can affect seawater biology. Through the interrelation of DIC, pH, and alkalinity, carbonate chemistry has profound effects on biological productivity, and oxygen availability. For example, excessive absorption or loss of carbonates can create an inhospitable seawater pH. Atmospheric CO_2 changes expected to occur over the next century (Clarke, 2003; Fung, 2001) may ultimately slow down the production of $CaCO_3$ in the surface ocean and its subsequent transport to the deep sea (Chung, 2003). CO_2 related changes in $CaCO_3$ formation have profound implications for the oceanic C cycle and may influence the ecology of calcareous phytoplankton. A corresponding decrease in $CaCO_3$ flux would significantly increase the oceans capacity to store atmospheric CO_2, resulting in a negative feedback to the present rise in atmospheric CO_2.

2.4 Oceans and Carbon Budgets

The amount of DIC in seawater in the oceans is far greater than the amount of DIC in the atmosphere (Schlesinger, 1996). While the concentration of CO_2 gas in the atmosphere is not chemically limited, seawater does have dissolved CO_2 carrying limits. The gas absorption limits in the ocean vary based on water temperature, DIC content, salinity and pressure as described under the carbonate chemistry section (Section 2.3). As a result, seawater can be a sink for the ever-increasing amount of anthropogenic CO_2 being added to the atmosphere, but the ocean's response as a sink is limited by gas flux and gas magnitude across the sea-atmosphere interface. Upwelling and downwelling processes with the deep ocean ultimately control surface concentration of DIC and alkalinity, and hence pCO_2. Warm, low latitude upwelling waters with decreased capacity to hold CO_2 release C to the atmosphere, but are not thought to control atmospheric pCO_2 (Schlesinger 1996). Gas exchange between the atmosphere and the ocean is driven by mechanisms called pumps, based on physical exchange, carbonate chemistry, and biology. This section considers seawater-atmosphere gas CO_2 exchange and composition over an Arctic ice-covered sea and the effects sea ice cover has on this transfer.

2.4.1 Surface Gas Exchange

Physical gas exchange happens when surface water mixes – usually accelerated by wave action. The surface water acts as an intermediary for the exchange, as it experiences ready mixing with the atmosphere due to wind in open sea conditions. Ice cover prevents direct surface air-water mixing. Wave action is limited in ice-covered seas, but brine input (not including seasonal melt) to the sea surface is active throughout the life cycle of FYI. During the cold winter season, the process of ice growth continues to deliver highly saline water to the surface layer immediately beneath the sea ice cover through brine drainage (Section 2.2.3). Ready exchange of CO_2 across the atmosphere-ocean boundary, and between different carbonate species, allows the existence of primary producers (fundamental organisms with the ability to make biomass by using sun energy via photosynthesis) to become a major part of the global C cycle.

The uniquely cold and saline Arctic Ocean is conducive to absorption of atmospheric gas constituents. Along with components of salinity, other dissolved solutes in seawater alter phase properties of the liquid. Horne (1967) points out that the

absorption of gases in an electrolytic (saline) solution decreases with increasing electrolyte concentration (Millero, 2002). However, this has negligible effect of the dissolving properties of gas compared to the effect of temperature. The Arctic surface seawater salinity is roughly 33.0 pss, slightly decreased compared to other sea water bodies, meaning Arctic seawater freezes at higher temperatures compared to more saline temperate oceans. For example, increasing a parcel of seawater's salinity increases the liquid phase range of the substance, therefore lowering the freezing point (and increasing the boiling point). This has further implications in sea ice brine chemistry where liquid salinities can reach very high values. Meanwhile, seawater's temperature range for holding gases is elevated compared to that of fresh water (Skirrow, 1965; Kelley and Gosink, 1979).

Shifting temperatures of the system change the capacity of liquids to hold gases. This allows Henry's Law to be represented as a constant. The equation derived from Eq. 2.2 to respond to temperature changes is:

$$k_{H,cp} = k_{H,stp} \bullet exp\left[-C \bullet \left(\frac{1}{T} - \frac{1}{Tcp}\right)\right] \qquad (2.9)$$

where k_H with subscripts *c* (the concentration of the solute in the solution) and *p* (the partial pressure of the solute above the solution) represents the value that differs from k_{stp}, or k_H at standard temperature (298 K) and equilibrium *p*. ; and C is a constant in the dimensions of k_H (C for CO_2, for example, is 2400). Therefore, Henry's Law recognizes that a cold liquid can hold a larger concentration of a gas than the same liquid at a warmer temperature (and vice versa) (Feely et al., 2001; Millero, 2002).

Equation 2.1 describes the exchange of CO_2 gas between the atmosphere and the ocean. The exchange can be described further with the bulk equation (Mills and Lobo, 1989; Snyder, 2001). The bulk equation is based on a derivation of Fick's first Law (1855), which is limited to steady state diffusion and can be used to tell us where the CO_2 is going:

$$J = -D \frac{\partial \phi}{\partial x} \qquad (2.10)$$

where J is the diffusion flux in dimensions of mol m^{-2} s^{-1}; D is the diffusion coefficient or diffusivity, m^2 s^{-1}; ϕ is the concentration in mol m^{-3} and; x is the position, in meters. The

bulk equation is used when the concentration within the diffusion volume changes with respect to time (s) becomes:

$$\frac{\partial \phi}{\partial t} = \mathrm{D}\ \frac{\partial^2 \phi}{\partial x^2} \qquad (2.11)$$

The Intergovernmental Panel on Climate Change (IPCC, 1996) has identified uncertainty in the gas exchange coefficient as a significant limitation in assessing the role of the ocean in absorbing anthropogenic CO_2 and has called for increased study of its global spatial and temporal variations in order to help close the global C budget.

Equation 2.11 indicates the system's attempt to maintain balance of the pCO_2 between the two mediums. Equations 2.3 and 2.5 (as shown) are further steps in the C cycle. Fick's Law shows that CO_2 gas has the ability to move within a medium, suggesting the possibility for it to move through the ice to the atmosphere or ocean. Using Equation 2.1, one can infer the direction of movement of atmospheric CO_2 by comparing seawater and atmospheric pCO_2.

2.4.2 Atmosphere-Ocean Carbon Movement

In seawater, surface gas exchange with the atmosphere ensures an abundance of CO_2. The solubility pump is a physical and chemical process that transports carbon (as DIC) from the ocean's surface to its interior. The solubility pump is driven by the existence of CO_2 as a function of:

- Henry's Law; CO_2 solubility is a strongly influenced by seawater temperature; and
- Thermohaline circulation driven by the formation of cold, deep water.

Since deep water is formed under the same surface conditions that promote CO_2 solubility, it contains a higher concentration of DIC than surface water. Consequently, Henry's law and thermohaline circulation act together to pump C from the atmosphere into the ocean's interior. One consequence of this is that when deep water upwells in warmer, equatorial latitudes out-gas CO_2 to the atmosphere because of the reduced solubility of the gas.

In seawater, the carbonate pump is regulated by a balance between precipitation and dissolution of carbonate particles. An example of carbonate formation in seawater uses $CO_{2(g)}$ as in Equations 2.3 and 2.5. The result of this is a reduced concentration of

the free $CO_{2(aq)}$ and bicarbonate. Thus, the greater the positive charge imbalance, the greater the solubility of CO_2. The charge imbalance is referred to as alkalinity. The ensuing equilibrium shift leads to an oceanic uptake of CO_2 from the atmosphere to restore balance.

Exchange of CO_2 between the atmosphere and the oceans is driven by the difference in pCO_2 across the air-sea interface (Lazar, 1983; Wanninkhof, 1992; Kier, 1993). Since natural systems strive for equilibrium a change in atmospheric CO_2 concentrations will result in a change of surface water pCO_2, and vice versa. Air-sea transfer of CO_2 tends toward the elimination of ΔpCO_2, but the lag time to equilibrate the surface layer with atmosphere means biological and physical processes dominate ΔpCO_2 distribution (Sarmiento et al., 1990). A response by one pump forces one or more of the other pumps to respond to maintain balance. Though the atmosphere is relatively well mixed, the processes that alter surface ocean pCO_2 and factors influencing ocean CO_2 exchange work slowly. Therefore, the ocean does not immediately respond to atmospheric gas changes.

The uptake capacity for $CO_{2(g)}$ varies markedly due to the carbonates (A_T) portion of DIC and salinity of seawater. The conversion of atmospheric CO_2 to carbonate is shown through Equations 2.1, 2.3, and 2.5. With a known value for alkalinity, a measure of saturation of carbonates in seawater can be found. The resultant measure of saturation indicates the ability of a water parcel to further absorb carbonates. Surface $CO_{2(aq)}$ will increase up to the saturation point; beyond it, carbonates are released to the $CO_{2(aq)}$ pool. In surface water, or the photic zone, photosynthesis can dominate over respiration. Thus, organic matter formation would tend to drive DIC down, and A_T slightly up. It is suspected that this would not be true in Arctic surface seawater during the ice-covered season due to lower primary productivity in the darkness relative to respiration (Tans et al., 1990; Gosselin et al., 1997; Lee, 2001).

One of the processes responsible for alkalinity changes in sea ice brines is precipitation and dissolution of inorganic matter. According to the brine discussion in Section 2.2.2 and Equation 2.5, the precipitation of $CaCO_3$ on the brine pocket walls can occur, assuming abundance of both Ca^{2+} and CO_3^{2-}. When this happens, the direction of Equation 2.5 continues forward to maintain equilibrium. The resulting $CO_{2(aq)}$ produced

to maintain balance leads to the return of $CO_{2(g)}$ within the inclusion. Each mole of precipitated $CaCO_3$ results in two moles of the total C (C_T) lost from the brine solution (Usdowski et al., 1979; Stiller et al., 1985; Papadimitriou et al., 1985; Delille et al., 2007). Therefore, if a sea ice system were open to exchange with the atmosphere, off gassing can occur. If the sea ice system were closed, however, off gassing would result in the accumulation of gas bubbles within the sea ice. Papadimitriou et al. (2003), and Zhang et al. (1995) go on to explain that this relationship can be seen by observing isotopic measurements of C_T and its components HCO_3^- and $CaCO_3$ and temperature. Knowing these relations helps determine the source or sink of the C in sea ice brines.

2.4.3 Biological Activity and the Biological Carbon Pump

Springtime solar radiation and air temperatures increase causing the ice to warm and ablate. Rising temperature decreases the ability of the surface seawater to hold carbon. At the same time, primary production increases due to improved availability of light (Gosselin, 1997). Biological processes are important to consider due to their strong direct effects on seawater chemistry (Redfield, et al., 1963). In the context of this research, biological activity at and near the surface of the euphotic zone[2] is of particular interest (Longhurst 1991; Rivkin and Legendre, 2001; Sarmiento and Orr, 1991). The sum of the biological carbon transport away from this surface zone is called the biological pump. Two primary biological C pumps can be distinguished at the sea surface: the organic carbon portion of this transport is known as the soft tissues pump, while the inorganic carbon portion is known as the hard tissues pump (Stoll, 1996; Raven, 1999; Millero, 2002). Hard tissue is composed primarily of calcareous shells or skeletons. For example, calcification occurs when a marine organism combines calcium with bicarbonate ions to make hard tissue (for example Eq. 5.1). Eventually these hard tissues sink dissolve, either in the water column or in the sediments. In seawater, primary producers consume CO_2, producing O_2, while consumers work in opposition, consuming the O_2 and producing CO_2.

The flux of C downwards from the surface seawater creates a CO_2 sink for the surface ocean in which each of the carbon pumps take part. Under these normal

[2] Euphotic, or photic, zone is the depth in a body of water that is exposed to sufficient sunlight for photosynthesis to occur.

conditions, the influences of the biological C pump on CO_2 levels, and thus on plants and animals in the sea, primarily affect the alkalinity and pH of seawater. The process of photosynthesis cannot be defined as a source or sink process for carbon. Though photosynthesis fixes CO_2 into more complex forms, the active surface layer of the ocean allows the C to remain in play as other organisms utilize the organic and inorganic C for metabolic purposes.

As sea ice growth continues through the dead of winter, months of darkness contribute to preventing photosynthesis from occurring, minimizing primary production. Respiration is the main biological activity converting organic C to inorganic C. The principle forms of surface water biological activity are heterotrophic species such as bacteria and zooplankton. Without photosynthesis to control metabolic C outputs, supersaturation of CO_2 in the surface layer below the sea ice would be expected and has been measured (Kelley, 1968; Semiletov et al., 2004; Delille et al., 2007); yet, supersaturation is not always present. Supersaturation is alleviated in part because biological conversion of C as organic matter influences levels of DIC and A_T. Respiratory C oxidation causes DIC to increase, and A_T to decrease slightly, due to oxidation of nutrients phosphorus (P) and nitrogen (N). Carbon species variation within the ocean occurs mainly due to these two biological processes (Lee, 2001; Rivkin and Legendre, 2001). CO_2 may be removed by downward or upward transport. The deepening of the mixed layer can spread CO_2 rich surface waters over a greater depth. These transport processes need to be further addressed by investigating the role of sea ice as an impediment or conveyor of C transport in the Polar Marine environment.

Through shifts in the equilibrium states of Equations 2.1 and 2.3, surface seawater pH can be altered, changing the conditions under which the biological pump functions. The physical and chemical pumping of CO_2 across the ocean-atmosphere interface is driven by the ΔpCO_2 resulting from changes in atmospheric pCO_2. The present increase in atmospheric CO_2 concentrations will inevitably modify the seawater carbonate chemistry when the surface ocean takes up more CO_2 (Revell and Seuss, 1957). As atmospheric CO_2 grows, so does the dissolved CO_2 content of surface seawater changing carbonate concentrations, as illustrated by Equations 2.1, 2.3, and 2.5. Instability of

$CO_{2(g)}$ and CO_3^{2-} in seawater cause Equation 2.3 to shift toward HCO_3^-. The net effect of adding CO_2 is a reaction with CO_3^{2-} to form HCO_3^- (IPCC, 2001). Most of the added CO_2 ends up as HCO_3^-; however, as the available CO_3^{2-} is used up leaving less to react with further CO_2 additions. CO_2 added after the carbonate saturation point remains $CO_{2(aq)}$. In other words, further CO_2 uptake will reduce the overall ability of surface seawater to take up CO_2.

2.4.4 Calculating Fluxes

Although no accurate method has been developed to measure CO_2 fluxes within sea ice to date, the eddy correlation system is showing promise in this area (Papakyriakou, 2004; Zemmelink, 2006). This method has shown that a carbon flux between the atmosphere and surface ice is occurring in the Arctic.

Measuring the seawater components of Equations 2.1, 2.3, and 2.5 along with atmospheric $pCO_{2(g)}$ can lead to determining short term direction of fluxes across the air-sea interface and to understanding fluxes at various stages of the C cycle. Determining degree of seawater CO_2 saturation in comparison to the atmosphere can indicate a finite position of the C cycle. Knowing the existence of CO_2 gas on both sides of the atmosphere-seawater boundary is not enough to indicate transport. It is also necessary to know the difference between atmospheric $pCO_{2(g)}$ and seawater $pCO_{2(aq)}$ (or $\Delta\, pCO_2$). Determining this value over time gives us CO_2 direction. The best estimates of CO_2 flux (FCO_2) across the ocean-atmosphere interface are computed from the gas-exchange flux equation (Liss 1983a, b; Liss and Merlivat, 1986; Etcheto and Merlivat, 1988; Tans *et al*., 1990; Landrum *et al*., 1996) using gas transfer velocity ($cm \cdot h^{-1}$), solubility of the gas in seawater as $mol \cdot l^{-1} \cdot atm^{-1}$, and the difference between the oceanic and atmospheric pCO_2 (ΔpCO_2). Detailed discussion of this work is beyond the scope of this project. For further discussions, refer to work performed by Wanninkhof (1992), Liss and Merlivat (1986).

Until such work as Gosink et al. (1976), Papakyriakou et al. (2004), Semiletov et al. (2006), Zemmelink et al. (2006), and Delille et al. (2007), it has been assumed that sea ice prevents the exchange of gas between the atmosphere and the ocean. The above literature review, combined with results of recent research (Papadimitriou et al., 2003;

Zemmelink et al., 2006; Delille et al., 2007), challenges this assumption. In particular, brine has been shown to move vertically within the sea ice, exiting into the seawater (Assur, 1960; Cox and Weeks, 1975; Cox and Weeks, 1983; Gleitz et al., 1995; Eicken, 1998). Brine has also been shown to have the capability to hold large volumes of gas (Kelley and Gosink, 1979; Cox and Weeks, 1983; Gleitz et al., 1995; Papadimitriou et al., 2003; Delille et al., 2007). In theory, brine can be supersaturated with CO_2 with respect to air upon the freezing of seawater. Laboratory trials performed by Papadimitriou et al. (2003) found the $[CO_{2(aq)}]$ showed sea ice brine to be close to the saturation level with the atmosphere. In the same experiment, the underlying seawater $[CO_{2(aq)}]$ was well below saturation levels until the end of the experiment, when the sea ice was thickest. Therefore, sea ice may play an important role in the global carbon cycle. This project attempts to contribute to a greater understanding of this role, and in particular, the role of FYI in the exchange of carbon between the atmosphere and the Arctic Ocean. The next chapter describes the project methodology.

CHAPTER 3: METHODS

This chapter provides a description of the *in-situ* measurement of pCO_2 in FYI. Section 3.1 gives an overview of the field site. Section 3.2 describes the physical and chemical sample collection; the custom in-ice gas-sampler design and deployment (3.2.1); sea ice and seawater sample collection for alkalinity (A_T) and related attributes (3.2.2), and a description of the micrometeorological data collection for basic MET and carbon flux specific attributes (3.2.3). Section 3.3 outlines laboratory analysis methods for gas chromatography (3.3.1) and aquatic chemistry (3.3.2). Section 3.3.3 describes computations used in Chapters 4 and 5, both in the data presentation and the discussion.

3.1 General Description of Field Activities and Site Description

This project was undertaken as part of the Canadian Arctic Shelf Exchange Study (CASES). The CASES study region was at the southwest corner of the Canadian Archipelago just north Canada's mainland coast. The CASES study region extended from 136°W to 121°W longitude and 69.5°N to 72°N latitude, with the stationary phase located at 126.30°W, 70.03°N (Figure 3.1). The region is bounded to the south by the 20 m isobath, the minimum depth of water the research ship *C.C.G.S. Amundsen* could safely navigate.

The geographic focus of this study is Franklin Bay, and it has elements of the interior continental climate of the Canadian mainland and archipelago to the south and northeast, and the polar marine climate of the Beaufort Sea to the northwest. The continental climate has severe winters with low amounts of precipitation. The maritime climate conditions differ from the continental climate, which prevail over the Arctic Ocean, coastal Alaska, Iceland, northern Norway and adjoining parts of Russia. The ocean significantly influences these areas. Winters are cold and stormy, while summers are cloudy but mild with mean temperatures about 10°C. Annual precipitation is generally much higher than in continental regions, with a cool season maximum and a snow cover when sea ice exists. The region is subject to seasonal insolation and the ocean's surface remains at or near freezing year round (Serreze et al., 1997; Andreas et

al., 2002). This unique and extreme environment leads to unique ecology, of which little is known due to logistical difficulties of researching such environment.

The CASES experiment consisted of two distinct sampling periods, mobile and over-wintering (ice camp). The ship was frozen in on December 5, 2003 and resumed the mobile sampling on June 2. During the ice camp phase, the ship was frozen into sea ice within Franklin Bay, NT (Figure 3.1). In the mobile phase, distributed sampling was undertaken throughout the Cape Bathurst flaw lead polynya system and Mackenzie shelf. Sampling was conducted from onboard *C.C.G.S. Amundsen* during fall of 2003 and spring and summer of 2004.

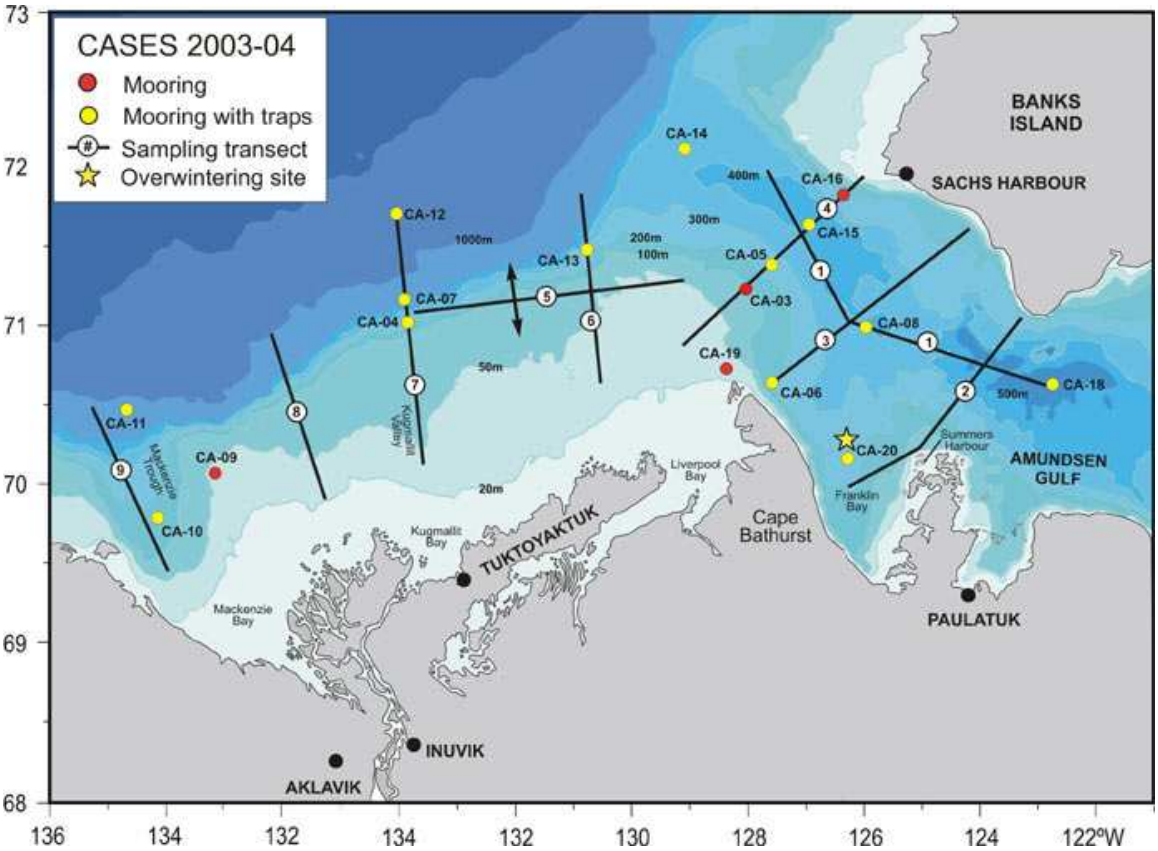

Figure 3.1: Map of the CASES, 2003-2004 region including ice station, ship transects and moorings locations. Adapted from CASES, 2004 data report.

At the ice camp, several areas were designated for different sampling activities to minimize disturbance on the experimental set-ups (Figure 3.2). Area C1, approximately 125 m ESE of the ship, was designated for gas chamber sampling and was equipped with

temperature sensors arranged in profile through the snow and sea ice. Specifics regarding the temperature sensors appear in Chapter 3.2.3.2. Area E was located approximately 350 m E of the ship, and consisted of a single hole in the sea ice where water sampling took place throughout the winter. Area F was located approximately 1320 m east of the ship and was designated for sampling snow and ice. Surface meteorology and flux measurements were made within Area G, located 220 m south of Area F. Between Area F and G was Area C2, a second location for sea ice gas sampling. Site locations are summarized in Table 3.1.

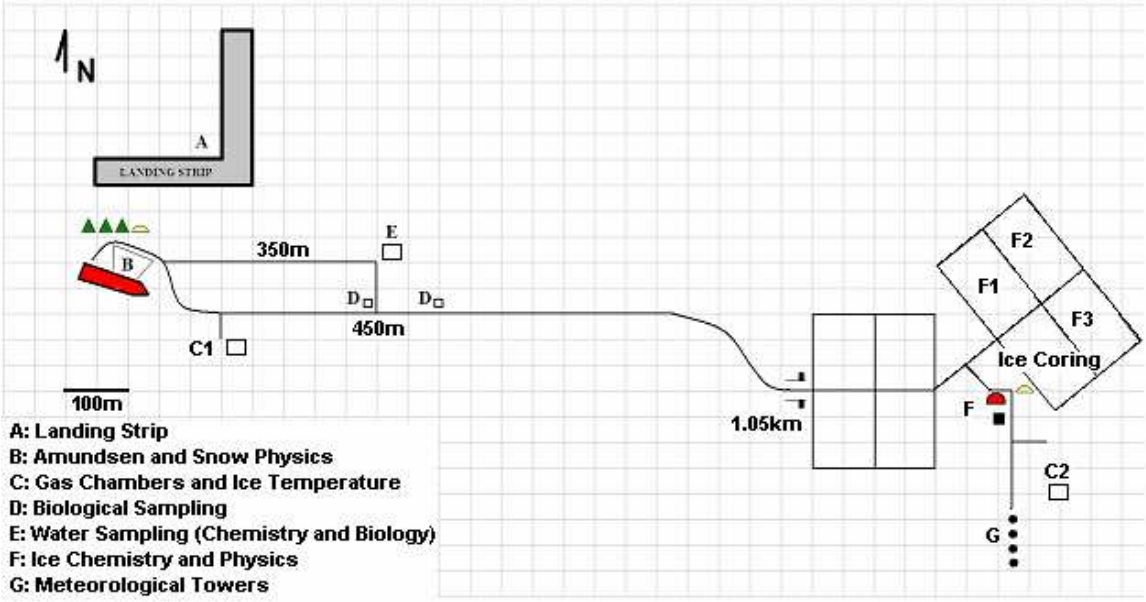

Figure 3.2: Map detailing the location of winter sampling sites with respect to the orientation of the C.C.G.S. Amundsen at the CASES over wintering site. Adapted from the CASES 2004 project.

On December 02, 2005, the ship was frozen into a pan of growing sea ice of uniform consolidation. The ice pan was approximately 3 to 4 km in diameter with the *C.C.G.S. Amundsen* positioned approximately in its centre. The sea ice surrounding the ship was 48 cm thick on 05 December 2003 and grew to 210 cm by 31 May 2004. Sampling at all sites occurred on the same pan of sea ice that ranged in thickness from approximately 70 to 205 cm. The maximum ice pan thickness observed was 220 cm, recorded in May. Snow cover was hard-packed and ranged from 2 to 10 cm on the date of site installations.

Table 3.1: Summary of the project activities and instruments locations.

Location		Distance	Activity(s)	Instruments
B	Ship	Origin	Laboratory	GC, $A_{(T)}$
C1	In-sea ice gas chambers	125 m ESE of ship	Collection of sea ice & atmospheric pCO_2;	Si chambers;
C2		150 m S of Area F		
E	Seawater sampling	400 m E of ship	Collection of seawater profiles for DIC and $A_{(T)}$	Kemmerer bottle; aquarium pump; Si chambers
F1	Ice chemistry	1320 m E of ship	Collection of: sea ice cores; ice temperature profiles; ice thickness	Kovacs core barrel; handheld temperature probe; measuring tape
G	Meteorological towers	220 m S of Area F	All meteorological data collection, including gas, energy, momentum fluxes	Air temperature, PAR, ice temperature

3.2 Sample Collection for Sea Ice and Seawater Chemistry and Micrometeorology

Vertical pCO_2 profiles were measured with a series of point samplers during growth and melt onset of sea ice during the over-wintering portion of the experiment.

3.2.1 pCO_2 Sampler Design and Deployment – Peepers

Traditionally, measurements of sea ice properties require that cores be extracted, sectioned and melted introducing contamination by new gases and an altered chemical state. Such destructive sea ice sampling was undertaken and is described in Section 3.2.2. In soil research, a similar problem has been overcome by the use of diffusion bags, or porous membranes, to form an isolated chamber from which a sample can be withdrawn (Hesslein, 1976). The diffusion bag method was adapted and used from procedures outlined by Kammann et al., (2001) for deployment in Arctic sea ice in this study. This method is appropriate because it allows an exchange of CO_2 between water and atmosphere within the porous Arctic ice (Untersteiner, 1968; Frere, 1975; Cox and Weeks, 1982; Wagenet, 1984; Wagenet and Hutson, 1989; Golden, 1998; Eicken, 2003). The Si chamber is more robust than the diffusion bags, a major advantage in this harsh

environment. The components of the devices used for non-destructively collecting gas for this project are listed in Appendix A.1. The sampling instrument consisted of two parts: silicone (Si) chambers to collect samples and a housing unit for deployment.

The Si chamber sample receptacle is shown in Figure 3.3. Here, the Si chambers consisted of 20.0 cm lengths of Si tubing[3]; outside diameter 13.4 mm, inside diameter 12.4 mm with a chamber wall of 2.0 mm. The tubes were capped with Si stoppers, and the stoppers occupied 1.5 cm at each end of the 20.0 cm tube section. The Si membrane is porous to small gas molecules including CH_4, CO_2, and N_2O, but is impermeable to water molecules ($H_2O_{(g)}$), making it suitable for the purposes of this project. The Si membrane allowed passive diffusion along a concentration gradient between the interior and the exterior of the chamber. Diffusion allowed the air space within the silicone tube to approach an equilibrium level with the surrounding sea ice.

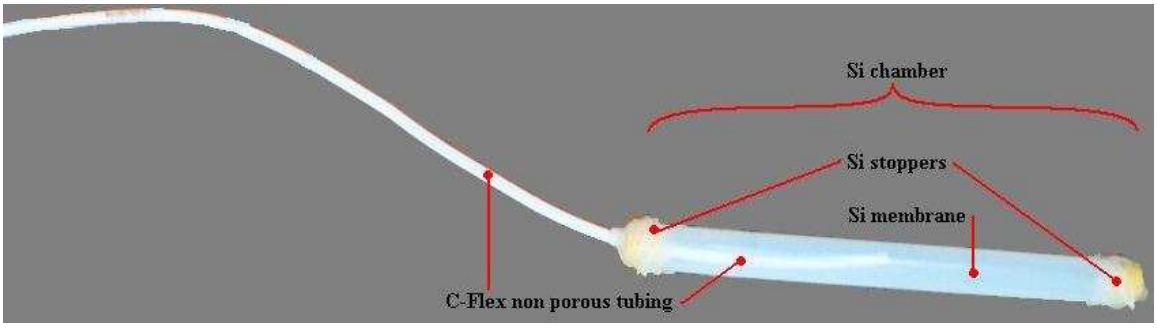

Figure 3.3: Si chamber components prior to installation in PVC tube (Figure 3.4): Si membrane tube, Si stoppers, C-Flex® tube, Si sealant.

A hole was punched in the stopper at one end of the chamber for inserting a narrow, non-diffusive artery (C-Flex®[4] tube) that extended from the chamber, through the sea ice or water to the surface. The C-Flex® tube length exceeded the depth at which each chamber was to be placed by 60cm. The chamber end of the C-Flex® tube was inserted half way into the Si chamber to allow for proper mixing during sample collection. The C-Flex® tube linked the Si chamber to the ice surface and was capped at the surface with a two-way stopcock in order to isolate the air in the chamber from the

[3] Cole-Parmer Si tubing; Tygon® 3360 silicone, platinum cured. Manufactured in Valley Forge, Pennsylvania, USA.

[4] Podisco, Inc.; Wilmington, North Carolina, USA.

outer atmosphere during inter-sampling periods. Membrane sampling ports were appropriately labelled for surface identification.

The housing unit was PVC tubing, 135 cm long by 4.08 cm outside diameter, separated into 20.0 cm long sections alternating between areas which exposed the inner chambers to the external environment (ice and water) and sections which prevented such exposure. The exposed sections consisted of twelve 20.0 cm long by 1.5 cm wide rectangular windows cut out of each PVC cylinder, four at each exposed depth. Each PVC tube supported three Si chambers to create a gas profile probe (Figure 3.4). The Si chambers were placed vertically in the exposed sections of the PVC cylinder (Figure 3.4) at predetermined heights for permanent placement at: 20 to 40 cm (depth 1; D1), 60 to 80 cm (depth 2; D2), and at 100 to 120 cm (depth 3; D3).

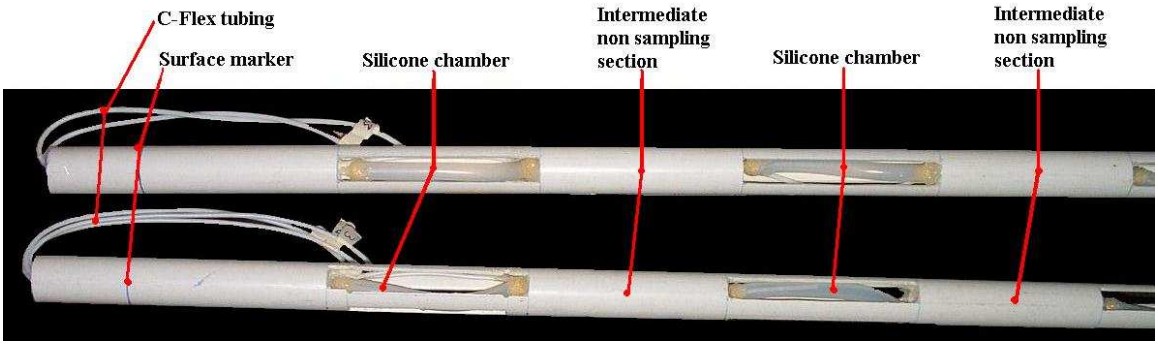

Figure 3.4: Constructed Si chamber sampling array with three Si chambers, a 130cm by 5cm PVC tube, and Great Stuff™ foam.

The non-exposed sections were non-sampling sections. Foam (Great Stuff™ [5]) filled the non-exposed sections to fix the Si chambers in place, add structural stability, and prevent vertical flow of ice and water and their constituents. The non-diffusive insulating foam filled the interior of the non-sampling zone, anchoring the position of the non-diffusive 0.3175 cm ID C-Flex® artery and, subsequently, the Si chamber. Care was taken to keep the Si chamber hanging free in the open section of the PVC tube. Rubber stoppers were used to plug both ends of the PVC tube to further prevent vertical movement of environmental constituents. The top stopper had a hole to allow the C-Flex® tubing through which samples were collected to exit the top of the sampling array.

[5] Dow Chemical; Marietta GA, USA.

3.2.1.1 Sea Ice pCO_2 Sampler Deployment

Six gas samplers were installed; three gas samplers at both sites C1 and C2 (location described in Chapter 3.3.1 and apparatus described in Chapter 3.2.1) with each site designated for day sampling and night sampling respectively. The gas samplers were inserted into 60 to 70 cm thick new ice prior to December 19, 2003. At the beginning of the season, the upper gas sampler was surrounded by sea ice and the lower two gas samplers were immersed in ocean surface water. The middle depth was covered in ice by the time sampling began, January 9, 2004. Each sampler is believed to have been completely enclosed in sea ice by mid-February, 2004. Gas was drawn from the probes roughly every second day to once a week by syringe through the C-Flex® tubing and immediately injected into evacuated 10 ml vials for analysis on a gas chromatograph (GC).

Repairs and redeployment were necessary because of damage to the units by foxes. Discovery of damages to samplers occurred December 28, followed by removal of all units the two following days. The sampling ports required reconstruction and 6L buckets were anchored to the ice surface over the exposed surface access ports for protection. The buckets were thoroughly perforated to allow airflow while acting as a protective cage and easily removable for sampling. Ice gas samplers were redeployed January 6th, 2004. After several months of operation, the seal between the Si chamber and the surface access port would break, and water would begin to enter the chamber preventing sample collection in these cases.

3.2.1.2 Sea Ice pCO_2 Sample Collection

Silicone tubing used to make chambers (peepers) by Kammann et al. (2001) had 3.0 mm thick walls and required approximately 2.9 hours (h) to achieve equilibrium with $CO_{2(g)}$ at 20°C. Holter (1990) used Si tubing of 1 mm wall thickness, at 22°C, and measured times of 0.7 h for CO_2 to reach 95% equilibrium. Increasing time to allow equilibrium did not improve the equilibrium conditions in both studies. Assuming a linear relationship between Si wall thickness and time to reach equilibrium, the 2.0 mm thick walls used in this experiment would need less than 2.4 hours for CO_2 inside the chamber to reach equilibrium with the environment outside the chamber at 20°C. The conditions used in this experiment meant the Si chambers were subject to temperatures

between -1°C and -21°C. Jacinthe & Dick (1996) report that N_2O took 2.5 times longer to reach equilibrium when the temperature was reduced by 10°C with Si chamber wall thickness of 2.4 mm. If I use the estimate of +2.5 times the length of time to reach equilibrium for N_2O every 10°C decrease, for a chamber in a CO_2 environment to reach equilibrium at 0°C would take 11.8 h; and 23.6 h at -20°C. These times of course are estimates.

Samples were taken every two to six days over a 120 day period that extended from January 9 to May 28, 2004. Collection occurred early in the morning from the gas chambers at site C2 (approximately 0900h, or roughly sunrise) to gather samples characteristic of the gas environment of the previous night. These samples are referred to as nighttime (NT). Late afternoon sampling occurred at approximately 1800 h (around sunset) from the gas chambers at site C1 to capture samples characteristic of daytime (DT) gas concentrations. Atmospheric conditions, such as air temperature, wind speed, direction and existence of precipitation were recorded at the time of measurement (Chapter 3.2.3).

The luer locks on both the syringe and Si chambers remained closed, except during the sample acquisition. Prior to sampling, the luer lock valve and C-Flex® line were inspected for the presence of snow or water and to ensure that they were undamaged. The presence of snow was a minor issue, as it blocked the closed stopcock. Simply blowing into the stopcock would effectively remove the snow, allowing sample withdrawal. Si chambers began to fail allowing seawater into the chamber. By May 30, 2004, when the ice-bound portion of the experiment was terminated, five chambers had failed. Air samples that could be extracted from these chambers were processed for $CO_{2(g)}$ concentration.

On sampling days (see sampling schedule in Appendix A.2), one sample was drawn from each of the three depths in each Si chamber probe and a fourth gas sample was collected by syringe from the atmosphere. To take a sample from the Si chamber, the luer on the syringe and Si chamber were connected. Both luers were opened and the syringe was pumped lightly three times to promote mixing within the chamber. A sample was then drawn into the syringe. Typically, 10 to 30 ml of gas would be drawn into the syringe. Both luer locks were then locked and separated. The cap was replaced on the

luer on the Si chamber port and a needle was attached to the luer on the syringe. The sample was then inserted through the septum of evacuated vials (Exetainer[TM6]). Refer to Chapter 3.3.1.2 for details regarding vial preparation. The entire sample was extricated out of the syringe into the vial. Confirmation that the vial had been properly evacuated was obtained by observing depression of the syringe plunger under the negative pressure within the vial. This extraction process was repeated for each depth of each sampling array. The atmospheric sample was taken at chest height while the operator held his/her breath and faced into the wind. Gas samples collected were analysed for CO_2 between 0 to 38 days after the collection. On average, the samples were analyzed within a week of collection. I did explore the stability of the samples by taking replicates, and running the replicates over varying lengths of time after sampling. I found that on average, the pCO_2 within the Exetainer decreased from elevated values by 0.9 to 2.2 ppmv CO_2/day over a period of greater than 100 days for samples with greater than 1000 ppmv CO_2. Since most samples were analyszed within a short time, and those samples most affected by the change in CO_2 concentration were samples with high pCO_2, the overall affect was small. For example, a sample stored for up to 38 days would see a maximum decrease of 84 ppmv CO_2. All samples were analyzed using a portable SRI 8610B gas chromatograph and procedures are described in Chapter 3.3.1.

3.2.2 Sea Ice and Seawater Chemistry

Seawater and sea ice sampling for A_T and salinity accompanied the measurement of the pCO_2 profiles. The sea ice chemistry component of the experiment took place during the ice camp study in Franklin Bay, and occurred between 10 December 2003 and 30 May 2004. Three sea ice cores were collected on a weekly basis, while seawater samples were collected roughly on a six-day cycle (sampling schedule Appendix A2) throughout the CASES project. The water sampling frequency was increased to every three days in mid-May with the onset of spring. The units and other details of analysis procedures are summarized in Table 3.2 and described in Chapter 3.4.

[6] Exetainer® of Labco Limited; Buckinghamshire, United Kingdom.

Table 3.2: Variables monitored in support of gas analysis.

Variable	Units	Description	Placement
[1]CO_2 concentration	ppm	NA	Surface atmosphere: 1m; Sea ice: 20-40 cm, 60-80 cm, 100-120 cm; Seawater: (calc.) 0.5, 2.5, 3.0, 4.5, 10 m
[2]Salinity	PSS	Measured from melted ice cores and sea water	Sea ice: 10cm sections from the surface; (Except Feb. 22: ice cut into 15 cm sections) Seawater (m): 0.5, 2.5, 3.0, 4.5, 10
[2]Alkalinty	µmol/ kg $CaCO_3$		
[2]Ice temperature	°C	Embedded thermocouple	(cm) 0, 5, 10, 15, 20, 30, 40, 50, 60, 70, 100
[3]Air temperature	°C	Embedded thermocouple	1.6 m above ice surface
[3]Photosynthetically active radiation	µmol m^2 s^{-1}	PAR	Flush with ice surface, below snow; 0 cm from ice surface

[1] Direct sampling for sea ice CO_2 gas concentration determination.
[2] Associated chemistry data is available for data interpretation. See Appendix D.
[3] Related meteorological data is available for data interpretation. See Appendix D.

3.2.2.1 Collection of Sea Ice for Chemical and Physical Attributes Analysis

Ice core samples were extracted from area E (Figure 3.2) starting on December 10th, 2003. From January 23, 2004 to May 30, 2004 ice core sampling occurred in area F1 (Figure 3.2) on a weekly basis for coincident ice physical and chemical analysis. Ice cores were brought to the ship for chemical analyses, which are described in Chapter 3.3.2. Core collection and sample analysis was typically performed by the same team of scientists. A corer (Kovacs[7] Mark II coring system) was used for ice sample collection. Cores were extracted in triplicate, and two of the three ice cores were cut into 10 cm sections, starting from the ice surface. If the lowest section were less than 5 cm, the final two sections would be divided evenly in two, creating two bottom sections of equal length, and were less than 10 cm each. The ice core sections were stored in 2 L Nalgene buckets and returned to the carbon chemistry lab onboard the Amundsen. Salinity (pss) and A_T (umol/kg) were measured each on one set of melted core sections (refer to Chapter 3.3.2.1 and 3.3.2.2, respectively). From February to May, some cores were used for DIC analysis. To prepare a collected core properly for DIC analysis, the ice puck was

placed into a plastic bag. Before sealing the bag, the air was pressed out and analysis conducted as described in Chapter 3.3.2.3. The measurement of ice temperature (˚C) was performed immediately following the core extraction. A hand drill and temperature probe was used for this purpose. Two individuals normally participated in sampling: one to drill holes in the core at 5 cm intervals and the other to insert the temperature probe into a hole to collect the temperature data from the liberated core. Generally, the temperature measurements were completed within 3 minutes after core extraction. When the ice was thicker than 90 cm, the top piece was measured first allowing the lower section to remain in place until processing.

3.2.2.2 Collection of Seawater for Chemical and Physical Attributes Analysis

Seawater samples were collected throughout the ice camp phase of the experiment at sampling site E (Figure 3.2). Site E was a small 20 to 100 cm diameter hole in the ice that was kept clear of ice throughout the experiment. A shed constructed with 2" X 4" pieces of wood and enclosed with thick plastic and placed over the hole approximately January 20, 2004 to assist the workers during sampling. Surface water pCO_2 samples were collected through this hole with a small salt-water aquarium pump, or Kemmerer bottle at 3 m, 5 m and 10 m from the ice surface. The procedure followed standard sampling practises (DOE, 1994; Almgren et al., 1983) for DIC, A_T and salinity samples with some modification owing to the ice cover as follows:

- A Kemmerer bottle, Nisken bottle or pump was lowered through the ice to 3 m, 5 m or 10 m depths from the ice surface. When at depth, the Kemmerer or Nisken was tripped, or pump turned on;
- A 25 cm Tygon® tube attached to the Kemmerer spigot or the water pump was used to introduce water to clean DIC/A_T and salinity glass bottles;
- Once the Tygon® was free of air bubbles, first the DIC/A_T glass bottles were filled slowly, with one bottle overflow as a rinse;
- Second, clean bottles for salinity samples were rinsed three times with seawater from the sample collector, filled and capped.
- DIC/A_T samples were poisoned with 200 µL saturated $HgCl_2$;

---

[7] Kovacs Enterprises, Inc.; Lebanon, New Hampshire, USA.

- DIC/A_T samples were capped with a greased glass stopper and clamped rubber band.
- DIC/A_T samples were stored in the onboard laboratory refrigerator until analysis 1 day to several months after collection.

When possible, samples for DIC and A_T analysis were collected in triplicate. Seawater salinity samples were analysed onboard by the CTD operator. When possible, salinity and pH samples were collected from the same Kemmerer bottle that supplied the DIC/A_T samples. The DIC, salinity, and A_T samples were analyzed onboard the ship.

3.2.3 Micrometeorology; Surface Radiation, Temperature and Exchanges of CO_2

Two guyed lattice masts, maintained by researchers from the University of Manitoba, were equipped to continuously record the components of the heat and radiation budget and atmospheric CO_2 flux (Table 3.2). The taller of the two towers (Flux Tower 1, 5 m) held equipment associated with the measurement of the CO_2 flux and heat flux (see Figure 3.5), while radiometers were deployed on the other tower (Tower 2, 2.5 m in height) to monitor the components of the radiation balance. Power to the sites was supplied by a 10 kW diesel generator that was positioned 200 m north of the instrumented towers and ran continuously during the ice camp campaign. Table 3.3 summarizes the coordinates of the towers and main reference objects and Table 3.4 shows distances and directions calculated from GPS locations. Meteorological and climatological variables of interest to this study include ice and air temperature (˚C), incident radiation in the photosynthetically active portion of the spectrum (PAR: 400 to 700 nm), and atmospheric CO_2 (ppm). Instrumentation, location, and data collection attributes are summarized in Table 3.5.

Table 3.3: Geographical locations of the CCGS *Amundsen* and meteorological towers of University of Manitoba during the ice-camp phase.

Point	Latitude	Longitude	Notes
AMUNDSEN	N 70.04553	W 126.30098	from ship GPS
Flux Tower 1 (UofM)	N 70.04193	W 126.26490	Tower 2 was 10 m NNE
Parcol	N 70.04392	W 126.26455	Shelter

Table 3.4: Distances based on GPS locations from the ship.

End Points	Distance (m)	Bearing (degree true)
AMUNDSEN - Parcol	1320	097
Parcol - Flux Tower 1 (UofM)	223	180

Table 3.5: Parameters monitored in association with the heat budget and radiation tower.

a) Atmospheric sensors

Variable measured	Sensor Manufacturer (model)	Height from ice (m)	Scan Rate (Hz)	Averaging Periods
Temperature and relative humidity	Vaisala (model HMP45C)	1.6, 5.12	0.3	1 hr
PAR irradiance	LI-COR® quantum sensor (LI-190)	~ 2.2	0.3	1 hr
Surface Temperature	Everest® IR Transducer (Model 4000.4 GL)	~ 2.2	0.3	1 hr
Wind Fluctuations	Ultrasonic anemometer (Campbell Scientific model CSAT3)	4.36	10	1 hr
CO_2 and H_2O concentration	Open path IRGA LI-COR® (model LICOR LI-7500)	4.36	10	1 hr

b) Snow and sea ice

Variable measured	Sensor Manufacturer (model)	Position relative to ice surface	Scan Rate	Averaging Periods
Snow temperature	Thermocouple sensors (24 awg – type T)	15 sensor at 1.5 cm increments starting at 0.5 cm	0.3 Hz	1 hr
Ice temperature	Thermocouple sensors (24 awg – type T)	-1 cm,-5,-10,-15,-20,-30,-40,-50,-60,-70,-80,-100	0.3 Hz	1 hr
PAR transmission (through snow)	LI-COR® quantum sensor (LI-192)	0 cm; under ~8 cm snow	0.3 Hz	1 hr

3.2.3.1 Surface Irradiance

Incident PAR was measured at site G at the ice surface with the sensor pointing vertically upwards beneath the snow cover. Sensor type and manufacturer are listed in Table 3.5. Sensor output was scanned at 3 second increments and stored as 10-minute averages by a Campbell Scientific (model 21X) data logger. Data are available from January 23 to May 25. The sensor was installed approximately 10 m E of the radiation tower (between the photographer and tower in Figure 3.5). Snow thickness (in cm) was observed alongside the heat exchange tower. A wooden dowel with a measuring tape attached was frozen into the sea ice surface with the zero point of the dowel at the ice surface. Data was collected during routine maintenance visits once every one to three days and after snow and wind events. Calculations for the estimation of solar irradiance at various depths within the sea ice are outlined in detail in Chapter 3.3.3.1.

3.2.3.2 Surface Heat and Momentum Budget

The sensors on the heat and carbon flux tower are summarized in Table 3.5. Two categories of sensors were in place: 1) basic meteorology and 2) CO_2 and H_2O flux. Variables associated with the basic meteorology were scanned at 3 s increments by a Campbell Scientific[8] 10x data logger and archived as 15 minute averages. Temperature-relative humidity sensors were oriented to the north, while anemometers faced south. The offset for the zeroing of the wind vane (on top of the tower) was –16.7°. Data are available from Jan 22 to May 25.

[8] Campbell Scientific 10X data logger; Logan, Utah, USA.

Figure 3.5: The 5m heat budget tower south of Takatuk.

Ice temperature was continually measured with one thermocouple rod at 10 locations (Table 3.5.b) extending from the ice surface to 1.0 m depth from the surface by thermocouple sensors (24 AWG, Type T) embedded into a 4.08 cm OD PVC tube. The sensor junctions were embedded in high conductivity epoxy and inserted into PVC plugs, which were in turn inserted into the PVC tubing. The plugs were inserted far enough so that the sensor tips were flush against the ice wall.

Atmospheric CO_2 concentration was continuously measured as part of the eddy correlation system mounted at 4.35 m on the heat budget tower (Fig. 3.6) and was oriented 190° from north. The system consisted of an open-path gas analyzer (LI-COR

model LI-7500) and an ultra sonic anemometer (Campbell Scientific, model CSAT3). Eddy correlation estimates of the atmospheric CO_2 flux were derived using the data collected. The flux sensors were scanned by a data logger (Campbell Scientific model CR23X) at 10 Hz. The raw high frequency data was transmitted to the *C.C.G.S. Amundsen* by RF telemetry at ten minute intervals and archived on a PC. The radio frequency transmitter was maintained above its threshold temperature of –25° by a 60 W light bulb located within the logger enclosure.

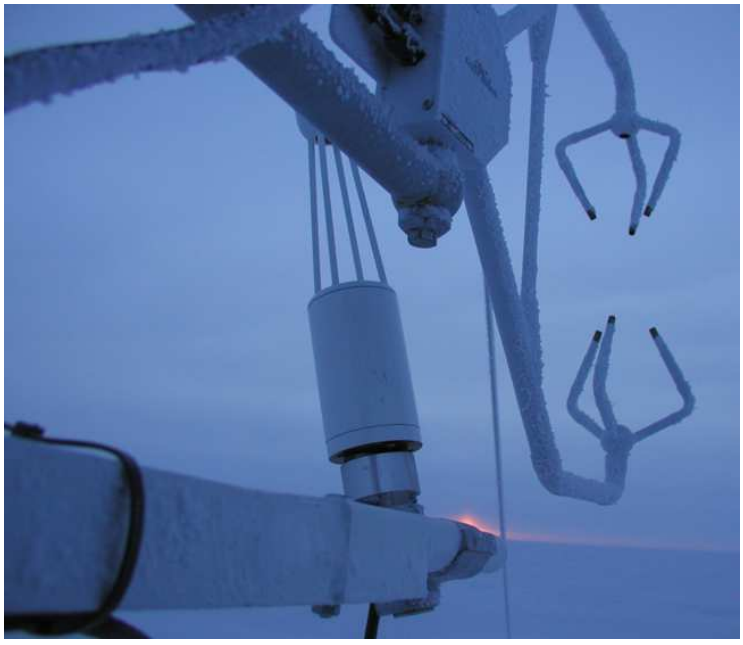

Figure 3.6: The eddy correlation system on the heat budget tower. CSAT3 (sonic anemometer) and LI7500 (CO_2 and H_20 gas analyzer).

The data output from the LI7500 included hourly averages of atmospheric CO_2 content and of CO_2 flux (FCO_2) determination. From the CO_2 hourly flux determination, a long-term calculation of FCO_2 was performed, described in 3.3.3. The flux of the measurement period was derived from system logs of the average CO_2 g/m^2/s over a period of interest.

3.3 Laboratory Analysis

Analyses were performed to determine two different forms of inorganic carbon content in sea ice. Gas chromatography (Chapter 3.4.1) was used to process the air samples extracted from Si chamber samplers for internal CO_2 concentration, while melted bulk ice samples were analyzed for A_T to determine dissolved carbonates (Chapter 3.4.2).

3.3.1 Gas Chromatography and Instrumentation

Gas samples associated with the peepers were analyzed by gas chromatography (SRI 8610B GC[9] - Figure 3.7). The portable SRI 8610B GC was equipped with a thermal conductivity detector (TCD). A TCD responds to flow of partitioned gas samples, each with different cooling abilities, cooling the heated filament as the sample flows over its surface by changing temperature. It is important that the filament heating and sample flow remain constant (Walker *et al.,* 1977). The TCD was set at 100°C and the GC oven temperature was set at 40°C. Concentrations are calculated with the integrated area under the curve corresponding to the system's CO_2 retention time (t_R). The instrument was accessed using PeakSimple 3D[10] software and the results from each analysis were presented in a graph showing separated substances (O_2, H_2O and CO_2, etc.). PeakSimple 3D software was used for curve interpretation and integration. The product also allowed post-analysis of the initial results, discussed further in Chapter 5. Appendix A.4 lists equipment required for the gas sample analysis. The gas chromatograph (GC) was calibrated daily throughout most of this process. Frequently, a standard sample was analyzed in duplicate at the end of analysis to detect instrument drift. The estimated error for the gas analysis is +/-40 ppmv CO_2, based on standard analysis throughout the project (Appendix B).

---

[9] SRI Instruments 8610B; Torrance California, USA.

[10] PeakSimple 3D software, supplied by SRI Instruments, Torrance, California, USA.

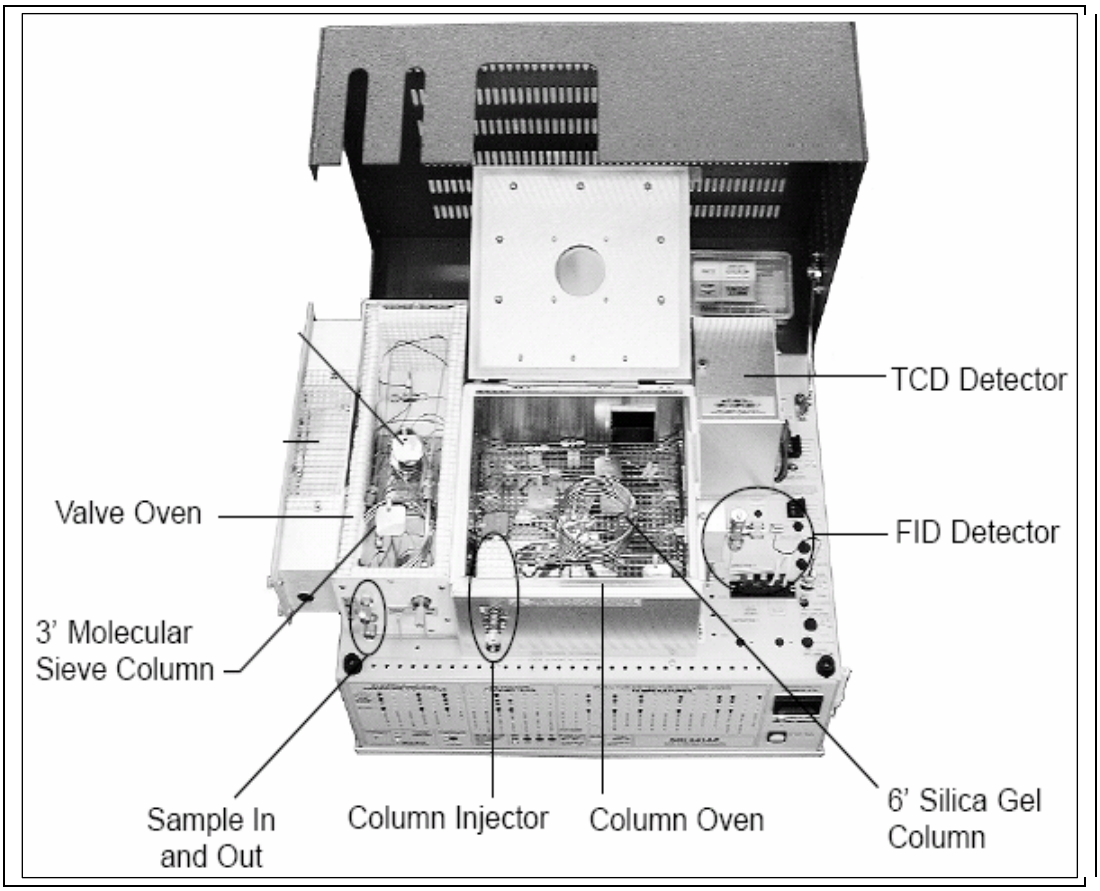

Figure 3.7: The SRInstruments 8610 line of GCs. The instrument used was slightly modified from this photo to accommodate a valve system for introducing gas samples to the GC column.

Helium (He) was used as the carrier gas and appropriate flow through the GC was confirmed and moderated with a flow meter. The He carrier gas remained on throughout the CASES experiment to protect the sensitive interior of the GC from over-saturation of non-exhausted sample molecules on the detector. The flow of He through the GC also allowed connections to be checked for leaks with a He gas detector. Figure 3.8 illustrates the path taken by a sample through the GC from injection to the data readout. The GC would be arranged as in Figure 3.8.A when the sample was being inserted in the injection port. Notice the gas goes in one end of the sample loop and out the other. The sample injection syringe was not attached to the sample loop during analysis or when not in use. Figure 3.8.B shows sample injection from the sample loop when the gas-sampling valve is switched to inject. The GC becomes a closed system with no access for sample input or output.

A.

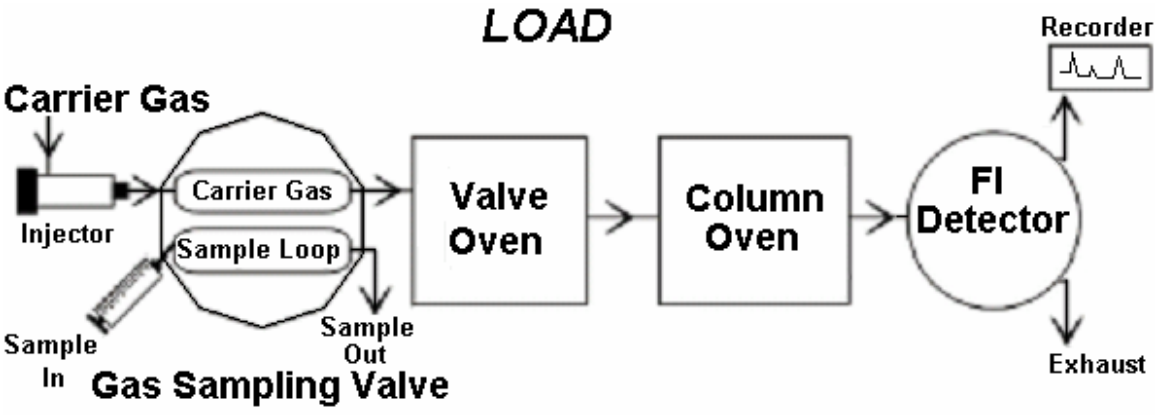

B.

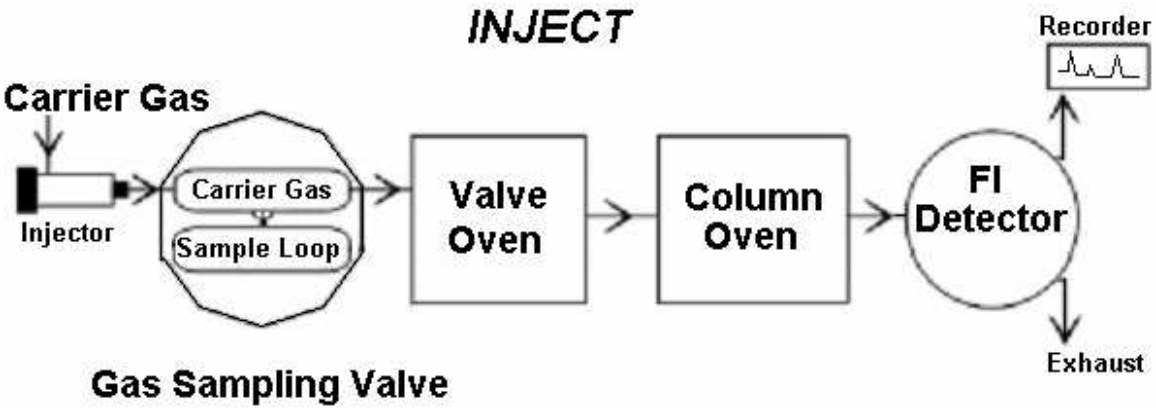

Figure 3.8: Basic functioning Schematic of a GC utilizing a TCD (not FI detector as illustrated). (Image modified from http://www.quadrexcorp.com/new/sri/mga1.pdf)

Three injection loop sizes (250 µL, 1 mL and 5 mL), called 'sample loops' in Figure 3.8, were used to handle samples with varying concentrations of CO_2. Each of the loops were used for calibrating the instrument. Typically, the 0.25 mL was used for field sample runs through the GC. Occasionally, the 1 mL loop and, less frequently, the 5 mL loop were used to run field samples when a low CO_2 concentration was suspected. The primary use of the 1 and 5 mL loop volumes was for calibration purposes.

One loop of appropriate volume was attached at any given time linking the injection port to the GC's oven. Samples from the end of March and early April were pushed through a $Mg(ClO_4)_2$ water trap approximately 15 cm long. Samples collected at the end of April and into May were pushed through a ~3 cm drying tube. A sample was injected into the insert port flushing out the previous sample and filling the loop with the new sample (Figure 3.8.A). The port was then closed to further sample injections and

became part of the GC partition column as in Figure 3.8.B. The loop volume determined the volume of the gas sample injected into the heated partition column.

The GC recorder provides two pieces of information in the results: retention time (t_R) and peak area (PA). The t_R is the time it takes the compound to reach the detector from injection. The PA is a direct measure of quantity, based on the number of molecules to strike the detector. Sample graphical output from the PeakSimple 3D computer program is shown in Figure 3.9.

Once PeakSimple 3D produced a graph of the sample analysis, the t_R was used to determine the peak representing CO_2. Typically, during this analysis the t_R for CO_2 was approximately 1.7 minutes. Predominantly analysts would inject at $t_R = 0.5$ minutes and the CO_2 peak would typically occur at $t_R = 2.2$ minutes. The actual t_R was recorded for each sample allowing for easier post analysis identification. The program was allowed to run for a minimum 4 minutes per analysis. PeakSimple 3D would auto integrate the peaks in the graphical output to give area under the curve. This area was recorded before a subsequent sample was analysed.

The graphical output from PeakSimple 3D provided real time feedback allowing for adjustments to the analysis process for subsequent samples. For example, if the loop size was not appropriate for the sample it could be changed to suit the volume of CO_2 entering analysis. Similarly, the automated integration performed by PeakSimple 3D was not able to use all the integration parameters available in the program forcing manual integration to occur in post analysis. Saving the file for each sample allowed for analysis of the data once the field project had completed. Post manual integration was required because the injections were performed manually by several workers, each with unique injection styles. Slight changes in injection style by various workers would render strict automated integration parameters less accurate.

A second analysis of the data was performed at the end of the project. This post analysis was performed blind, meaning the researcher knew the injected sample t_R, but not the sample ID. Post integration of PAs was carried out for several reasons:

- To double check original integration from any overlooked erroneous results;
- To be sure the PA included all of the CO_2 of the sample and excluded other molecular species; and

- To standardize integration and ensure all curves had been integrated using the same interpretation.

Therefore, when referring to the data, the term "original" is used to describe the PA results from integration that was performed in the field. This includes both auto integration and any modifications to the automation and results recorded in the logbook. The term "new" is used to describe data that resulted from post integration of PAs, performed some time after analysis had completed. Results used in Chapter 4 and Chapter 5 use the new PA integrations.

The technician could readily observe whether the output exhibited unsatisfactory results. Ideally, the spectral peaks should be symmetrical, narrow, separate (not overlapping), and made with smooth lines. The size of the peaks, more precisely the area, is proportional to the quantity of the corresponding substances in the specimen analyzed. The peak is measured from the baseline to the tip of the peak. The characteristics of the SRI GC TCD should provide a normal response and follow the Gaussian concentration profile of the eluted peak as shown in Figure 3.9. The TCD detector provides better results if PA is used to determine gas concentration in a sample (Harris, 2003). A larger PA indicates a larger amount of analyte present in the sample. Height and width are affected by the speed at which the analyte moves through the column to the detector. An analyte that moves slowly will produce a short, broad peak. Faster movement of the analyte will produce a tall, thin peak.

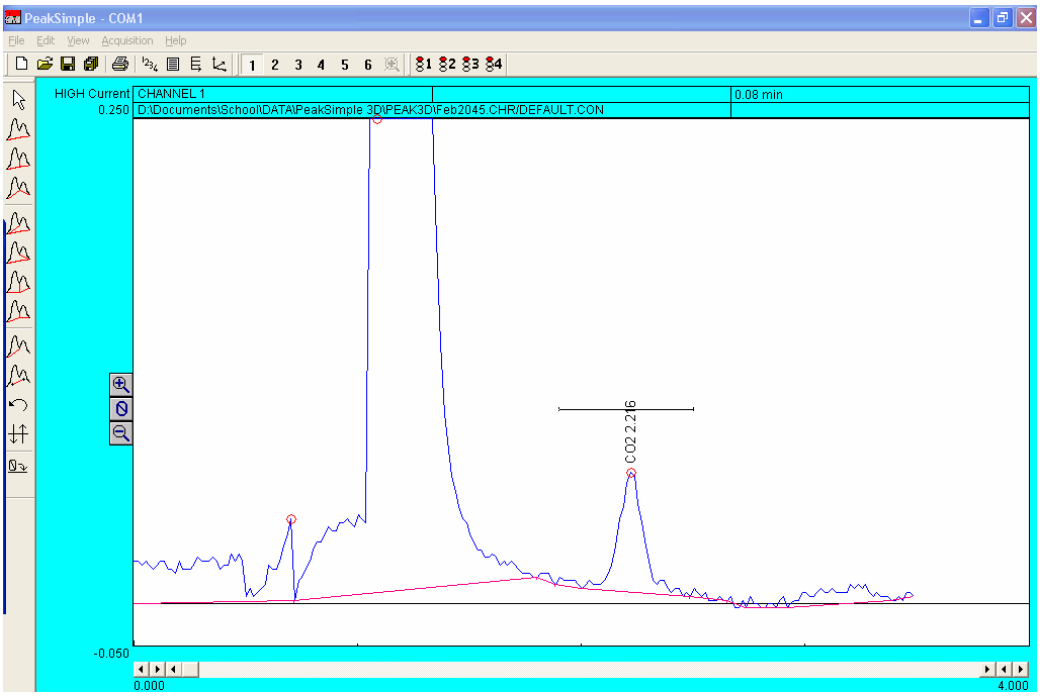

Figure 3.9: Example of a clean output from the GC. Screenshot of data output from PeakSimple 3D for gas sample #45 (February 2, 2004). CO_2 t_R is 2.216 minutes.

For the curve analysis in Figure 3.9, auto integration provided the r_t, and the baseline curve - in red. The baseline represents the bottom of the curve from which integration occurred. The red circle indicates a curve peak from which an area was automatically determined by PeakSimple 3D. Typically, two peaks resulted from analysis of commercially available gas and field samples. The first expected peak (second peak in Figure 3.9) was $O_{2(g)}$, and was large compared to the following peak. Other peaks, such as the first peak (on the left in Figure 3.9), would occasionally occur. In Figure 3.9 the horizontal line above the peak at t_R 2.216 minutes indicates the expected position of the curve of the $CO_{2(g)}$ response. The range provided here was 1.9 min. To 2.5 min. This expected range was correct as long as the CO_2 sample was injected at the correct time of each sample analysis.

While examining Figure 3.9, it is important to notice the location of the CO_2 peak with respect to the previous peak. Though peaks are expected to be very narrow and not have a tail, the combination of ensuring the SRI unit would be robust, versatile and accessible meant that an arrangement of column selection in conjunction with the TCD had to be made to elute the CO_2 and O_2 independently. Therefore some peak overlap

could occur. The CO_2 peak is, therefore, found to be partly on the tail of the previous peak. Integration based on a horizontal baseline for CO_2 would capture some of the TCD response of the previous sample. Integrating this curve meant that the base had to follow the projected contour of the previous peak.

An example of poor peak separation is seen in Figure 3.10. Here, two peaks occurred close together. Using the data logbook to determine the expected t_R for CO_2, the second peak, labelled CO2 2.400, was determined to be the peak of interest. The base line of the CO_2 peak was estimated based on the expected trajectory of the previous peak. Peaks are typically smooth allowing for easy baseline predictions. This figure is an example where PeakSimple 3D was able to accurately separate the two different peaks.

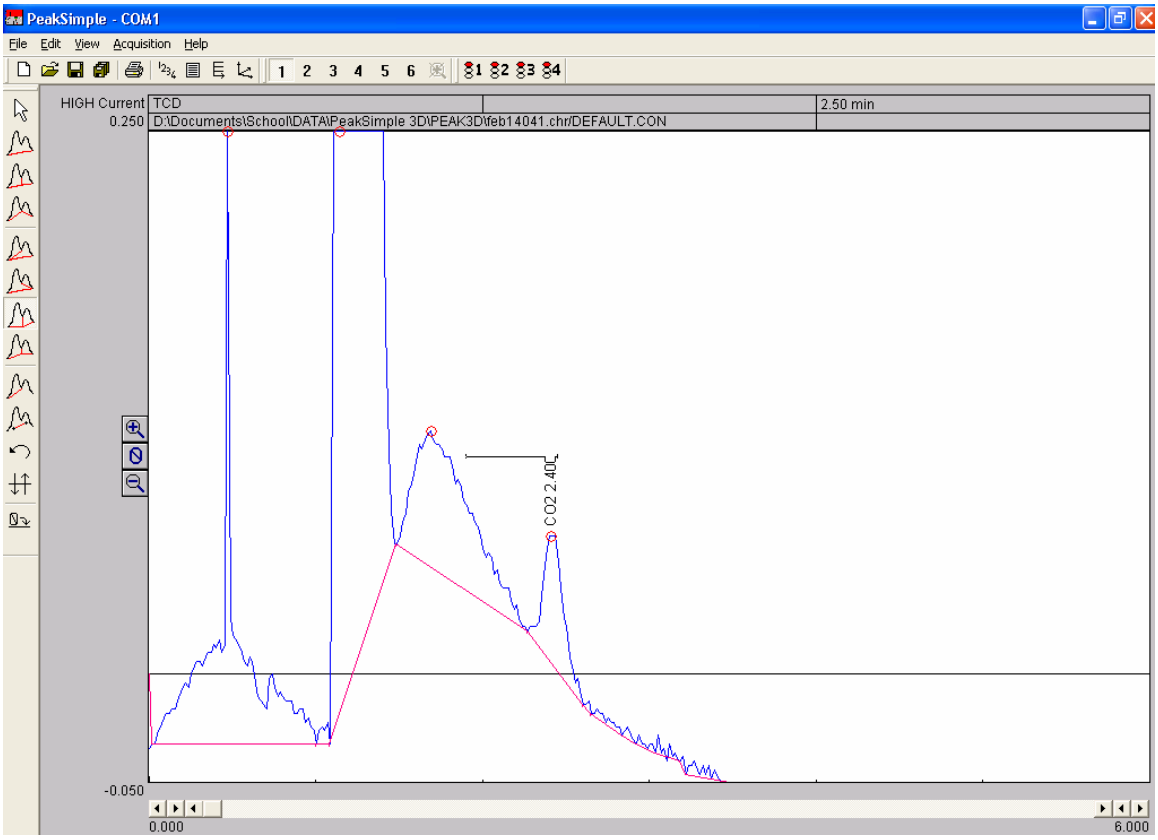

Figure 3.10: Example of a double peak or a peak within a peak. The previous peak is ignored, and the CO_2 baseline is estimated with respect to the previous peak. Screenshot for gas sample #41 (February 14, 2004). CO_2 t_R is 2.40 min.

A common error by PeakSimple 3D was to integrate an extended tail on either side of the sample peak (Figure 3.11). In this example the integration area continues in a

tail to the right of the main peak body. Figure 3.12.A and .B magnify the result of the auto and manual integration respectively of the peak from Figure 3.11. Automatic integration errors occurred in 30% of the data outputs. These integration errors were correctable with confidence in 60% of the corrected data outputs. The remaining 30% of the curves requiring correction, equivalent to 10% of the total output in the experiment, had 2 or more acceptable results. Less than 1% of results had to be ignored due to an unclean curve.

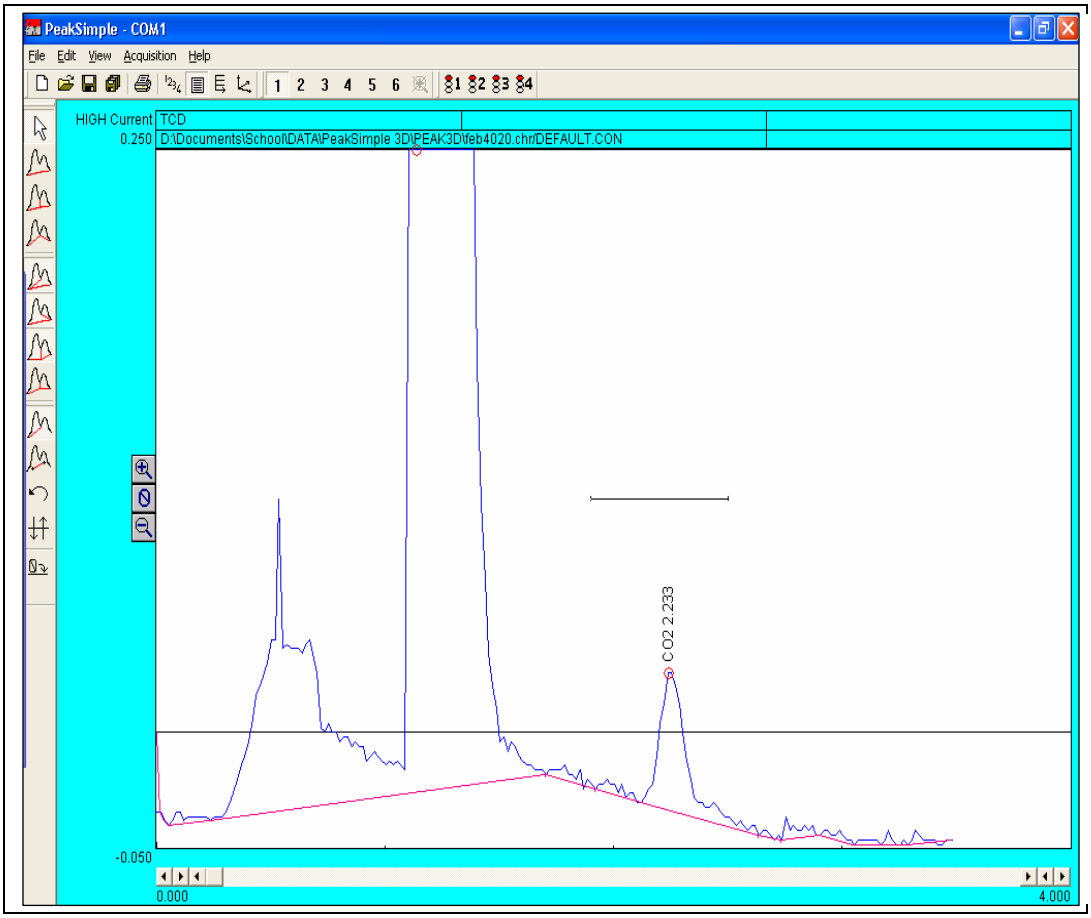

Figure 3.11: Example of an extended tail, falsely increasing the peak area of the sample. Screenshot of gas sample #20 (February 4, 2004). CO_2 t_R is 2.233 min.

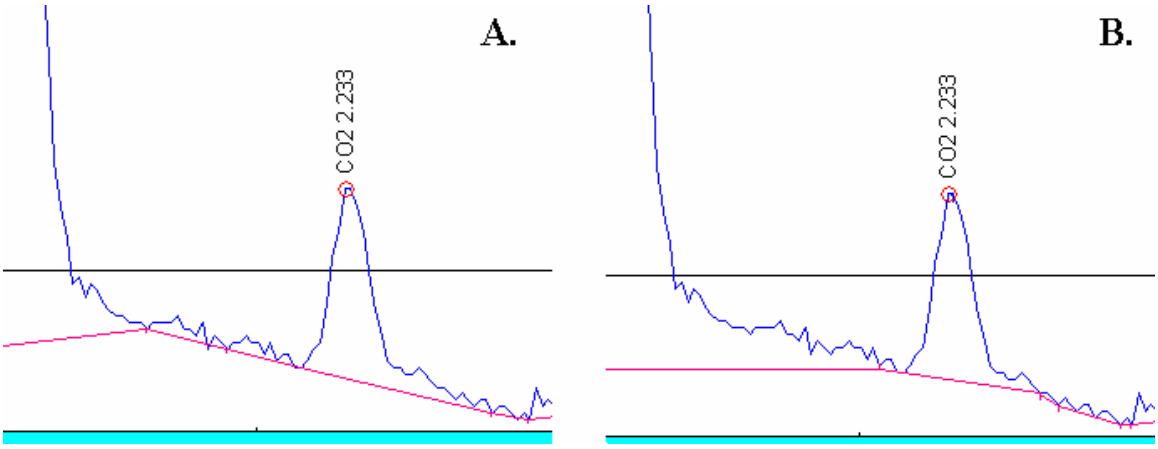

Figure 3.12: Magnification of the CO_2 peak in Figure 3.11 showing over-representation of the CO_2 result in the extended tail. A. Shows the auto integration by the PeakSimple 3D with a tail on the right. **B**. Shows the manual integration correction provided for A.

Cases where a curve from a gas analysis was rejected occurred for two reasons, presence of multiple indistinguishable peaks, or a sample with a long tail. Both indicate contamination and inability to correctly find the start/end of sample detection. The latter would result from a bad injection; over-saturation of the detector, or presence of residual gas from previous samples. An example of a curve that was rejected due to a long tail on the CO_2 peak follows in Figure 3.13. The CO_2 peak (third from left) appears smooth in this example but it is severely asymmetrical, unlike the two previous peaks (Figure 3.10 and 3.11). Note the left hand side of the CO_2 peak has a good shape with a sharp starting point and steep slope.

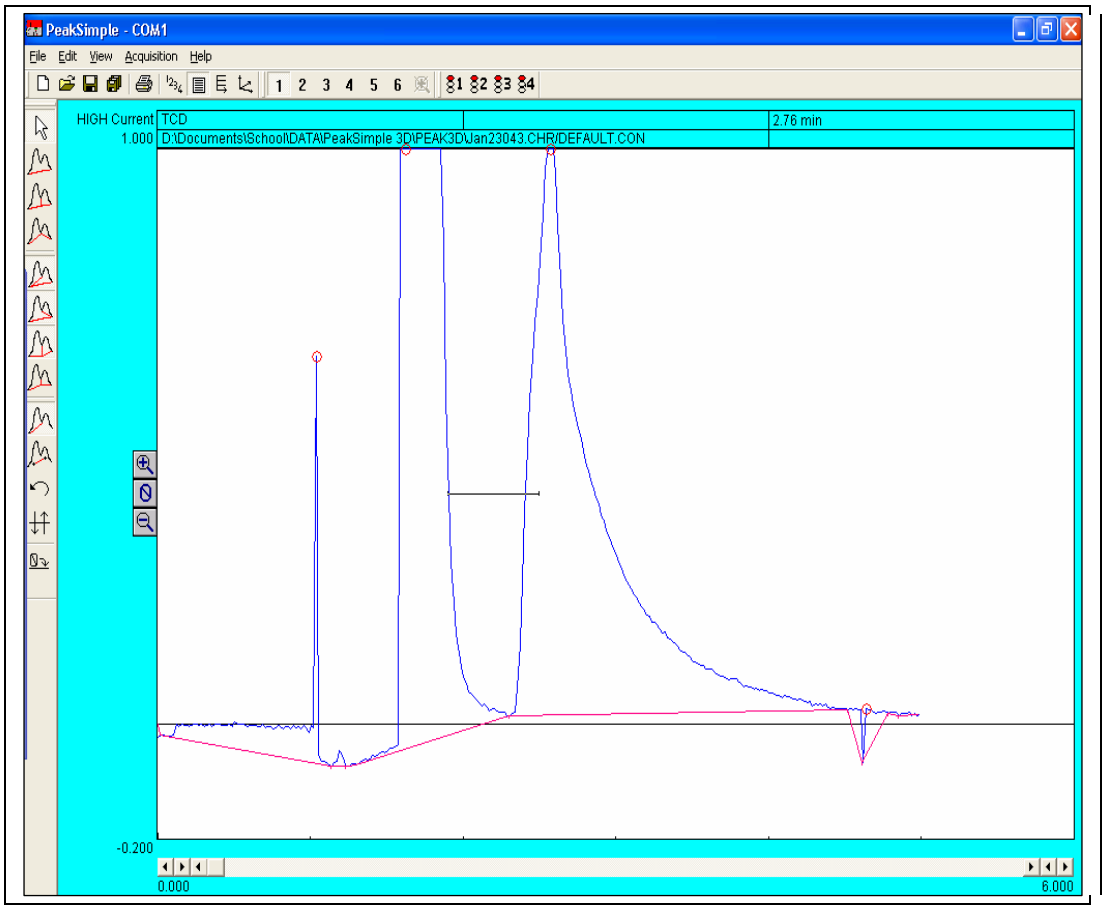

Figure 3.13: Example of a rejected curve output due to a long tail. Note the peak appears smooth, but the long tail makes the curve asymmetrical and therefore unreliable. Sample # 43 (January 23, 2004). CO_2 t_R is 2.216 min.

3.3.1.1 GC Calibration

A 412 ppmv +/- 2% CO_2 standard was used as the gas standard. The CO_2 standard was introduced to the GC via the three different loop volumes providing different amounts of CO_2 analyte to respond to. The three loop sizes gave an opportunity for a three point, linear calibration for the GC. Three samples from the CO_2 standard were analysed through each of the three loops. These results were used to produce an average PA of CO_2 from each loop. The three averages were plotted as mole fraction vs. PA. A graph, like the one shown in Figure 3.14, provided a linear regression curve for calibration purposes. The line should theoretically pass through the origin (0,0): if zero CO_2 is inserted, zero CO_2 should be measured. Therefore, the line was forced through

the origin (0, 0) in the calculation. This practice can skew the actual best-fit slope through the physical range of use.

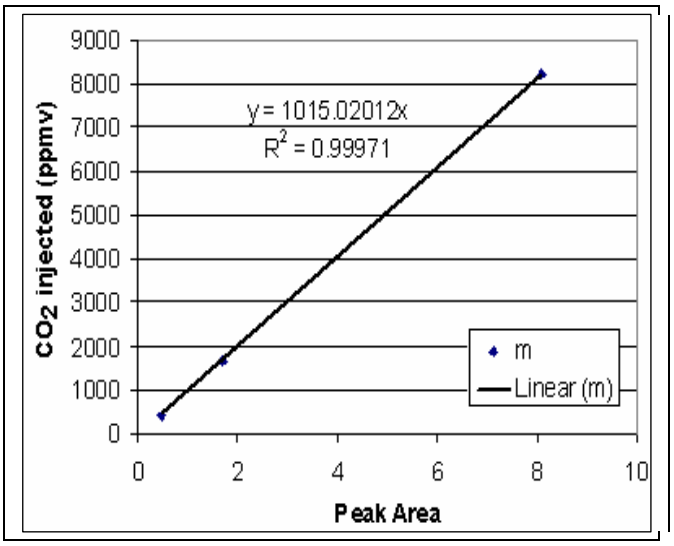

Figure 3.14: Example calibration curve produced by 412 ppmv CO_2 standard injection using all three loop volumes, forced through (0,0) (January 26, 2004).

The slope of the calibration curve (i.e. Figure 3.14) was used to calibrate subsequent analysis. The calibration was applied to the integrated CO_2 area under the curve of a CO_2 standard sample recorded from the graphical printout from the PeakSimple 3D program. Calculation of gas concentration from PA is based on the equation for ideal gasses,

$$P V = n R T \qquad (3.1)$$

where P is barometric pressure (Pascals), V is volume (L), n is number of moles, R is the ideal gas number ($R = 8.314472\ L \cdot kPa \cdot K^{-1} \cdot mol^{-1}$) and T is temperature (K). From the ideal gas law, the raw PA from a CO_2 standard sample was combined with the slope determined from the raw data calibration curve (m):

$$[CO_2] = m * PA * R * T * P^{-1} * V^{-1} * 1000^{-1} \qquad (3.2)$$

where the multiplier 1000^{-1} was used to convert the result to ppm.

Equation 3.2 shows the application of the calibration slope (m) to the raw area under the CO_2 peak resulting in the pCO_2 of the sample (ppmv). To deal with atmospheric pressure changes during a course of analysis, barometric pressure was monitored. This was verified post analysis with the barometric pressure data from the MET site. Each data output included a time stamp of the moment of analysis. This time was matched with the corresponding barometric pressure and inputted into the calculations. A thermometer was posted along side the machine and traffic through the GC room was minimized to maintain a stable ambient temperature.

3.3.1.2 Vial preparation; Exetainer™ Evacuation Protocol

A manifold was used for the evacuation of the sample vials (Figure 3.15). Appendix A.5 summarizes the components of the evacuator their role in the evacuation process.

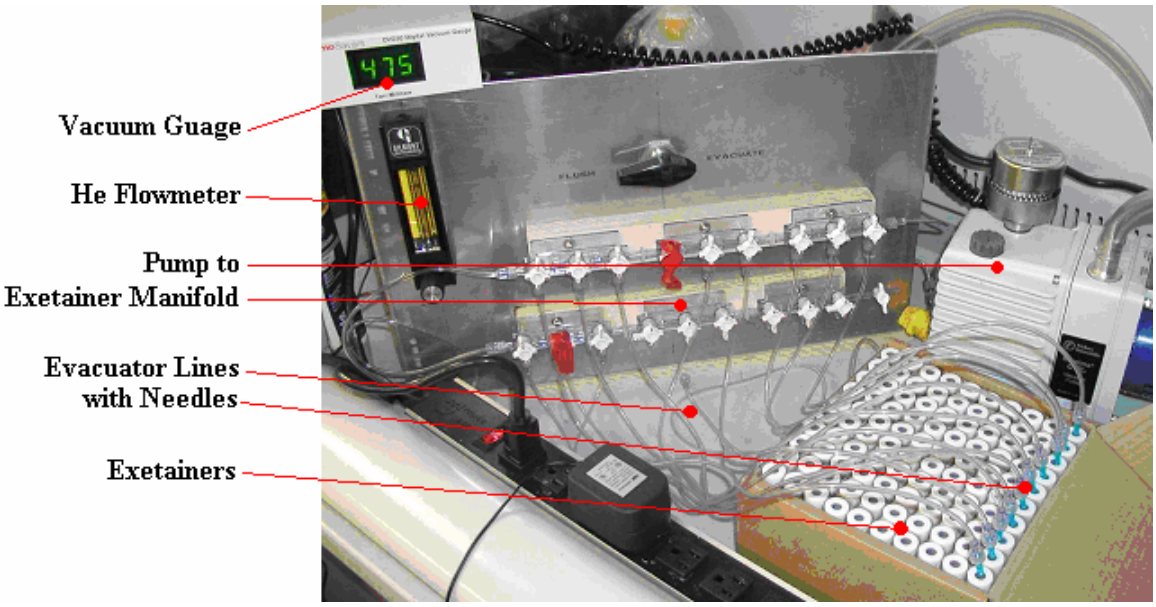

Figure 3.15: Exetainer evacuator in use. Note manifold ports are open, Swag-lock is set to evacuate, and the gauge pressure is 475 millitorr. Appendix A.5 lists items required for construction of the evacuator.

A Fisher Scientific Maxima Plus M2C[11] air pump was used to evacuate the vials. The He gas was used to flush the vials, leaving a He headspace upon the final evacuation. The luer lock array was used to evacuate up to ten vials at one time. Needles were

[11] Fisher Scientific Maxima Plus M2C, manufactured in Pittsburgh, Pennsylvania, USA.

replaced after approximately 25 insertions into a septum. The vials were evacuated using the following procedure:

- All valves and luer locks on the apparatus were closed sealing the vials from the He gas and atmosphere. The large manifold switch was set to evacuate to open the connection between the vacuum pump and the vials;
- Needles attached to the luer manifold via rigid tubing were inserted into the septum of the vials;
- Luer locks on the luer manifolds connected to sample vials were opened (all others remained closed);
- Vials were evacuated to below 1.0 mTorr;
- The manifold was toggled from "Evacuate" to "Flush" allowing He gas to flush the vials;
- Steps 4 and 5 were repeated an additional two times;
- A final evacuation was performed so the vials were left empty with an internal pressure of less than 1.0 mTorr;
- Once the fourth evacuation was complete the luer locks and the large manifold switch were closed and the needles removed from the vials;
  - Note: the value on the digital vacuum gauge should not increase as the needles were removed one at a time, signifying that no leak existed within the system;
  - The septum of each vial was covered with a bead of silicone sealant to ensure longevity of the vacuum inside the vial.
- A random sampling of vials was performed to ensure evacuation was consistent;
  - About one in 20 vials had their cap twisted off while the worker listened for the sound of air rushing into vial proving evacuation,
  - These vials were returned to the collection of vials requiring evacuation.

Once all vials were evacuated, the vacuum pump and the He gas tank were turned off.

3.3.2 Chemical Analyses

Ice chemistry was performed on ice cores that were brought to the ship from Site E and F1 (Figure 3.2, described in Chapter 3.3.4) for analysis of salinity, A_T and/or DIC. The core samples were transported back to the ship in two different ways. One was to wrap the cores samples in a plastic bag or a sleeve tied at both ends. This was done for entire core pieces (up to 1 m in length because of the length of the Kovacs core barrel and laid on their side) and to 10 cm sections that were cut promptly in the field. Often, 10 cm sections were placed in 2 L Nalgene buckets (sometimes wrapped in plastic) for easier transport. The ice was melted in 10 cm sections at room temperature in paleo lab for approximately 12 hours, at which point they were ready for chemical analysis. Analysis procedures for sea ice are described in Chapter 3.3.2.1 for salinity and Chapter 3.3.2.2 for A_T. If A_T analysis did not occur promptly after melting, the samples were poisoned with 200 µL saturated mercuric chloride ($HgCl_2$) and stored in a cool and dark location until analysis was possible as described in the DOE (1994). Surface seawater samples were poisoned promptly upon returning to the Amundsen laboratory. Poisoning retains C chemistry properties of the sample after its extraction.

3.3.2.1 Salinity

Salinity was measured promptly after ice core samples melted using a WTW Cond330i[12] sensor. The clean dry probe was inserted into the liquid sample. Once the instrument readout had settled on a value, this value was recorded. The probe would be removed, rinsed with Milli-Q[13] water and wiped dry with a Kimwipe®[14] prior to subsequent immersions in a sample. At the end of analysis, the probe would be rinsed with Milli-Q water, dried and packed away in its storage container. The precision and accuracy of the measurements was 0.002 units.

3.3.2.2 Alkalinity

Alkalinity is the acid-neutralizing capacity of an aqueous solution. If the bottled sample was used for both DIC and A_T analysis, A_T was run after DIC/TCO_2 analysis so as not to bias the DIC measurement.

---

12 WTW Wissenschaftlich-Technische-Werkstätten GmbH; Weilheim, Germany.
13 Millipore **Milli-Q**® Biocel Ultrapure Water Purification System, USA.
14 Kimwipe®: Lagasse Bros Inc, manufactured in New Orleans Louisiana, USA.

A TitraLab 865 Potentiometric Titration Workstation[15] was used for A_T analysis (supplies list Appendix A.6). The software used to operate the titrator was the TitraMaster85 (Radiometer Analytical). The electrodes were an $HgSO_4$ reference electrode (ref. 201 no. 237-12-017) and a platinum electrode (M241Pt no. 243-11-005). The apparatus allowed numerous modes of analysis. The IP (inflection point) continuous mode of titration was used with a maximum titrant flow of 1mL min^{-1}. The potential range in the program was 70 mV to 120 mV. The theoretical titrant concentration was 0.03 N HCl for the ice core (and seawater) A_T analysis up to March 30, the cores after that date were analysed using 0.005 N HCl. Seawater A_T analysis continued to use titrant concentration of 0.03 N HCl after this date. The same program was used for analysis with both titrant concentrations, with only the titrant concentrations being different between the two programs. The purpose was to obtain a higher inflexion point. Therefore, the titrator could calculate a more precise inflexion point for the sea ice samples with lower error. The actual titrant concentration was determined with every titration series. Dickson CRM, described below, was used to calibrate the titrant.

This automated method was validated with CRMs prepared and distributed by A. G. Dickson of SIO (Scripps Institution of Oceanography under the U.S. Department of Energy Global Change Research Program) (Dickson et al., 2002). Titrant acid concentration was calibrated to CRMs prepared and distributed by A. G. Dickson of SIO. Appendix A, Table 6 lists items required for A_T analysis.

Sample mass was used during stationary (ice camp) phase for A_T analysis. When the ship was in motion it was not possible to measure the mass of a sample to determine an accurate volume. Nevertheless, an accurate volumetric technique was required for A_T samples run in December and January. For this purpose, a pipette was filled using a bulb pump. To allocate a volume of melted sea ice for analysis the first step was to flush the pipette by filling it once with sample and drained. The second step was to refill the pipette providing a sample for titration. The bulb was emptied into the sampling beaker. The pipette was calibrated in the Institute of Ocean Sciences[16] prior to the CASES project and was roughly 80 ml in volume. Using salinity, temperature and known volume of the

[15] TitraLab 865 Potentiometric Titration Workstation; manufactured in Lyon, France.

[16] Institute for Ocean Science, Department of Fisheries and Oceans, Sidney, B.C. V8V 4L1

pipette at standard temperature, the pipette volume could be determined. This complex problem is discussed by Fofonoff and Millard (1983).

The following steps were performed in this order on *duplicates* of each of:

1. junk seawater (enough to properly warm up the titrator),
2. Dickson CRM or secondary standard samples,
3. field samples (sea ice - SI or seawater - SW), and
4. another set of Dickson CRM or secondary standard samples.

The process for running a standard, a sample or a junk was as follows:

- Approximately 75 g or 75 mL was allotted for analysis of a sample.
- Following the TitraMaster85 on screen prompts, the sample ID was entered while sample salinity, sample temperature and sample weight were recorded in the logbook.
- The beaker containing the sample and a stir bar were prepared and placed on the stir plate with the electrode and dosimat diffuser positioned in the sample at least 2cm below the water line avoiding contact with the stir bar.
- The TitraMaster85 program was started and the stir bar and controlled acid addition began.
- Following the complete initial acid addition (1.6 ml), mV readings were recorded as further smaller additions occurred.
- Periodically, 0.05 ml acid was added to the solution. The potential was recorded continuously and the process continued as long as the standard deviation between subsequent readings was below 0.1.
- The readings and 0.05 ml additions continued until the mV readings plateau and the final acid volume was added. The inflection point was determined by the TitraMaster85 program from this graph. At the inflection point, the potential was recorded from the x-axis and the titrant volume from the y-axis.
- Following the completion of the acid additions, the volume of titrant added and the final eV value reported were recorded. The titrant volume was used to calculate the samples A_T.

- The sample was dumped down the drain. The titration beaker with stir bar was rinsed with Milli-Q water, dried with a Kimwipe and placed upside down until the next sample was ready for analysis.
- Replicates (of the standard or samples) within 0.05 mmol/kg of each other were deemed to be statistically similar.

Figure 3.16 is a recreation of the data output from the TitraMaster85 program. The titrant volume that had been added, as in Figure 3.16, was used to calculate the samples A_T by finding the greatest change in the measured pH per unit volume of acid added, known as the inflection point. The computer calculations used here follow the alkalinity measurements method using a calibration curve derived from the PC TitratION[17] software that calculated results of calibration standards. Further detail on alkalinity measurements in the chemistry in Stumm and Morgan (1981).

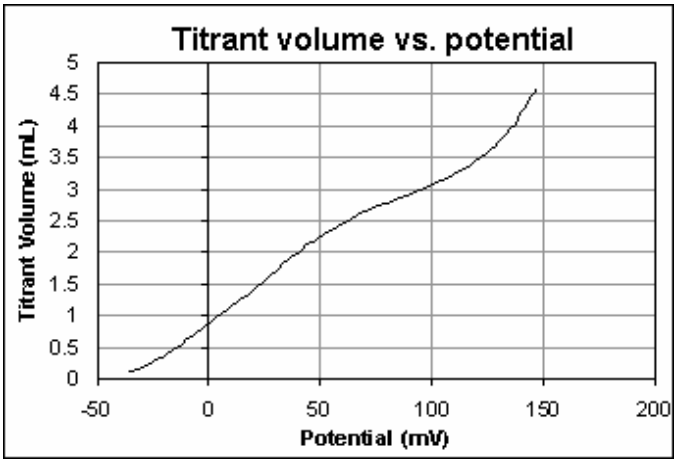

Figure 3.16: Results of titrant addition to melted ice by the TitraLab 865 Potentiometric Titration Workstation.

At the end of analysis the computer and analyzer were shut off. Care was taken to remove the electrode from sample containers. The electrode was rinsed and stored in pH electrode storage solution of KCl, with the hole in the electrode probe covered to prevent evaporation of the solution within the electrode. Occasionally, the solution in the electrode required refilling when electrode solution dried out.

[17] Product of Radiometer Analytical

3.3.2.3 DIC

A SOMMA (*s*ingle-operator multi metabolic analyzer) Coulometer system was used for accurate DIC measurements (DOE, 1996; Dickson, 1993; Johnson et al., 1993; Goyet et al., 1992). This method offers reproducible (~0.02%; ~0.4 μmoles kg^{-1}), accurate (to better than 0.025% or ~0.45 μmoles kg^{-1}), and rapid sample analyses (20 to 30 minutes). The SOMMA-coulometer instrument has been widely used for ocean carbon cycle studies. It is transportable, rugged, sea-going, and reliable. Calibration and certification procedures are complete, tested, and well documented. The SOMMA system semi-automatically controls the sample handling and extraction of CO_2 from seawater samples. The SOMMA control the pipetting and extraction of DIC from seawater samples. The SOMMA is interfaced with a personal computer and coupled to a CO_2 coulometric detector.

The SOMMA system is a coulometer based DIC analyzer with the following components: sample dispensing and extraction (glass pipette; stripping chamber; reservoir for phosphoric acid controlled by valves and flow regulators for the various gases, such as carrier gas (e.g., Helium)); sample temperature regulation (water bath), electronic interfacing (computer, basic software and printer), and conductance cell (coulometer cell solution, containing ethanolamine, dimethylsulfoxide (DMSO) and thymolphthalein indicator). The SOMMA system is calibrated forcing a known volume of gas to the coulometer for detection. The SOMMA system coulometric cell solutions get exhausted after some time, and therefore, preparation of new cell solutions and recalibration of the SOMMA system is necessary.

The same sampling technique as described for the alkalinity procedure (3.3.2.2) was followed here for the purpose of using many of the same samples for DIC analysis. When the same bottle was used for both alkalinity and DIC, the DIC analysis occurred first.

During analysis, a known volume of seawater sample is acidified with reagent grade phosphoric acid, converting all carbonate species to free CO_2. The evolved CO_2 is then extracted from seawater using an inert carrier gas such as ultra high purity inert carrier gass. The CO_2 is absorbed by the coulometer cell solution. Reaction between CO_2 and ethanolamine produces hydroxyethylcarbamic acid, causing a colour change in

the solution. Hydroxyl ions are electrochemically generated to maintain the absorbing solution at a constant, colorimetrically defined pH. The current generated by this titration is related by the Faraday constant to the moles of CO_2 absorbed by the solution (Johnson et al., 1993). The SOMMA system was routinely calibrated with CRM standards, supplied by Andrew Dickson, Scripps Institution of Oceanography. CRM's have a certified DIC concentration determined at the Scripps Institution of Oceanography lab overseen by A.G. Dickson.

3.3.3 Derived Variables

3.3.3.1 Light Penetration

The amount of light reaching the different ice depths was calculated using Beers Law, modified by the method proposed by Arrigo et al. (1991). Fundamentally, the Beer-Lambert Law is an empirical relationship that relates the absorption of light (A, unitless since $A = \log_{10} K_0 / K_z$, where K_z is radiation at depth z, and K_0 is incident radiation) to the properties of the material through which the light is travelling and states that:

$$A = \alpha z c, \qquad (3.3)$$

where; α is the absorption coefficient or the molar absorptivity of the absorber ($L \bullet mol^{-1} \bullet cm^{-1}$), z is the distance that the light travels through the material (m) and; c is the concentration of absorbing species in the material ($mol \bullet L^{-1}$). Transmitted radiation was estimated at depths corresponding to the midpoint of each of the three pCO_2 gas sampler depths. The photon flux densities calculated are daily maximum values ($mmol*m^{-2}s^{-1}$). Snow is more opaque and reflective than sea ice and affects total daily PAR penetration to ice depths (Grenfell and Maykut, 1977; Grenfell, 1994). Light extinction in snow (A_s) is a function of depth and α was set at 12.5. The estimate of FYI light attenuation (A_i) used here was determined by Arrigo et al. (1991), as 1.4 (Perovich, 1993; Manizza et al., 2004 and 2005). This value was used to determine irradiances at desired sea ice depths ($K\downarrow z$), necessary to approximate irradiation depletion from the ice surface ($K\downarrow_0$), according to the model that includes an extinction coefficient (α). The formula transforms to:

$$\log_{10} K\downarrow_o - \log_{10} K\downarrow_z = \alpha z c \quad (3.4)$$

$$\log_{10} K\downarrow_z = z\alpha(\log_{10} K\downarrow_o) \quad (3.5)$$

$$K\downarrow_z = e^{(K\downarrow_o - z\alpha)} \quad (3.6)$$

where $K\downarrow_z$ is downward radiation at depth z, and $K\downarrow_0$ is downward incident radiation. This formula was used on PAR data collected as described in Chapter 3.2.4.

3.3.3.2 Eddy Correlation

The instrumentation in Chapter 3.2.4.2 used for determining CO_2 gas flux is part of a method called Eddy Correlation. Discussion in Chapter 5 uses flux data collected through the eddy correlation technique.

Eddy correlation measurements for CO_2 fluxes are based on the correlation between turbulent motions of the air, and the abundance of transported CO_2 by the turbulent motions (Campbell and Norman, 1998). The primary transport mechanism by which heat and CO_2 moves between the ice and the atmosphere is by the turbulent motion of the air near the surface. The average vertical wind speed above a flat land surface is considered to be zero, because the ice surface is neither a source nor sink for air. Similarly, for $CO_{2(g)}$ to undergo turbulent transport from the ice surface to or from the atmosphere, air motions in one direction must contain more CO_2 than the other. The time-averaged correlation of high frequency fluctuations in vertical wind speed and $[CO_2]$ is positive during periods of net $CO_{2(g)}$ production. In turn, the correlation is negative during net CO_2 absorption. The eddy correlation method uses high frequency (~10 Hz) measurements of vertical wind speed, temperature, and $[CO_2]$ to directly calculate the correlation between vertical air motions and the constituent of interest. Fluxes, means, covariances and variances were calculated over one hour integration periods using standard methods (e.g., Massman and Lee, 2002), complete with pressure density corrections. Twenty-four hours of this data was averaged to produce daily CO_2 flux rates for the whole experiment, and each period individually. From this data,

average daily flux direction and magnitude (FCO_{2D}) were calculated by multiplying the average daily flux rates ($FCO_{2/s}$ as $g/m^2/s$) by the number of seconds in a day (t, t = 86400 s).

$$FCO_{2D} = t \bullet FCO_{2/s} \quad (3.7)$$

One final calculation was performed to determine the total CO_2 moved in a period (FCO_{2P}). To obtain this value, the average daily CO_2 flux (FCO_{2D}) was multiplied by the number of days in the period (P_D).

$$FCO_{2P} = P_D \bullet FCO_{2D} \quad (3.8)$$

Small gaps in raw data in the order of seconds to a few minutes are typically caused by erroneous or error data due to instrument malfunctions, or short periods when the instrumentation is under service. These small gaps may be subject to data filling in which each missing value is filled in with the average value of all the non-missing adjacent neighbours. If more than 15 minutes of data were missing in an hour, then the hour's data were rejected and not processed.

3.3.3.3 Tests for Statistical Significance

The analysis of variance (ANOVA) was used to partition observed variance into components based on various dependent and independent variables. The analysis assumes that the data populations differ only in their means, and that each case is independent, normally distributed, and that the variance of data in groups should be the same. One-way ANOVA was used to test for differences among two or more independent groups. The One-way ANOVA was used to test for differences among at least two groups. Although a T-test can be used for two-group scenarios, ANOVA works as well.

A null hypothesis is a hypothesis set up to be disproved in order to support an alternative hypothesis. When used, the null hypothesis is presumed true until statistical evidence, in the form of a hypothesis test, indicates otherwise. In other words, when there is a certain degree of confidence, here 95%, that the data does not support the null hypothesis. It is possible for an experiment to fail to reject the null hypothesis. To test a hypothesis, several groups with different dependent variables are identified. Usually the

groups appeared to be similar. Of course, under close scrutiny, each group is probably different. The purpose is to determine if we take this difference as evidence that the groups in fact are different; perhaps caused by the dependent variable. Note that even if there is not a real effect on the population (the null hypothesis), the groups are likely to be different.

The likely range of variation of the averages if our effect hypothesis is wrong, and the null hypothesis is correct, is a term related to standard deviation called the sum of squares. The deviation of the i^{th} data point (x_i) from the mean of the data set ($\bar{x}$) is written as:

$$x_i - \bar{x} \tag{3.9}$$

If all deviations are squared, then summed we get the "sum of squares" for the data, as in:

$$\sum_{i=1}^{n} (x_i - \bar{x})^2 \tag{3.10}$$

As the size of the data set increases, so does the sum of squares of the data set. Therefore, the sum of squares is normalized with the number called the degrees of freedom. Here, the degree of freedom is defined as the number of data in the collection, minus one, or $n - 1$, where n is the number of data points. The result of dividing the sum of squares by the degrees of freedom is the mean of the squares.

The F ratio can be computed from the mean of the squares. A table of critical values of the F-distribution was used at this point to determine the 5% significance level. This is interpreted to mean that there is a 5% chance that the null hypothesis is not true.

CHAPTER 4: RESULTS

In this chapter I review the physical environment within which the study was conducted. Presented is the seasonally evolving data record associated with atmospheric and surface characteristics, including measurements of air and ice temperature, ice thickness, day length, and surface incident photosynthetically active radiation (PAR). Aspects of sea ice geophysics and sea ice pCO_2 are described, followed by a presentation of the basic available attributes of surface seawater and sea ice carbonate chemistry. In figures of this chapter the three ice gas sampling depths correspond to the midpoint of each of the three pCO_2 gas sampler depths: 30 cm for D1 at 20-40 cm; 70 cm for D2 at 60-80 cm; and 110 cm for D3 at 100-120 cm.

4.1 Bulk Meteorology and Site Microclimatology

The day-to-day variation in air and sea ice temperature is shown in Figure 4.1. Ice temperature was monitored at MET site G (Figure 3.2), and measurement practices are described in Section 3.2.3. Ice temperatures in the upper 20cm to 100cm ranged from –28.11ºC to –2.90ºC throughout the winter and spring season with the coldest ice being near to the sea ice surface in March. Air temperature was colder than –20ºC for at least a portion of each day for 81% of the days. Daytime length ranged between 0 and 24 hours during this experiment (Figure 4.1), and was 24 hours in length after May 15. Daytime length refers to the amount of time the sun is above the horizon on a given 24 hour time period.

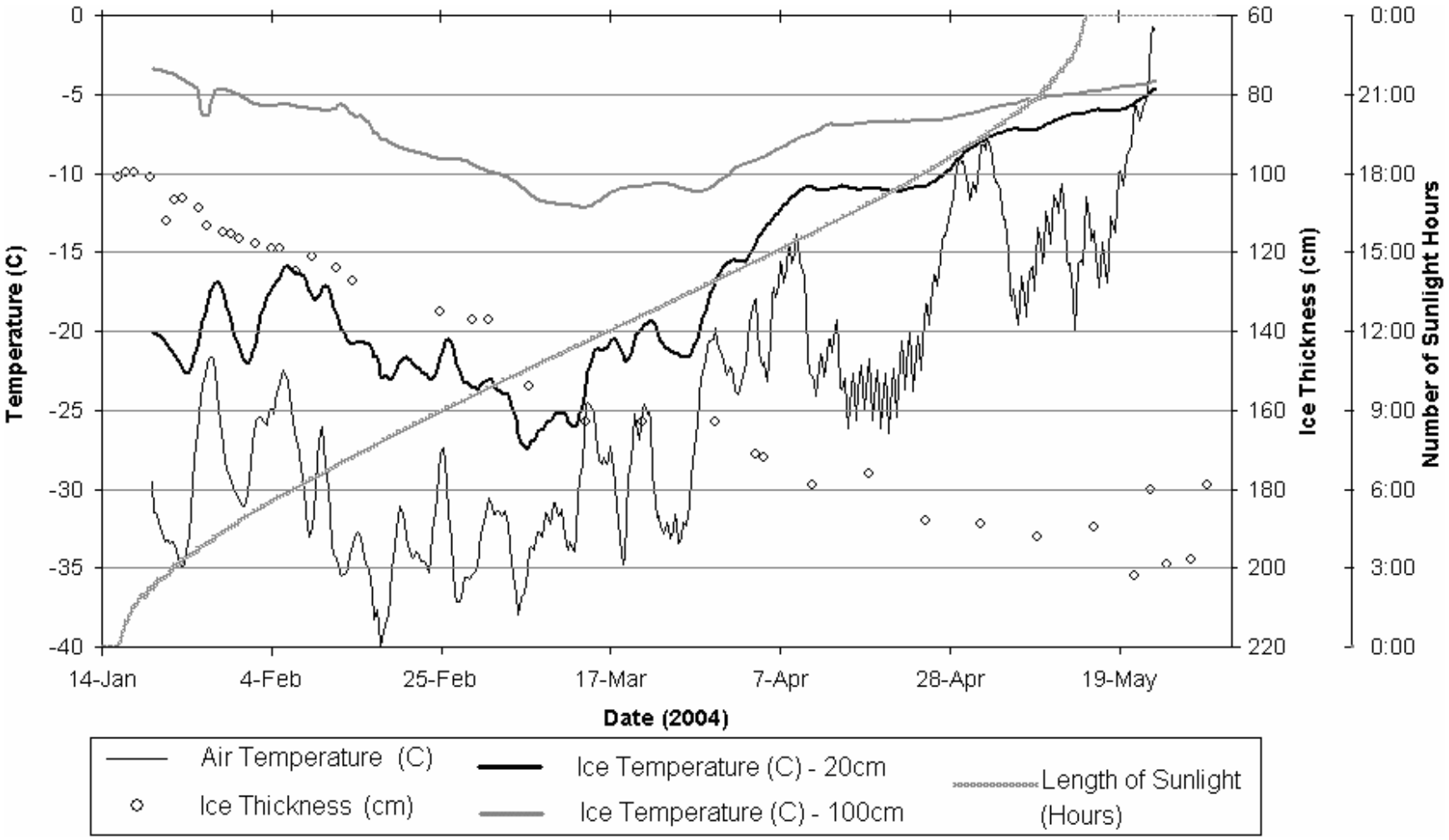

Figure 4.1: The day-to-day variation in *daytime* sea ice pCO_2 at all three depths within the sea ice and air temperature. The (very small) whiskers associated with the pCO_2 average data point represent the ± 2 standard deviation units from the reported average. Normalized sea ice pCO_2 is defined in the text.

Ice thickness increased for most of the experiment, doubling from 86cm to 204 cm, (Figure 4.1). The growth rate at the beginning of data collection was 1.40 cm/day decreasing throughout the measurement period. The decreasing rate of ice growth in the CASES region (2004, cm/day) is quantified in the polynomial curve (Equation 4.1) generated from the plot of weekly average ice growth (y):

$$y = -0.0002\ x^2 + 0.0235\ x + 0.1397 \qquad (4.1)$$

where x is day number ($1 \leq x \leq 150$ of year 2004). From the spring equinox to the end of the measurement period, the sea ice grew an average of only 15 cm across multiple sites of measurement. Observed thinning of the ice cover during the final days of the experiment provided evidence of *in-situ* ablation.

The temperature data presented in Figure 4.1 was recorded automatically on the meteorological tower as described in Section 3.2.2. The temperature record at the 20 cm depth does not reflect the rapid fluctuation in air temperature. Both the sea ice and air temperature showed a general cooling trend to mid-march, increasing thereafter. There is, however, pronounced variability in both time series of short term warming and cooling superimposed on the general trend. Minimum air temperature occurred on February 18 (-39.59ºC) while the coldest sea ice at the 20 cm level (D1, Section 3.2.1) occurred at March 7 (-30.15ºC). Of note are periods that show extreme fluctuation relative to the general trend. These include the period between April 12 to 26, where a 12ºC drop in air temperature occurred over 14 days interrupting increases in sea ice temperature at the 20 cm depth, remaining at –10.5ºC. After March 21, 20 cm sea ice temperature rose rapidly to about –12ºC by 10 April, with a gradual increase thereafter to the end of the experiment.

The ice temperature structure is shown for the surface 1 m in 12-day intervals throughout the experiment in Figure 4.2. The temperature at any level in the ice is a function of ice thickness and of the temperature difference between the ice surface and its base (Lake and Lewis 1970; Jones, 1973; Lepparanta, 1993; Killawee et al., 1998). The profile is slightly negative (ocean warmer than atmosphere) until late March, after which the sea ice abruptly approaches an isothermal state by 9 April. The upper 1m of ice is near isothermal, close to –5ºC by 15 May, and by 25 May, the entire upper ice is above –5ºC, with enhanced warming at the upper 20 cm. Because of the temperature gradient

over much of the experiment, one would expect differences in each of the ice physical and chemical properties across the ice profile, particularly given that brine chemistry and migration are strong functions of temperature (Section 2.2.2).

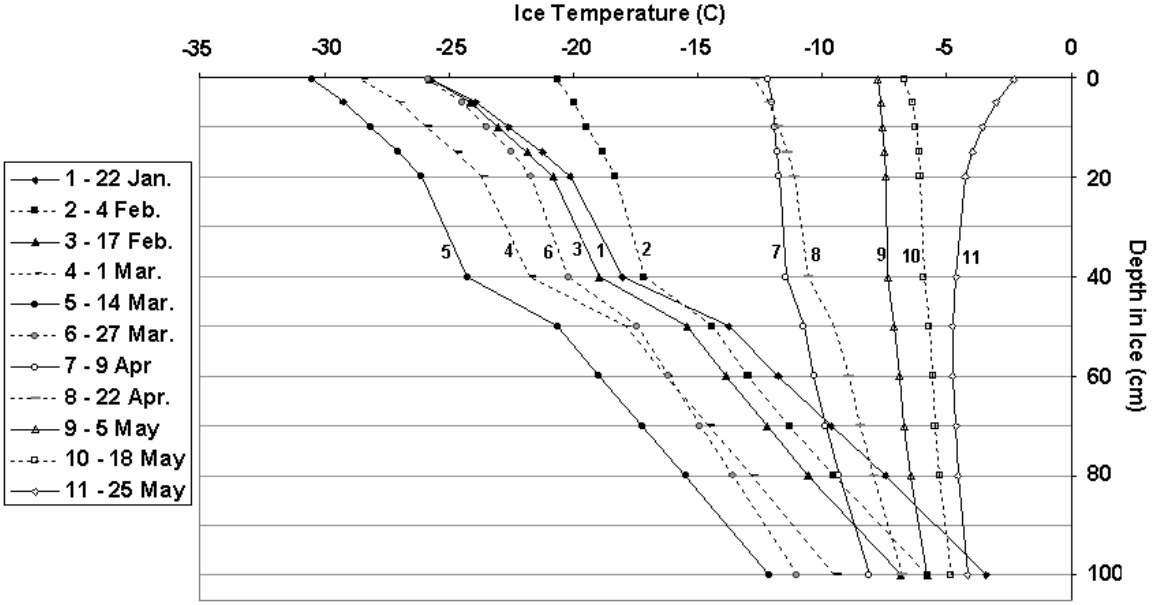

Figure 4.2: Ice temperature profiles. Temperature profiles within the upper 1 m of sea ice from every 12th day of the experiment.

The observed variation in the PAR is associated with the seasonal increase in daytime length, varying cloud cover and changing snow thickness. Figure 4.3 shows the record of daily maximum PAR at the ice surface. PAR transmission through the snow and into the sea ice was calculated using Equation 3.6 following methods outlined in Section 3.3.3.1. PAR was reduced from the surface value shown in Figure 4.3 at depths ice gas sampling depths D1, D2 and D3 to 65.7%, 37.5% and 21.4% respectively. According to Gosselin et al. (1985) ice algae require a minimum of 4 mmol $m^{-2}s^{-1}$ for active production to occur. The light levels at the depth of the peepers exceeded this threshold daily at the two upper depths, D1 and D2; and from January 28 to the end of measurements at D3.

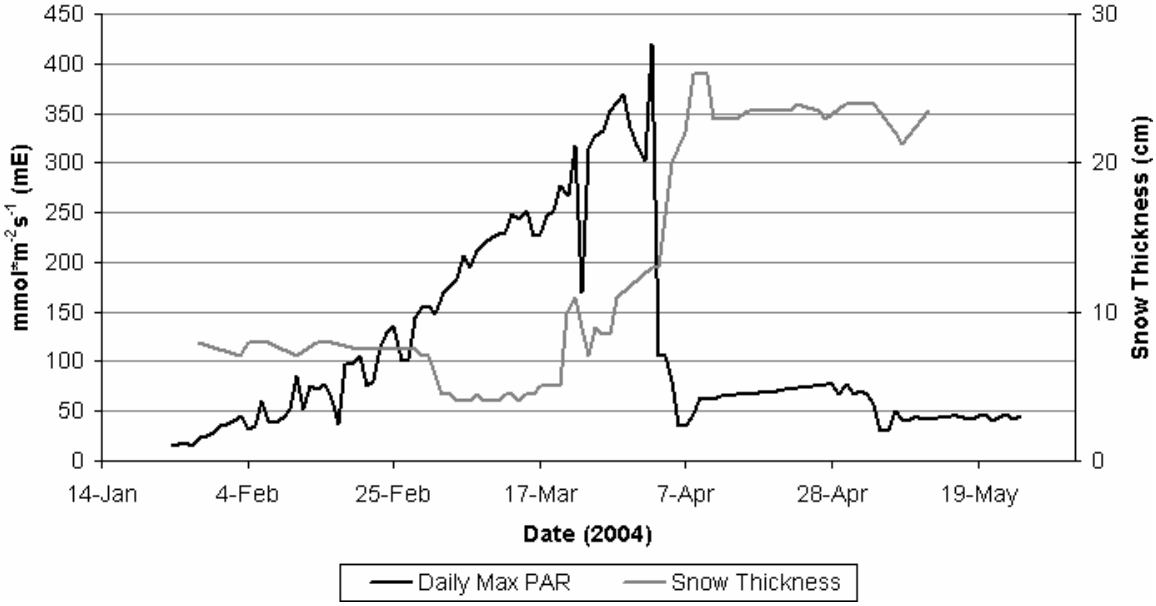

Figure 4.3: Daily snow thickness and maximum calculated PAR at the ice surface.

Heavy cloud cover and precipitation on February 16, March 2 to 3, and April 2 lowered the available solar radiation at the snow surface. On April 2, the snow thickness increased by a factor of 3.5, from 7.5 cm to 24 cm, causing an 80% decrease in PAR reaching the ice surface. Daytime PAR maximums were relatively consistent after April 7 coinciding with increased snow thickness.

4.2 Sea Ice pCO_2

4.2.1 General Characteristics and Diurnal Variation

In-situ sea ice pCO_2, as measured using the ice peepers (Chapter 3.2.1), is shown in Figures 4.4 and 4.5 representing DT and NT conditions, respectively. Of the six samplers that were located at each depth across our sites, three were sampled in the morning to represent nighttime (NT) gas conditions, and three were sampled in the late afternoon to represent daytime (DT) gas conditions (Section 3.2.1.2). The sea ice pCO_2 in the figures represent the average among the three ice gas depths collected at the same time period (Ex.: all DT samples on a particular date are averaged together in Figure 4.4, with the same process occurring for NT samples in Figure 4.5). Sea ice thickness reached 120 cm by February 9, completely covering the deepest ice gas samplers. Prior to this date, the bottom-most sampler (D3) measured seawater pCO_2 and was not included in the ice pCO_2 average. In Figures 4.4 and 4.5, the plots are an average of all

samplers, at all depths encased in ice during the DT and NT, respectively. Atmosphere pCO_2 is also included in these figures. Normalized sea ice pCO_2 refers to the ratio of sea ice pCO_2 divided by the atmosphere pCO_2 of that same day. This ratio shows the relative stock of pCO_2 in the ice relative to atmosphere levels and provides a way of comparing relative levels between days without having to worry about variation in the gas sampling analysis associated with uncertainties in GC calibration. Normalized calculations were performed on ice and atmosphere samples that were analyzed in the GC during the same analyzing session. I discuss the test for statistical significance in Section 3.3.3.3, and an example of the process is in Appendix B. In Appendix B, I also examine quality control activities and other environmental factors that may cause elevated or depressed sea ice pCO_2 values. Appendix C examines the effects of the ship on sampling.

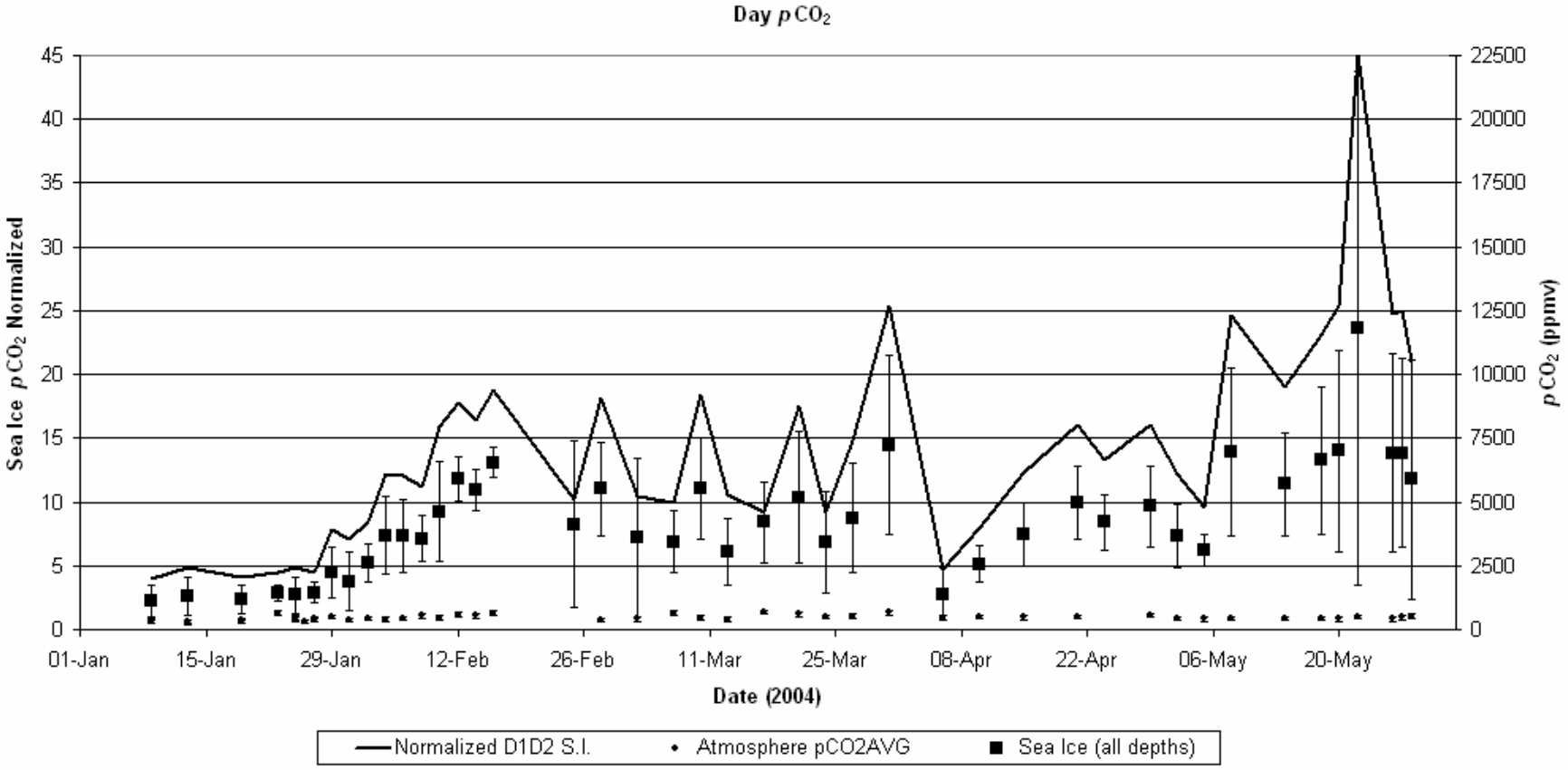

Figure 4.4: The day-to-day variation in *daytime* sea ice pCO_2 at all three depths within the sea ice and air temperature. The (very small) whiskers associated with the pCO_2 average data point represent the ± 2 standard deviation units from the reported average. Normalized sea ice pCO_2 is defined in the text.

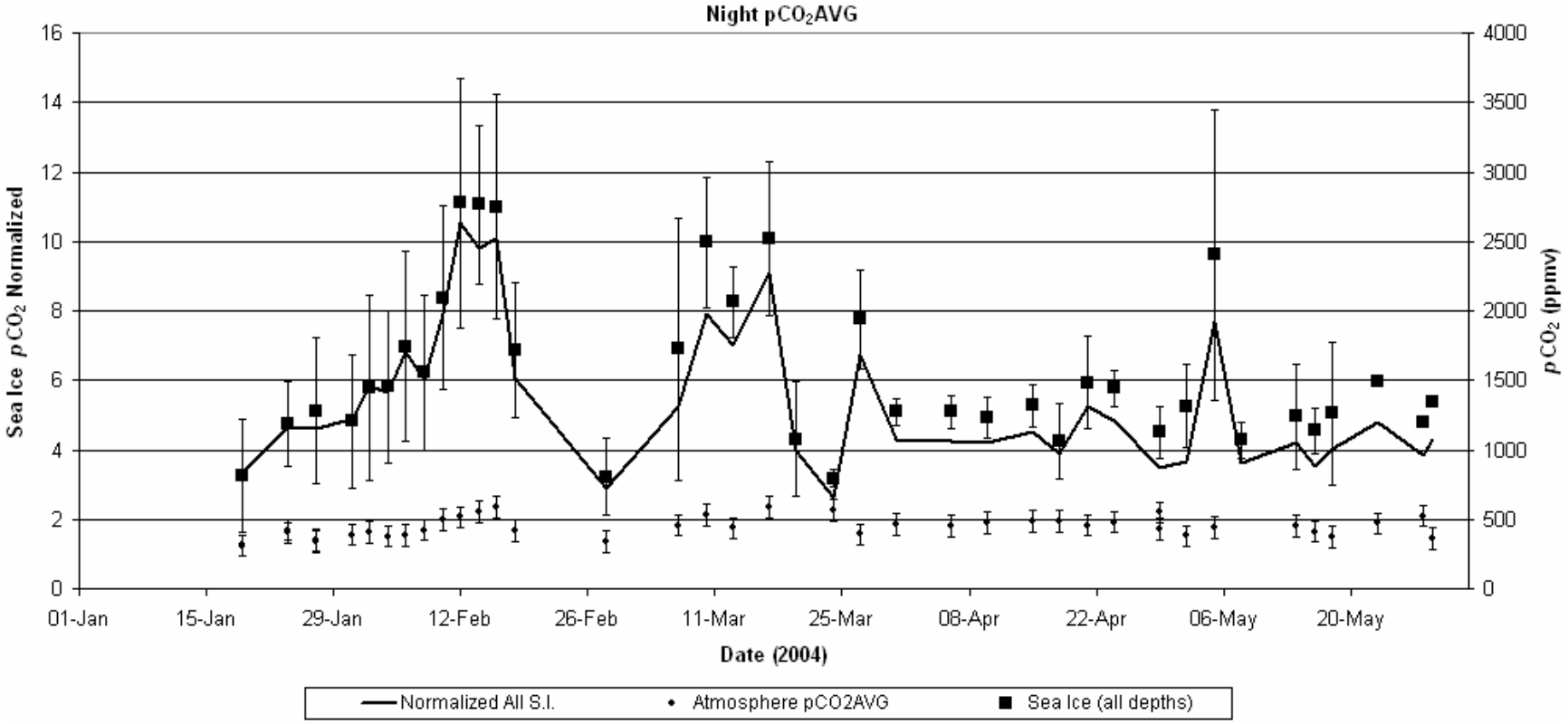

Figure 4.5: The day-to-day variation in *nighttime* sea ice pCO_2 at all measurement depths within the sea ice and air temperature. See description in Figure 4.5 for details.

With few exceptions, DT sea ice pCO_2 was much larger than NT measurements of sea ice pCO_2 by factors of between 2 and 7 over the experimental periods, hence, there is a need for different y-axis scales between Figures 4.4 and 4.5. The immediate observation is that the pCO_2 in the sea ice is much higher than ambient levels. The normalized values range between approximately 2.0 and 5.4 at night and between 2.5 and 24.0 during the day, with mean values of 3.6 and 9.7, respectively for night and day. Three main features are observed in the time series of DT values: a rise of sea ice pCO_2 from January to the end of February; steady, but lower levels in March and April; and a late season rise during the first two weeks of May. The first two features are seen from the NT data, but the end of season rise is poorly defined. On the basis of our observations, the time series can be divided into three periods for discussion of results. The periods are shown in Table 4.1 along with average temperature in the ice for the given date and average DT and NT pCO_2 values.

Sea ice pCO_2 increased from the beginning of sample collection to the middle of February. Daytime pCO_2 increased from 2500 ppm to 10000 ppm, while NT pCO_2 increased from 1400 ppm to 2900 ppm. pCO_2 increased rapidly over seven days, due in part to complete emersion of D3 in sea ice. During this time, the air temperature range was -19°C to -37°C (Figure 4.1). Further cooling occurred between the middle of February to the end of March. The sea ice pCO_2 decreased slightly during this cooling period, from approximately 9000 ppm to 6000 ppm during the DT, while NT samples changed from 2500 ppm to 1500 ppm.

We observed a general lowering in DT and NT sea ice pCO_2 in association with rising air and sea ice temperature during the March equinox. In early April, from the 4^{th} to the 10^{th}, a 25% decrease in DT sea ice pCO_2 was associated with a short period of air and sea ice warming. Between the 10^{th} and 15^{th} of April, the DT sea ice pCO_2 increased approximately 2500 ppmv for the upper two samplers, and approximately 500 ppmv at D3. Nighttime samples experienced a negligible increase of approximately 100 ppmv at each depth during this time interval. Nighttime CO_2 concentrations remained unchanged to the end of May. Subsequent to this observation, the sea ice temperature surrounding the upper two sea ice gas samplers increased by up to 5°C, remaining warmer than –8ºC

over this period. The sea ice temperature around the lowest gas sampler, at 100 cm depth, increased an average of 3.5°C between April 15 and the 25th of May (Figure 4.1). Colder atmosphere conditions returned from April 12 to April 26, however, the sea ice remained warm for approximately 16 days because of the insulation effects of the snow cover. Coinciding with the warmer sea ice and colder air was an increase in sea ice pCO_2 to pre-warming levels. At the beginning of May mild air and sea ice temperatures (up to –6ºC) were observed. On May 22, DT pCO_2 values at D1 and D2 began to increase to values 1.5 times greater than any other time measured in this FYI. Consequently, DT pCO_2 maximums were approximately seven times larger than NT pCO_2 values during May.

4.2.2 Seasonal Periods

The pCO_2 in the ice ranged between 2.5 and 24.0 times ambient air values during the DT and 2.0 to 5.4 times ambient levels at NT. Three periods (P1 to P3) are observed in Figures 4.4 and 4.5: (1) rising levels to Feb 16, (2) decreasing levels between February 17 and May 6, and (3) rising levels from May 7 to the experiment's end (Table 4.1). The first period (P1) occurs entirely in winter. This period is characterized by rapid ice growth and short day length (Figure 4.1). A significant portion of this period (January 9 to 18) was characterized by a complete lack of sunlight (Figures 4.1 and 4.4). Day length reached 7.5 hours by the end of this period. Period two (P2) is marked by the lengthening of the DT period, continued, albeit slower ice growth (Equation 4.1) and the gradual warming of the near-surface atmosphere. February 18 was also when the crew working on this project on the ship was changed. Although precautions were taken for continuity of the project, this marks a time when systematic change in sample collection and analysis may occur. The sea ice temperature dropped over the period until March 13, after which a general rise in ice temperatures occurred with infrequent interruptions. At the end of March another crew change occurred. The third period (P3) was characterized by significant warming of the ice and dramatic increases in DT sea ice pCO_2. One week after the period began, another crew change occurred. By May 25, the ice temperature range was close to –4.5˚C throughout the top 120 cm of sea ice (Figure 4.2).

Table 4.1: Sea ice temperature and pCO_2 characteristics on the start date of seasonal sub-intervals P1, P2 and P3 and end date of P3.

Period	Date (2004)	Sea Ice Temperature (°C)			Sea Ice pCO_2 (ppmv)	
		D1[1#]	D2[2#]	D3[3#]	DT[**]	NT[**]
P1	January 9	-18.00	-9.50	-3.33	3443.8	1903.9
P2	February 17[@]	-18.83	-11.89	-6.38	4534.4	1756.0
P3	May 7[$]	-7.09	-6.44	-5.57	7546.7	1313.0
P3 *	May 25	-4.45	-4.63	-4.20		

1. Depth 1 gas sampler located 20 to 40 cm beneath the ice surface as described in Section 3.2.1.
2. Depth 2 gas sampler located 60 to 80 cm beneath the ice surface (Section 3.2.1).
3. Depth 3 gas sampler located 100 to 120 cm beneath the ice surface (Section 3.2.1).
Value at start of period.
* May 25 is the final date of meteorological data collection from Site G; P3 ends on May 30.
** Average for entire period.
[@] February 18, crew change.
[$] May 14 crew change.

4.2.3 Vertical Variation

The distribution of pCO_2 is shown as a function of the location in the sea ice and seawater in Figure 4.6. Box and whisker plots in Figure 4.6 represent sea ice pCO_2 as a function of depth. The boxes mark the centre of the data and the first and third quartile spread, and the whiskers complete the overall range of distribution of results. This range of the data makes up the inter-quartile range *(*IQR*)*. The lower quartile is the median of all values smaller than the population median; the upper quartile is the median of all values larger than the population median. The whiskers to the right and left the box show the locations of maximum values up to +/- 1.5 × IQR respectively. This dataset has displayed some outliers, usually high maximums. The circles are suspected outliers: 1.5 × IQR to 3 × IQR.

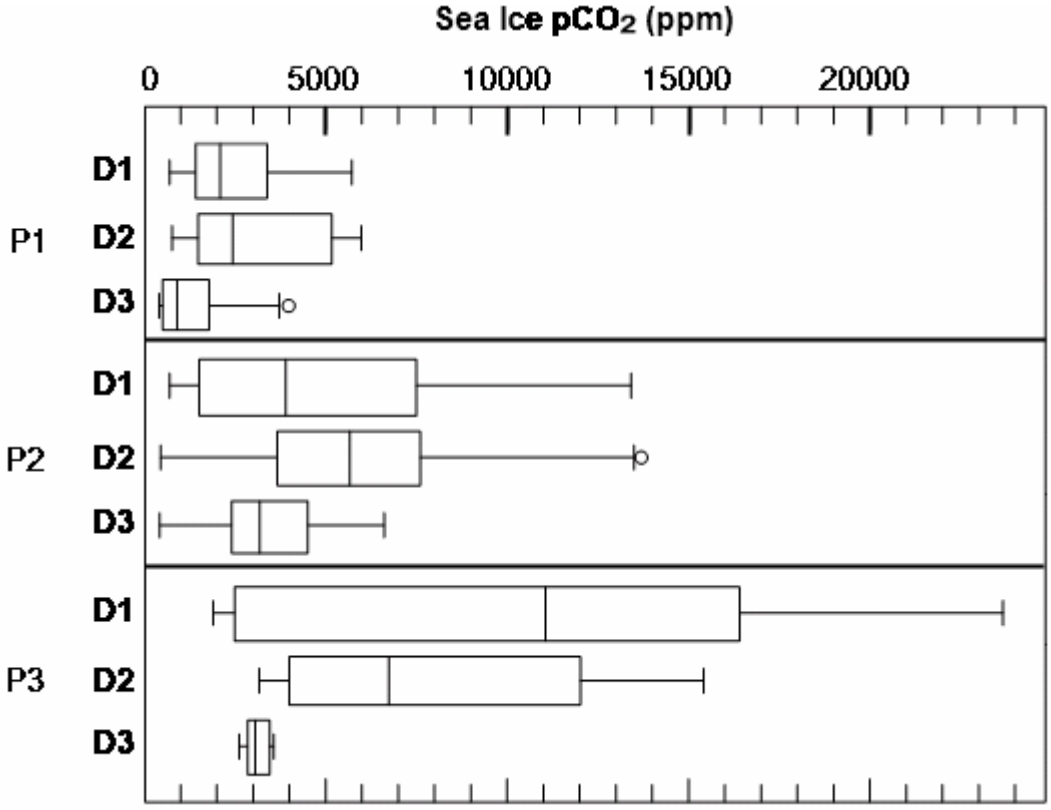

Figure 4.6: DT pCO_2 of three ice depths by period. Boxes represent the 1st and 3rd quartiles around the sample medians and the whiskers represent the 10th and 90th percentiles, respectively.

Immediately, the dynamic range in sea ice pCO_2 among the three depths, and over the three periods becomes evident. The concentration of CO_2 gas measured in the upper two samplers, D1 and D2, were within 7% of each other throughout most of the experiment. pCO_2 at D3 on the other hand was about 40% less than at D1 and D2 on average from complete immersion in sea ice on February 9 until mid-May. The difference between pCO_2 in the DT sea ice environment at D1 and D2 from sea ice pCO_2 at D3 was statistically significant. The test for statistical significance was performed following the ANOVA method outlined in Section 3.3.3.3, and an example of the process is in Appendix B. The upper sea ice undergoes the greatest variation, particularly during P3. Values at the ice surface (D1 and D2) are larger than at D3, and show greater variation. Of note is the small range in pCO_2 observed at the 120 cm during P3. With few exceptions, DT sea ice pCO_2 was much larger than NT measurements of sea ice pCO_2 (Table 4.2) by factors of between 2 and 7 over the experimental periods; hence,

there is a difference in y-axis scales between the two figures. The diurnal variation increased from P1 through to P3.

Table 4.2. Period ratios of DT pCO_2 over NT pCO_2 (DT/NT).

Period	DT pCO_2 : NT pCO_2 Ratio Averaged by Period			
	Depth 1	Depth 2	Depth 3	*Average of Period (+/- St. Dev)*
P1	1.77	2.06	2.28	*2.04 +/- 0.63*
P2	2.71	3.19	2.08	*2.70 +/-1.38*
P3	12.54	4.84	3.11	*7.17 +/-6.42*

In Table 4.2, only days that samples were collected both in the morning and the evening are represented. The value for DT pCO_2 was divided by NT pCO_2 of the same day. A rapid increase in CO_2 concentration occurred over seven days following complete emersion of D3 in sea ice (Figure 4.5 and 4.6). pCO_2 at D3 remained approximately 40% lower for the remainder of the experimental period.

4.3 Ice Chemistry and Associated Seawater and Atmosphere Characteristics

The sea ice pCO_2 measurements at depth were accompanied by measurements of sea ice and seawater A_T, DIC and salinity (refer to Section 3.2). The distribution of sea ice A_T, DIC, and salinity are presented in Figure 4.7 in monthly sections. In the figure, monthly median values for each parameter (A_T, DIC, and salinity) are marked and whiskers have been added to indicate the associated first and third quartiles for each set of measurements. A_T is represented throughout the five months in the figure. In general, A_T profiles in the sea ice did not exhibit the pronounced seasonal change observed in sea ice pCO_2. Ice within approximately 20 cm of the ice-atmosphere and ice-seawater interfaces exhibited greater chemical variation than does the main body ice. Sea ice DIC is represented in the figure throughout March and April, but only the latter ten days of February and first ten days of May (data collection summarized in Appendix A.2). Surface seawater DIC and A_T chemistry evolved in a similar manner and are roughly 5 to 6 times greater than in sea ice. The DIC increased through the experiment with the final two months being statistically different from January's DIC since the error ranges for the

two sample groups did not cross each other. As with the seawater A_T, the monthly increases were greatly, with only March and April not being significantly greater. The test for statistical significance was performed following the ANOVA method outlined in Section 3.3.3.3. The sea ice A_T formed an S-shaped curve in March, but smoothed out to a more vertical line in April, indicating brine movement caused by gravity drainage and increased brine flow due to increasing ice temperature.

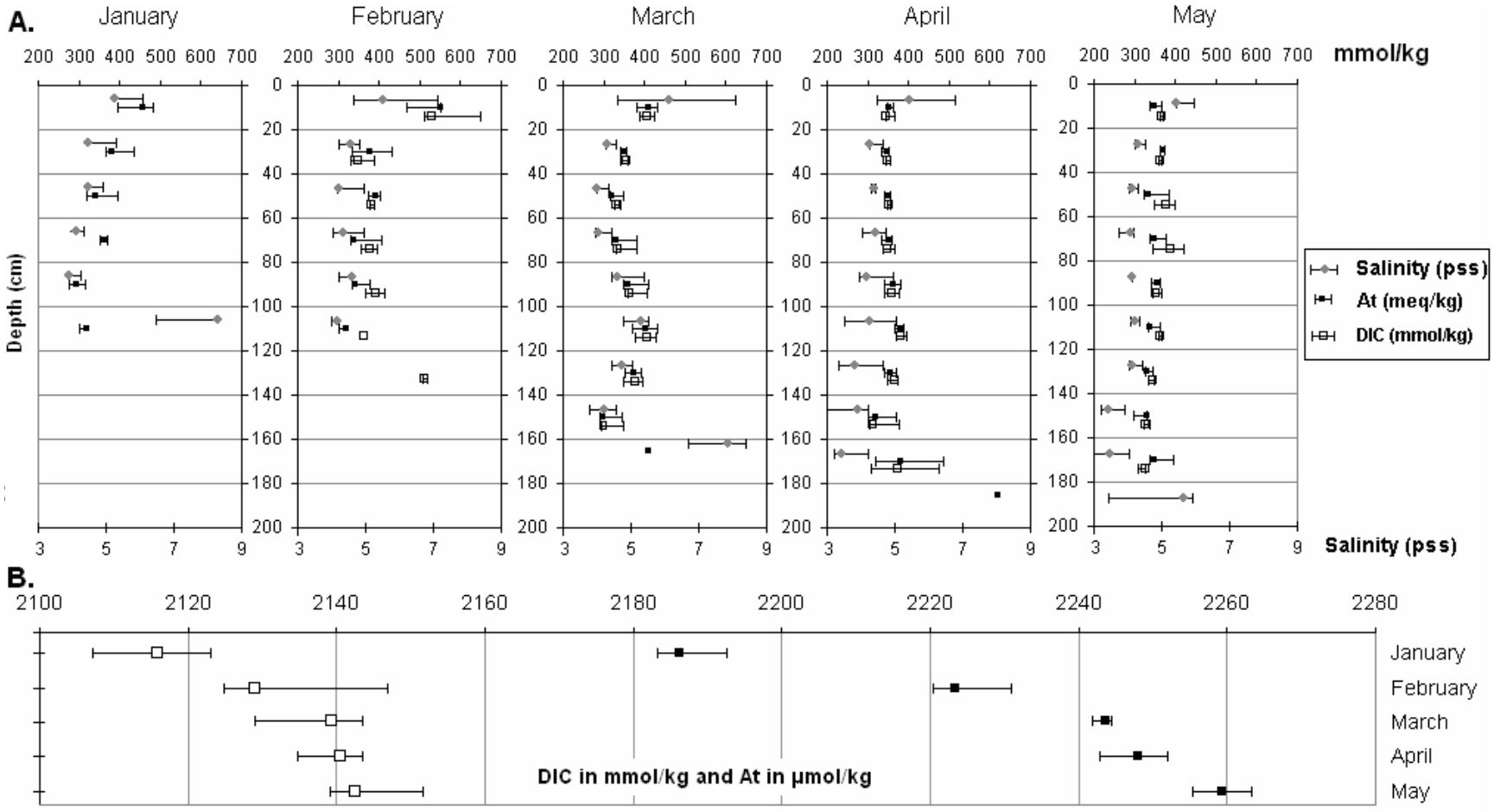

Figure 4.7: Alkalinity, DIC and salinity of sea ice and surface seawater. A. Data from 20 cm sections of sea ice profiles. Data is represented as the median and the whiskers reach to the first and third quartile. **B.** Monthly surface seawater plot of DIC and A_T. Whiskers indicate first and third quartiles. Note: Sea ice DIC measurements were limited to the latter ten days of February and first ten days of May.

A method of determining carbon fluxes to and from a surface is currently the eddy correlation technique. This technique was performed at this study site for much of the time that the above data was collected. In Figure 4.8, hourly atmospheric pCO_2 (— —), as ppm, is averaged over 24 hours. The atmospheric flux of CO_2 (—), measured as grams per square meter per second ($g \cdot m^{-2} \cdot s^{-1}$), is averaged over 12 hours with negative values representing a draw-down of CO_2. Atmospheric CO_2 concentration at the study site was lowest in March and early April. Atmospheric CO_2 at the beginning of the measurement period was approximately 380 ppm CO_2, reached a short-term minimum on the first of April at less than 330 ppm CO_2 with an average minimum of approximately 350 ppm CO_2, finally increasing to 375 ppm CO_2 at the end of May. Based on only 1 data point, seawater pCO_2 at the end of February was (379 ppm CO_2) and therefore greater than atmospheric pCO_2.

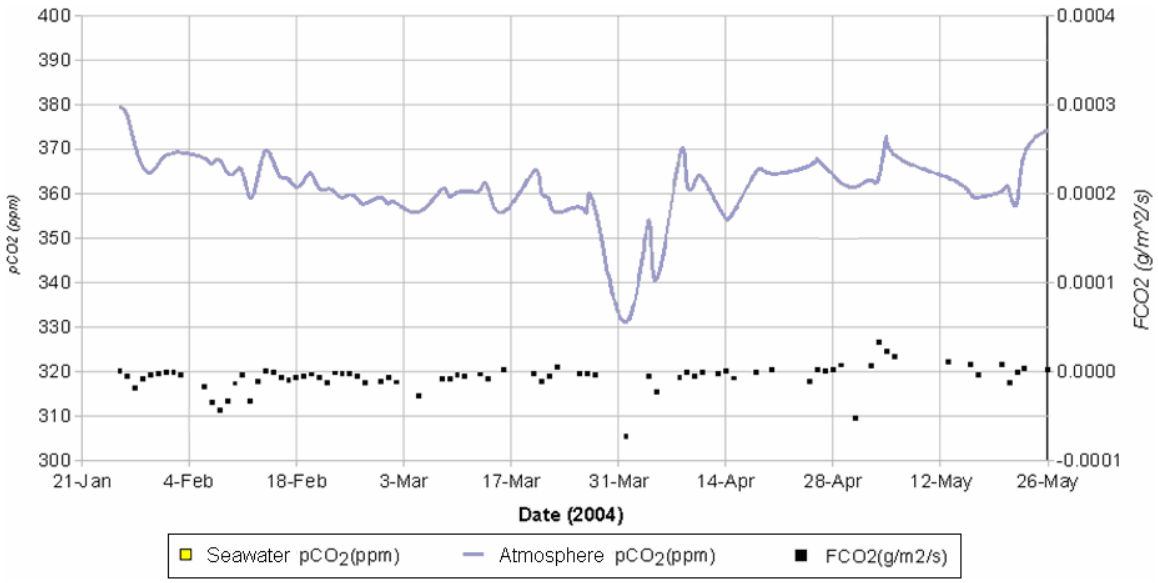

Figure 4.8: Atmospheric pCO_2 and FCO_2 (at 2m) and seawater pCO_2 (at –0.5 cm). Atmospheric (—) CO_2 (ppm) and the flux of carbon (—) measured in the atmosphere ($g/m^2/s$). Negative flux represents downward movement of carbon.

Flux data as measured on the Flux tower shows a near zero flux of CO_2 throughout the winter season with a total downward flow of CO_2 of 63.55 g/m^2, measured during the 126-day period (Table 4.3), or an average uptake of 0.5 CO_2 g/m^2/day for the entire measurement period from the atmosphere to the ice (further breakdown of period

flux rates is in Table 4.3). Long term averages, or totals, are sensitive to small systematic biases in computed flux and therefore care should be taken when interpreting these results. The possibility of flux underestimation (i.e., smaller positive flux or larger negative flux) using the eddy covariance technique with an open-path gas analyzer has been suggested in recent flux research (Burba et al, 2006). The cause of the bias remains unknown. Without independent flux measurements we can not confirm the uptake totals reported in Table 4.3. However, there is nothing in the literature to suggest that episodes of large uptake or efflux should not be real. Large uptake was observed on or around February 8, April 1, and May 2. The spring season uptake periods correspond to times of rapidly increasing air temperature. In the above figure (4.8), the parameter FCO_2 is marked for each 24 hour period, or day, with at least 20 hours of data. Separating the whole season into periods, the largest difference CO_2 draw-down rate was during P1 (0.83 CO_2 g/m^2). During the subsequent two periods, pCO_2 differences decreased by approximately 50% from the previous period (Table 4.3). The change of flux rates coincided with ice thickness growth of 130 cm during P2, and negligible ice thickness changes during P3.

Table 4.3. The CO_2 flux over the ice surface as measured by the eddy correlation flux system.

Period		CO_2 flux x10^{-6} g/m^2/s	CO_2 /day g m^{-2}	Total CO_2 g/m^2
$Total_{AVG}$	Jan. 21 to May 25	-5.839	-0.504	-63.5496
P1	Jan. 21 to Feb. 17	-9.57	-0.8268	-23.0822
P2	Feb. 17 to May 6	-5.085	-0.4393	-34.6884
P3	May 7 to May 25	-2.444	-0.2112	-4.0126

4.4 Summary

Ice temperature responded to variations in air temperature diurnally and on longer scales. Snow cover thickening decreased diurnal to daily temperature variation in the sea ice. After two months of cooling, general warming occurred at the study site. The study spanned a period beginning with 24hrs darkness and ending with 24 hrs of light. Ice

surface PAR exposure variation occurred as a result of solar elevation, hours of sunshine at the top of the atmosphere, weather events, and snow thickness.

The pCO_2 of the atmosphere and water surface are used to further the understanding of the fate of the sea ice pCO_2. Patterns of change in atmospheric pCO_2, seawater pCO_2 (Figure 4.8) and sea ice pCO_2 obtained in this experiment do not match, indicating that the forces of change among the different environments were in different forms at each location. This will be explored further in Chapter 5. General trends of $CO_{2(g)}$ in the sea ice included:

- High values of pCO_2 in the sea ice relative to seawater and atmosphere,
- Differences in DT versus NT sea ice pCO_2 values,
- Variation in sea ice pCO_2 with depth, and
- Seasonal shift in sea ice pCO_2, apparently related to temperature.

Sea ice A_T and DIC were measured in bulk ice samples to monitor changes in carbonate chemistry. Seawater A_T and DIC were also monitored. General trends of seawater and sea ice chemistry observed included the following:

- Sea ice A_T and DIC changed the most in the upper portion of the ice pack (approximately 10-20 cm),
- A decrease in A_T and DIC content in surface ice (i.e. the upper 60 cm) by the end of the experiment was measured,
- Shifts in seawater DIC occurred with time, and
- Seawater A_T patterns did not match those observed in seawater DIC patterns.

CHAPTER 5: DISCUSSION

In Chapter 4 I presented results surrounding the site's general meteorology, climatology, sea ice bulk properties, within and under-ice pCO_2 and basic sea ice carbonate chemistry. Results of note include sea ice pCO_2:

- that was much larger than values observed within the atmosphere and ocean,
- differences between day and night, and
- variation observed over the measurement period.

These results may be explained by considering the theoretical and chemical controls over the pCO_2 in saline solutions in relation to changing atmospheric and sea ice thermodynamics and characteristics. Also, errors in procedures are discussed as measurement and analysis procedures may have contributed to the observed variation.

5.1 Sea ice pCO_2

The primary determinant of climate in the polar regions is extreme variance in solar radiation. The data sets presented in Chapter 4 extend from polar night (where sun is always below the horizon) to 24 hours of sunlight (where sun is always above the horizon), with the transition into 24 hours of daylight occurring on May 15. The response of pCO_2 levels in the upper sea ice (20 to 40 cm beneath the ice surface) to emerging sunlight for both day and night samples is shown in Figure 5.1. Period 1 (Section 4.2.2) occurs entirely in winter, characterized by rapid ice growth and a significant portion of this period (January 9 to 18) was characterized by a complete lack of sunlight (Figures 4.1).

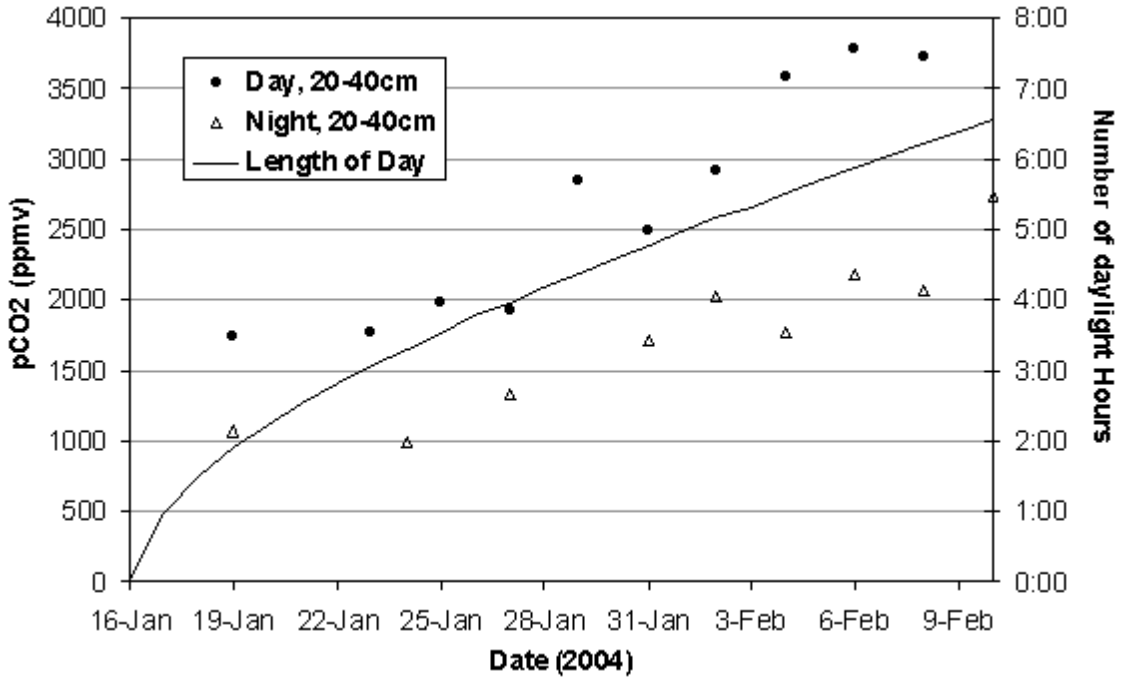

Figure 5.1: 20-40cm pCO_2 vs. length of daylight hours. The seasonal increase in top of the atmosphere sunshine hours and sea ice pCO_2 during P1 (16-Jan and 9-Feb).

Surface sea ice pCO_2 appears to increase with increasing daytime length as the period transitioned away from polar night. Polar sunrise occurred on January 18, 2004 at the study site and day length was 6.5 hours by February 9. The correlation (r) of length of day to both DT and NT ice pCO_2 is 0.953. The strong co-varying relationship between pCO_2 and day length disappeared after February 12. We refer to period before Feb 12 as P1. From polar sunrise to the end of P1, D1 sea ice pCO_2 increased from approximately 1600ppmv to 4500ppmv CO2 in the DT, and 1100ppmv to 3750ppmv CO_2 in the NT (Figure 5.1). The observations suggest photochemical reactions may be occurring in the ice, which can occur independently of temperature (Xie and Gosselin, 2005). The diurnal variability of pCO_2 and solar input during P1 provides a baseline for the sea ice pCO_2 response to solar input. During P1, the D1 sampler measured the least diurnal variability of CO_2 while the greatest changes were measured at D3 (during complete sampler immersion in sea ice).

A study on photomineralization of organic matter in the Beaufort Sea region by Belanger et al., (2006) indicates that photo production of DIC occurred in seawater. Due to similarities in the components of seawater and brine, photomineralization may also occur in ice brines. The observation that sea ice pCO_2 increased simultaneously with ice PAR availability lends credibility to this supposition. The rates of DIC creation in brine compared to seawater will be affected by the availability of source components for the photochemical reactions, such as organic carbon. For example, photo-oxidation of CDOM affects the relationship between CDOM and DOC concentrations in surface waters. One of the products of photochemical oxidation of natural dissolved organic carbon (DOC) is CO_2 (Miller and Zepp, 1995). The results of one simple model (August, in the Middle Atlantic Bight) suggest about 10% of the DOC in the mixed layer was directly converted photochemically to DIC (Vodacek et al., 1997). Also, the lower brine temperatures decrease reaction rates leading to that understanding that though the surface ice has increased PAR availability, the typically lower temperature and loss of ice brine components due to precipitation may prevent further production of CO_2 in isolation of another process.

Day-night differences in sea ice pCO_2 were observed throughout the project. Figure 5.2 displays the ratio of the DT pCO_2 through the entire profile divided by NT pCO_2 of the same day, on days where both day and night sea ice pCO_2 were collected. The DT sea ice pCO_2 is 2 to 7 times greater than NT pCO_2 throughout the experiment. Table 4.2 indicates that the smallest difference between DT and NT pCO_2 measurements within a day was during P1 with DT pCO_2 being 2.70 (+/-1.38) times greater than NT pCO_2. By comparison, DT pCO_2 was 3.04 times greater during P2 and 7.17 times greater in P3. The DT to NT difference increases with increasing daytime lengths from P1 through P3, suggesting that solar radiation and/or temperature plays a significant role in pCO_2 values.

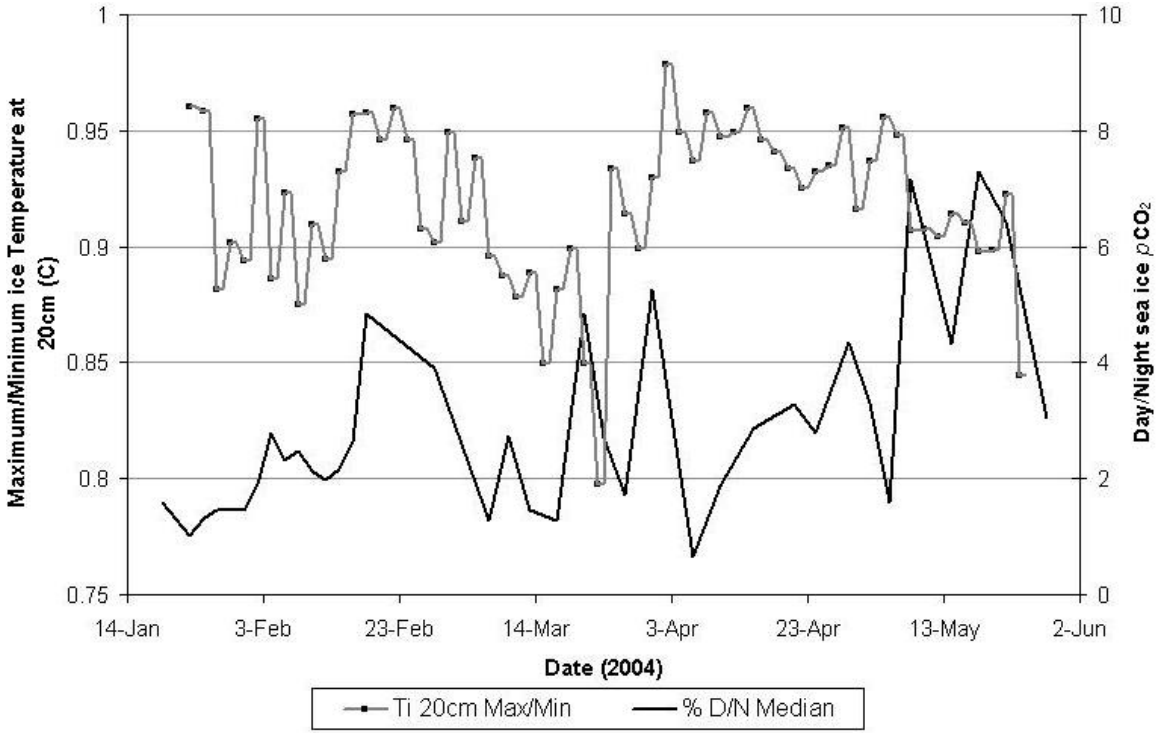

Figure 5.2: Ratio of DT and NT sea ice pCO2 (ppm) as ▬ and upper sea ice temperature (Ti in °C) fluctuations as ▬■▬.

To assist with exploring the effect of temperature on pCO_2, Figure 5.2 compares, the ratio of maximum diurnal ice temperature over minimum ice temperature to the ratio of DT ice pCO_2 over NT ice pCO_2. The ratio of NT over DT temperature at the 20cm depth is 0.92 +/-0.08. (The ratio between DT and NT pCO_2 is the heavier line.) When tested, no significant correlation (correlation coefficients (ρ) in the range of 0.09 to 0.34 for the different samplers vs. time lags to account for heat transport through the ice) was found between sea ice pCO_2 and changes in the magnitude of diurnal temperature changes, over the experiment. However, some similarity does appear in the form of the two curves in the figure, particularly for the period before April 3. No relationship seems present during the period after around April 23, where we see small temperature fluctuations, but extremely large fluctuations in pCO_2 (3 to 4.5 times).

Work on temperature and seawater solute relations (Assur, 1960; Cox and Weeks, 1975; Weeks and Ackley, 1982; Killawee et al., 1998) indicates that ice brine chemistry should respond to changes in sea ice temperature, and indirectly to air temperature. Recall the elevated capacity of colder seawater to dissolve gases such as CO_2. Revisiting

the seasonal evolution of ice temperature profiles from Figure 4.2, Figure 5.3 uses the same data capturing the multi-day to seasonal shape of the gas curves and 20 cm depth temperature in relation to each other. The reverse temperature axis is to illustrate the inverse relationship between the two ice characteristics at temperatures colder than -8ºC, when the relationship is expected to become direct.

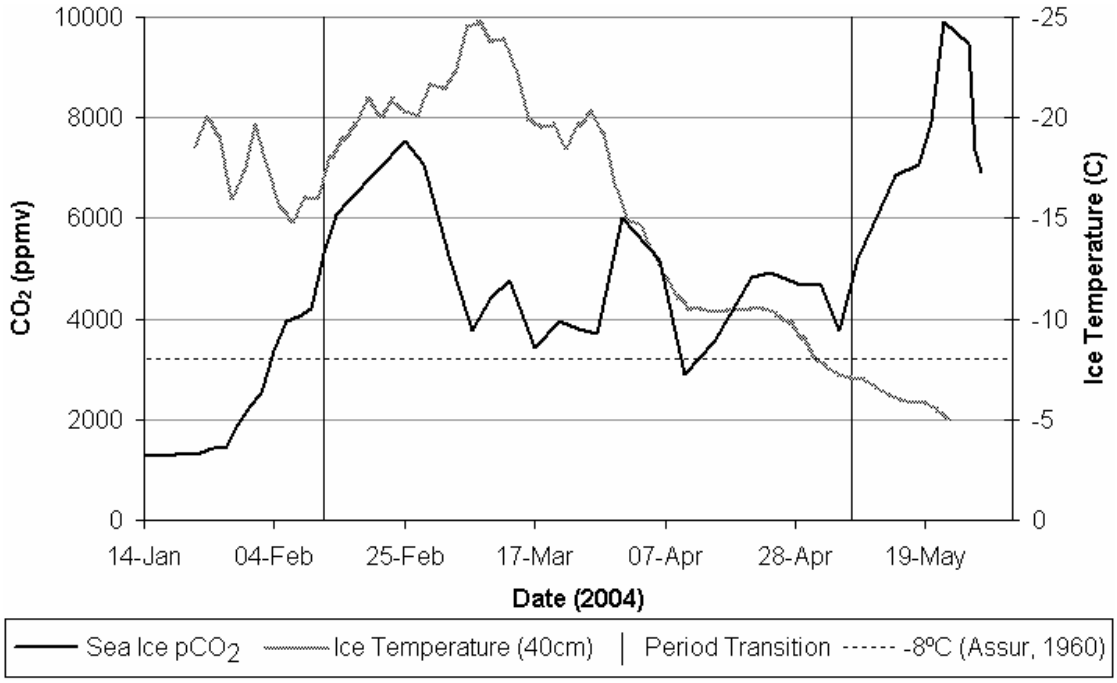

Figure 5.3: Full DT sea ice column pCO_2 and bi-daily average temperature.

In Figure 5.3 the temperature and sea ice pCO_2 curves appear to be related most strongly at the beginning and final half of P2. Period two is marked by the lengthening of the DT, gradual warming of the near-surface atmosphere, and continued, albeit slower, ice growth (Eq. 4.1). If the sea water solubility-temperature relationship holds for high salinity and low temperature solutions (Millero and Laferiere, 2002), then colder brine (cooling sea ice) will not accommodate higher pCO_2, all else being equal. The precipitation of carbonates during cooling should liberate CO_2, in turn, the dissolution of carbonates during warming should consume CO_2 as follows:

$$Ca^{2+} + 2HCO_3^- \rightarrow CaCO_{3(s)} + H_2O + CO_{2(aq)} \quad (5.1)$$

$\rightarrow$ cooling

$\leftarrow$ warming

Equation 5.1 indicates precipitation of $CaCO_{3(s)}$ during cooling releases CO_2 while the dissolution due to warming consumes CO_2. The methods of DIC and AT analysis on core melts would occur when Equation 5.1 was shifted far to the left due to warming and the $CaCO_{3(s)}$ would have heavily re-dissolved. In turn, the method of CO_2 sample collection described in Chapter 3.1, using peepers, would allow for measurements of CO_2 analysis that would point to shifts in the equilibrium.

The third period (P3) was characterized by significant warming of the ice. Temperatures at D1, D2 and D3 were –7.1˚C, -6.4˚C, and -5.6˚C, respectively at the start of the period. By May 19, the ice temperature ranged between –4.2˚C and –4.6˚C (Figure 4.1) in the top 120 cm of sea ice. The final rise in sea ice pCO_2 observed in DT P3 is poorly defined during the NT period. The reason P3 ice temperatures and pCO_2 diverge from the relationship formed in P2 is based on ice temperatures. Recall Assur's (1960) phase change Figure (2.1). The transition from P2 to P3 is marked by the attainment of the -8ºC temperature threshold through much of the sea ice depth. On warming, CO_2 should be consumed in the dissolution of the carbonate salts. Things however don't act in isolation. At this time increasing amounts of solar radiation had been entering the ice. Therefore, photochemical production may be an important factor affecting in-situ sea ice pCO_2.

Due to the ice temperature gradient, two factors lead to differences in brine chemistry observed within the sea ice: varying ice age due to downward growth of ice over a winter season; and temperature differences through the vertical profile (Figure 4.2). The downward growth and further cooling causes chemical and physical changes to occur within the sea ice brine (Lake and Lewis 1970; Jones, 1973; Lepparanta, 1993; Killawee et al., 1998). The seasonal progression of the ice temperature profile (Figure 4.2) displays several features about the ice's changing temperature. The figure shows the variation of ice temperature over a short vertical distance and temporally during the course of the season. Brine mobility in growing ice relocates brine constituents under

two conditions: in the warm growing ice at the base of the pack, and the cooling mid-to-upper ice layer. The brine of the older ice that is closer to the air-ice surface has had an extended opportunity to evolve chemically. This ice is colder than the lower and newer sea ice layer. Figure 5.4 shows the change in absolute salinity and percentage alkalinity between layers with brine drainage from January to May. In the figure, ice cores from February 2 to the end of P1 were used to produce an average alkalinity profile for P1. Ice cores collected throughout P3 were used to produce an average alkalinity profile data for P3. A decrease in salinity and alkalinity should be observed over the ice profile (Perovich and Elder, 2001). In Figure 5.4, a difference in total saline and alkaline composition from the beginning of the experiment and the end of the experiment is shown. The change is calculated as the difference in amount of AT between January and May (i.e., ATMay - ATJanuary) and expressed as a percentage along the upper x-axis and salinity as pss on the bottom x-axis. Calculations for Figure 5.4 end at 120 cm deep because of limited ice thickness in P1. The alkalinity and salinity measurements were performed on melted bulk ice samples, leaving the in situ dissolved solute volume in the brine solution unmeasured in this experiment (Section 3.3.2.2). Brine analysis alone provides alkalinity data unique to the ice temperature at the point of extraction. Point temperature and salinity data can be used to determine brine volumes using methods devised by Cox and Weeks (1983). Although we can calculate brine volumes, original composition of source seawater, relocation of brine constituents, and the solutes known to exist in brine at various temperatures (Assur, 1960), it is difficult to estimate the salt composition of brine. The following data discussion includes all A_T dissolved in the brine solution and precipitated on the brine channel/pocket walls. The upper 60 cm of the ice cover underwent two to three times greater changes in alkalinity and salinity from January to May than the lower 60 cm of ice.

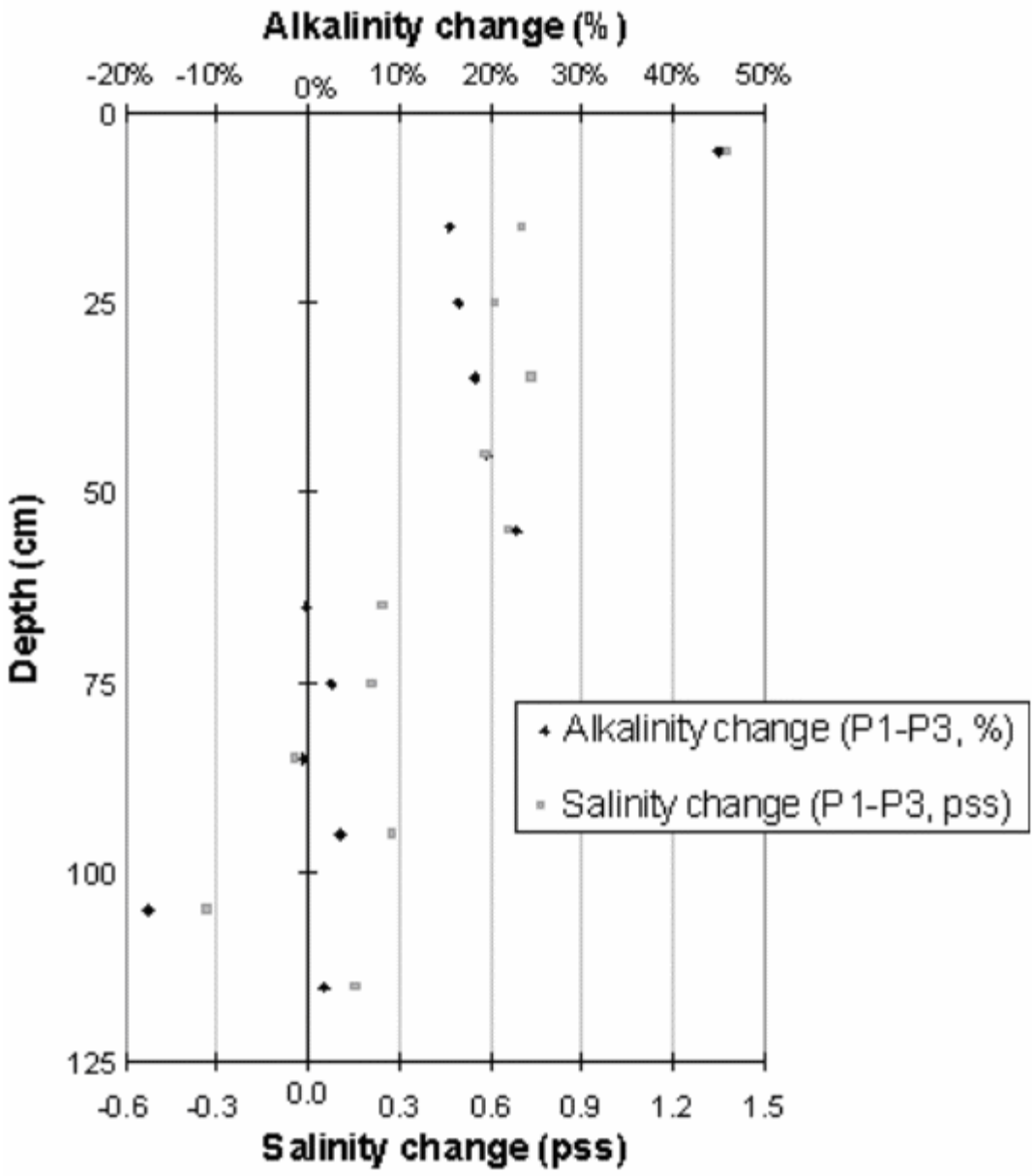

Figure 5.4: P1 to P3 alkalinity and salinity changes in bulk ice cores. Changes in absolute salt content (▒) and alkalinity percent (♦) of the sea ice from P1 to P3 by depth. The right hand side of 0%/0pss indicates loss of solute from P1 to P3.

Flushing from surface melt ponds had not occurred by the end of the experiment. This contributed to the fact that salinity and alkalinity did not completely wash away into the seawater below by the end of measurements. Had the experiment extended longer into the spring season, further solute loss should have been seen in the sea ice due to elevated rates of brine drainage at temperatures above approximately -5ºC (Golden et al.,

1998). At the beginning of P3, D1 and D2 reached –8°C, and the ice at D3 had been warmer than this for 21 days. The extended period of warmer conditions in the ice at D3 would allow for greater mobility of AT components than for the upper two samplers (Cox and Weeks, 1975; Eide and Martin, 1975). The uppermost gas sampler, D1, was placed in the portion of sea ice that experienced a greater loss of alkalinity (16% to 18%) and salinity (21% to 25%, Figure 5.4). At D2 similar changes occurred in alkalinity and salinity (both 22%). Both temperature and pCO_2 were similar at D1 and D2, except for alkalinity at these depths in April. Therefore, only small changes in the bulk sea ice solute volume was observed of during this project in concurrence with the high changes in sea ice pCO_2.

Experimental work by Assur (1960) and more recently by Marion et al., (1999) shows that the precipitation of salts in cooling brine occurs along a sequence. This can mean that mobility of each salt is different at each temperature. Upon cooling, the carbonate salts, which tend to precipitate first, leave a large proportion of the salinity components in solution for a greater range of temperatures (Weeks and Ackley, 1982). Because the mobility of the brine and the salt precipitate need not be the same (Rysgaard et al., 2007), brine movement provides a mechanism for the separation of the DIC components. Both the amount and chemical composition of brine can change spatially across the ice profile and temporally at any position in the ice. This is because brine mobility increases with increasing temperature and the sea ice is exposed to a persistent temperature gradient and subject to temperature fluctuations (Untersteiner, 1968; Eicken, 1992). For these reasons we should not expect an identical temperature— pCO_2 relationship at each of the three sampling depths.

As seen in Figure 5.4, rates of solute content change are different between alkalinity and salinity, suggesting that brine solutes travel at different rates. Specifically, the components that make up alkalinity (the carbonates) comprise a portion of the components that make up salinity. The additional components that make up salinity are the non carbonate salts NaCl, as the ions Na^+ and Cl^-. Figure 5.4 shows a decrease in ice alkalinity occurred in the upper 10 cm by as much as 44.5%. The portion of the sea ice from 10 cm to 60 cm that included the sea ice gas sampler D1 (20-40 cm, Chapter 3.2.1),

showed alkalinity losses from 16% to 22%. The location of the bottom two samplers, below 60 cm to as deep as 120 cm, did not measure significant decreases in alkalinity content during the determination of alkalinity difference. The changes were below 5% and not seen as significant when compared to the much greater changes in alkalinity that were over 15%. Measured differences between these bottom two depths were below 4% and therefore probably insignificant. Sea ice pCO_2 changes by depth were not in concurrence with changes in the sea ice alkalinity. Recall from Chapter 4.2.3, D1 and D2 sea ice pCO_2 values were established to be within 7% of each other through the experiment, while the AT of the sea ice behaved differently. Meanwhile, D3, which typically measured 40% lower pCO_2 by volume than D2, actually saw an increase in alkalinity through the experiment (Figure 5.4). Contrary to the profile of sea ice pCO_2 data (pCO_2 at D1 and D2 similar, yet different from D3), it appears (Figure 5.4) that D2 and D3 are in a zone that experienced similar changes in sea ice chemistry, but different from D1. The ice at depth 100 cm to 115 cm (gas sampler D3) increased in alkalinity by 18% from the start to end of the experiment. The earliest samples measured at this depth were the bottom 10 cm of the ice pack, which is typically at a level of elevated salinity given a characteristic C-shape salinity distribution in first-year sea ice (Ono and Kasai, 1985). For much of the season, D3 was at or near the temperature (-4ºC to -12ºC) established by Assur (1960) where carbonate phase changes begin. Therefore, ice growth will have affected the salinity and alkalinity levels across the experiment.

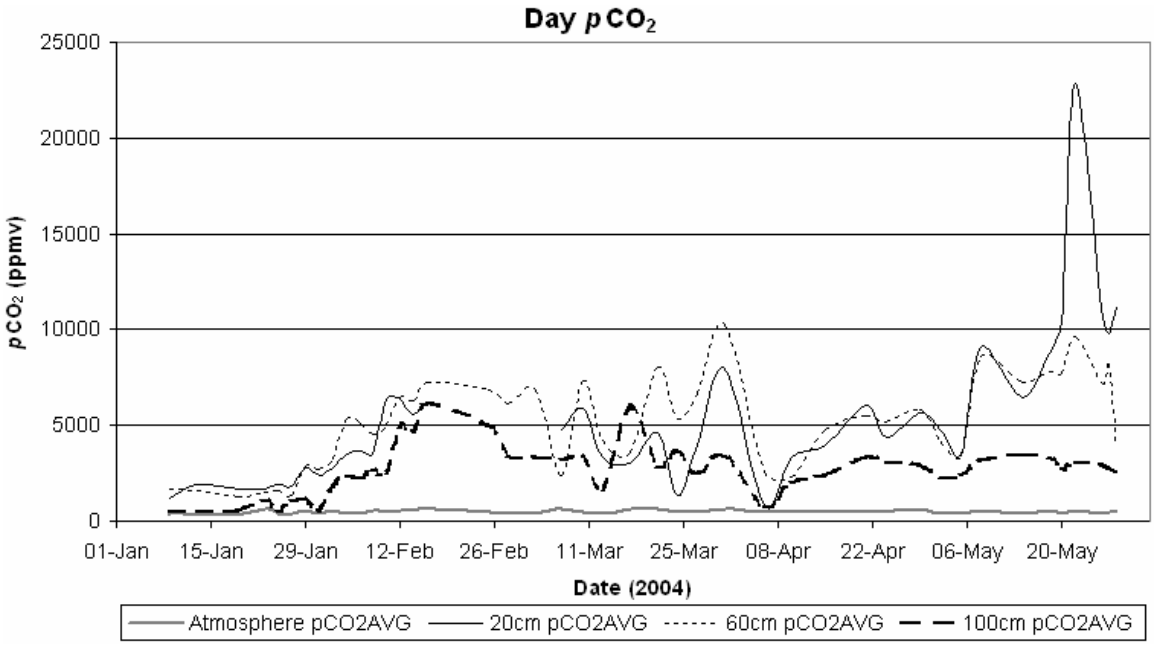

Figure 5.5: Daytime sea ice and atmosphere pCO_2 (ppmv). Upper two gas samplers D1 and D2, indicated by solid thin lines, meanwhile D3 is represented by a dashed thick line.

Correlation calculations were performed for ice pCO_2 vs. temperature at every hour from 12 hours before sample collection to the time sample collection occurred, without improved R^2 values. There is not a strong mathematical correlation between sea ice pCO_2 and sea ice temperature, despite the observed association in Figure 5.3. This reminds us to keep in mind that carbonates phase changes play a role in the dissolved gas content in the brines. The poor statistical association may be attributed to several factors. For example, the samplers closest to the surface measured greater pCO_2 fluctuation in accordance to atmospheric temperature, while the deeper samplers saw smaller diurnal changes (Figure 5.5). The upper two samplers' pCO_2 were in ice that responded more quickly to air temperature. The temperature profile within the sea ice is affected by the heat budget at the upper and lower boundaries with the atmosphere and seawater respectively (Figure 4.2), as well as the thermal properties of the ice. Meanwhile, the bottom sampler, D3, was under different temperature conditions causing the different pCO_2 response observed. Thus, correlation calculations across multiple depths have not produced meaningful results. In fact, D3 had spent most of the experiment in conditions between –8°C and –12°C, partially explaining the perpetually lower gas concentrations measured. The D3 sampler also exhibited a smaller seasonal range and diurnal

fluctuation of temperature and pCO_2 than the upper samplers. Also, the response time of the gas sampler to the sea ice temperature is experimentally unknown for these conditions.

5.2 Sea Ice pCO_2 and Connection among the Air-Ice-Sea Systems

Irrespective of the surface state and characteristic (ice cover or water), the near surface flux of CO_2 is driven by the gas concentration gradient. Sustained uptake requires a carbon sink and observed loss requires a source. It is interesting that our measured fluxes were largely directed from the atmosphere to the surface, whereas the sea ice pCO_2 concentration is far in excess of atmospheric values, which would otherwise drive large CO_2 transfer rates from the sea ice into the atmosphere. The eddy correlation may be prone to a small underestimation in the flux (Burba et al., 2006), however, there is nothing in the literature that would suggest that the system would miss a strong sustained upward flux under the cold conditions that were experienced during the CASES experiment. Irrespective of biases in the flux, the measurement of atmospheric CO_2 concentration with the open path sensor should be both precise and accurate within the sensors operating temperature range (-40°C to 0°C). From P1 to several weeks after the transition to P2, the decreasing atmospheric pCO_2 coincided with increases in sea ice pCO_2. The sea ice pCO_2 decrease that was observed in P2 corresponded to a period of relatively unchanging atmospheric pCO_2 (Figure 4.4, 4.5 for sea ice pCO_2 and Figure 4.8 for atmospheric pCO_2). During this period, there was a small net transfer of CO_2 (0.44 g/m2/day) from the atmosphere to the ice (Table 4.3). If the flux is legitimate, then two scenarios may be in play. One, the carbon is further transported to the surface seawater through downward brine flushing. Two, though the sea ice pCO_2 is decreasing, the thickening ice and increasingly cold temperatures create an environment where CO_2 may be captured the brine during carbonate precipitation (Rysgaard, 2007). Brine content and mobility are dependent on ice temperature and cooling conditions increasingly limit both brine content and mobility (Cox and Weeks, 1983). These scenarios affect the sea ice permeability.

Coinciding with downward gas flux in P2 is an observed increase of ice pCO_2 (Figure 4.8). The upper ice at this time is still fairly cold in the upper 50 cm. But the ice had just undergone a brief period of warming, having reached between -8°C and -12°C throughout each gas sampling depth, increasing brine mobility. During the final week of P2, the atmospheric CO_2 concentration remained within a narrow range and a net flux of CO_2 toward the atmosphere from below was measured. The ice had undergone further warming at this time of approximately 2°C to 5°C at the lowest and highest samplers respectively to -6 to -7ºC. At the onset of P3, the atmospheric CO_2 concentration measured by the IRGA decreased by 10ppm, coinciding with the increase in DT pCO_2 in the sea ice.

The large temporal changes in the sea ice pCO_2 are not reflected in the air-surface exchange of CO_2. Instead, the changes must be related to processes occurring within the sea ice, including the transformation of pCO_2 into and out of the other components of DIC, and perhaps biological processes. Semelitov et al. (2004) suggested that biological processes may be responsible for some sequestration of CO_2 from an atmospheric source may be incorporated into the sea ice, acting as a biological pump.

Original assumptions regarding the impermeable nature of sea ice are based in part on biological studies. For example, an early study by Zubov (1945) measured FYI, in comparison to atmospheric air, lower oxygen, higher carbon dioxide, and similar nitrogen gas concentrations were found in these pockets. At the time, Zubov concluded that sea ice was impermeable to gas flow and these observations were due to biological activity.

The Zubov study has been followed by many others (for example, Goto et al., 2000; Thomas and Dieckmann, 2002a; Krembs et al., 2002; Trevena et al., 2003; Carpenter, et al. 2000; Johnston, et al., 1991; Price, 2000) that have shown that biological activity occurs in sea ice. Other environmental factors such as light and nutrient availability means that biological activity was not constant throughout the experiment. In fact we would expect primary productivity to have increased particularly near the end of the experiment as the light availability increased. We know this because basic life-forms

such as bacteria, algae and virus have been observed to varying degree within sea ice. For instance, changes in the seawater carbonate chemistry are expected to affect the production of marine micro algae. The ratio of calcification to photosynthetic C fixation has decreased with increasing pCO_2 from pre-industrial levels (270 ppmv) to current values (Wigley, 1983; Barnola et al., 1991; Etheridges et al., 1996). In contrast to plant photosynthesis, which results in net CO_2 decrease in surface seawater, marine animals produce a net increase in CO_2 as they breathe. As with the absorption of $CO_{2(g)}$ by seawater, free CO_2 released during respiration reacts with water/brine producing carbonic acid (H_2CO_3), resulting in a lowered seawater pH. This additional C input follows Equations 2.1, 2.3, and 2.5, in that order. The respired CO_2 can be expelled from the seawater if saturation and a route of escape exists. Otherwise, it is re-used by primary producers or continues to Equations (2.1) and (2.3).

5.3 Implications of Measurement Uncertainty

The method of extracting sea ice pCO_2 used here is new and experimental. Thus, the technique requires further thought and modification to attend to issues discovered during its implementation. Issues involved with the gas sample collection and analysis are discussed under two categories: measurement bias, and sample collection bias.

5.3.1 Measurement Bias

5.3.1.1 Wind and the Measurement of Atmospheric CO_2 Concentration

The possibility exists for the ship's exhaust to contaminate the samples that were pulled from the atmosphere. The sea ice pCO_2 sampling sites were located on a compass bearing 74º from North of the *CCGS Amundsen*. Wind coming from the sector between 287º and 301º will first travel over the *CCGS Amundsen* before arriving at the sampling sites, potentially carrying stack effluent with it. The C1 sea ice pCO_2 sampling location site was located 1450m away from the Amundsen with C2 located another 1250 m from C1. Atmospheric pCO_2 was collected by workers at these sites (Chapter 3.2.1) for analysis by GC (Chapter 3.3.1). Therefore, under some conditions our air measurements

for pCO_2 may be affected. In total, eight sample days have been removed from the data batch (Appendix C).

Other anomalously high atmospheric pCO_2 measurements may have been associated with stable atmosphere conditions caused by low wind speeds. Air inversions are common over cold surfaces (Oke, 1987), particularly when wind speeds are low. Under such conditions, the effluent from the ship may pool and spread out along the surface. Air inversion and low wind speed made it possible for the ship's exhaust to be low lying and within the region of drawing of bulk atmosphere samples. High wind speeds possibly alleviated this issue. Human respiration may be a source of error on days with low wind speed. Here (Appendix C), low wind speeds are considered to be less than 2 m/s. Caution was taken by each worker during sample collection to prevent exhaled breath from entering the sampling receptacle. High pCO_2 values coinciding with wind direction/speed combinations that could bias measurements have been identified (Appendix C).

5.3.2 Time, temperature, pressure, and analysis modification

5.3.2.1 Physical Pressure: Vacuum induced in silicon receptacle and over pressurization in the GC

Atmospheric pressure has an affect at sample collection (Equation 3.1) and analysis. One, drawing of a sample from the Si tubing within the sea ice will induce a negative pressure within the Si chamber. Our analysis assumes that the tube is in equilibrium with the surrounding environment. However, low pressure is created by drawing air from the tube. The decreased pressure would alter the balance of the chemical equilibriums within the ice. Returning to Equations 2.1, 2.3, and 2.5, if the gaseous components are decreased in the system, the equations would shift to return to equilibrium for the given temperature conditions. Two, the process of sample analysis of pCO_2 samples by GC is dependant on barometric pressure and temperature, both parameters have a part in the ideal gas law (Equation 3.2). The process of correcting for pressure is described in Section 3.3.1.1.

5.3.2.2 Time of day sample collection

Sea ice pCO_2 measurements were made from samples collected in the morning and the evening for comparison of day-night processes. The terms day and night are perhaps more reflective of low and high sun angle given that part of the experiment occurred during polar summer (24 h with the sun above the horizon). The time when samples were collected in relation to sunrise and sunset varied throughout the experiment, which does complicate a day versus night comparison. The sampling schedule was also affected by other factors, including the schedule of other scientists (sampling required two individuals) and weather. Samples were typically collected between 9am and 10am for night samples and 6pm or 7pm for morning samples.

5.3.2.3 Effects of the Silicone Chamber

Questions surround the use of silicone for chambers, given that CO_2 is a product of a silicone photo reaction (H. Xie, pers. comm., 2004). An experiment was performed to determine if this was an issue in our settings. For the experiment an Si chamber was sealed in a glass container connected to a LI-COR closed path IRGA for 96 hours exposed to full sun conditions in about -5 to -15°C weather. The experiment did not produce results indicating the internal environment of the silicone chamber was being altered. The maximum daily variation of CO_2 concentration measured within the glass container was +/10 ppmv CO_2 from the mean concentration of CO_2 within the container. This is well within the expected variation of the instrument. Further, the results from the GC of sea ice pCO_2 did not follow a pattern that could be attributed to the volume of light that reached the chambers throughout the experiment.

The silicone membrane was selected for its permeability to CO_2 and ability to withstand the harsh Arctic environment. The C-Flex was selected to allow access to the in-ice gas from the surface via an impermeable conduit. The C-Flex[18] is listed as being impermeable to CO_2. The material is slightly permeable to O_2, making it possible to change the concentration of the gases within the chamber when pressure is changed.

[18] C-Flex product specifications webpage: http://www.masterflex.com/techinfo/techinfo.asp?htmlfile=Tubing_Cflex.htm&id=762

Although should be minimal because the Permeability to several gases through the Si chamber walls is much greater than just O_2 through the C-Flex walls.

5.3.2.4 GC Specific Issues: Standards, Water Traps and Sample Carry-over

The calibration process enabled the investigation of results produced by the three different loop volumes (Appendix B.1). An estimation of drift in the instrument by various analysis periods was conducted using calibration data from the beginning and end of each analysis series (Appendix B.2). Analysis by the GC of a CRM valued at 412 ppmv CO_2 (Section 3.3.1.1) resulted in an observed variation of +/- 40.3µl L^{-1} pCO_2, or 40.3 ppmv, over 10 iterations. Figure D.2 shows atmospheric pCO_2 results from both the GC and the MET tower IRGA. Table 5.1 lists basic statistics of GC and IRGA analysis. In Table 5.1, the IRGA, DT GC and NT GC columns list the average of good atmospheric pCO_2 samples analyzed with their respective instruments. The DT and NT columns show the average and median differences between atmospheric pCO_2 results produced by the IRGA and GC (for DT and NT). For further details on IRGA and GC analysis see Appendix B.

Table 5.1: Statistical analysis of IRGA and GC data and differences between the measurements analyses.

	IRGA (ppmv)	DT GC (ppmv)	DT (GC – IRGA)	NT GC (ppmv)	NT (GC – IRGA)
Average	361.71	503.30	140.86	481.09	118.92
St Dev (of the average)	7.11	85.37	87.16	87.98	89.46
Median	361.37	488.44	129.45	471.38	110.88

Three configurations of water trap were used at the GC injection port for this project (Chapter 3.3.1). The water trap was used to dry the gas entering the GC system to prevent H_2O from affecting the results and to increase the longevity of the TCD detector. The water trap consists of a tube packed with a water absorbing dessicant with minimal absorption of $CO_{2(g)}$. The principle cause for elevated pCO_2 results when using a water trap would be the occurrence of trapped gas within the water trap and loop column.

Proper flushing of the previous sample may not have occurred when pushing a new sample through the trap. A majority of atmosphere samples were run immediately after a sea ice sample because three times more sea ice pCO_2 samples with high CO_2 concentration were analyzed than atmospheric samples. An injected sample would flush the water trap as well as fill the injection column. This was noted by the worker as increased resistance placed against the plunger during sample injection.

There exists a problem in chromatography with contamination from high sample volumes carrying over into subsequent analyses of low sample volumes. This issue was not quantified. Sample carry over could very well be an issue with our lower concentration samples, such as atmosphere samples, particularly since some of the ice samples were so very high. Therefore strong suspicion is placed on any air sample run right after a high concentration ice sample. The issue appears to be alleviated with the standard gas calibrations, because the loops were well flushed. This issue is compounded when the water trap is in use.

Samples analyzed in January and February were not pushed through a water trap. Subsequent samples from the end of February, March and early April were pushed through a water trap approximately 15cm long and samples analyzed during the remainder of April and May were pushed through a shorter, 3cm, water trap. The water traps were not always used for CRM analysis. We are unable to asses the effect of the water trap on pCO_2 analysis of sea ice samples. Table 5.2 uses normalized atmospheric pCO_2 data. The GC gas data was normalized against the IRGA data to account for seasonal drifts in atmospheric pCO_2. From the data in Table 5.2, it appears that there is a noticeable increase in atmospheric pCO_2 measurement using the water trap. The use of Q1 (quartile 1), Q2 (quartile 2) and the IQ (inter-quartile) range in Table 5.2 is described in Appendix B.1 where similar data analysis is used.

Table 5.2: Atmospheric pCO_2 output during use of various water trap arrangements. Median output value when the GC was run with no water trap, a long trap and a short trap.

Trap type	Median pCO_2	Q1 pCO_2	Q3 pCO_2	IQ range (Q1 to Q3) pCO_2
No trap	1.17	1.11	1.36	0.25
Long trap	1.38	1.33	1.60	0.27
Short trap	1.30	1.20	1.36	0.16
No trap/ Short trap	0.906	0.922	0.996	

To ensure an unbiased consideration of this issue, this discussion includes atmosphere samples deemed not affected by error factors such as contamination by ship's exhaust, worker breath, and questionable calibration (reviewed in Appendix B). The April and May samples run through the short water trap produced a median value 16.6% greater than samples that were not run through the trap. As a result of the elevated water trap results, atmosphere pCO_2 measured in the GC using a water trap that were outside the IQ range of the no trap samples have been omitted from the analysis.

5.4 Further discussion

The results of this investigation indicates that

- pCO_2 levels in FYI brine are far in excess of atmospheric and sea water levels,
- DIC and A_T values in the under-ice seawater are greater than in the sea ice, and
- FYI DIC and A_T vary from the winter to summer periods.

The observed changes in sea ice pCO_2 appear related to environmental factors, including solar radiation and temperature, although the exact nature of the relationships is not yet known. Solar radiation may drive photochemical reactions in the sea ice brine involving organic material and dissolved CO_2. Temperature and temperature variation affects phase equilibrium within the sea ice brine and brine solubility, the former affecting dissolved CO_2 concentrations through the formation and dissolution of carbonate minerals. An air-sea ice exchange of CO_2 was measured and largely directed to the surface, although this direction is opposite to the direction that would appease the

observed air-surface difference in pCO_2. Apparently, the pCO_2 measured in the sea ice is not readily available for transport with the atmosphere, as suggested by our flux measurements. The sea ice DIC and A_T decreases between stages of the spring transition, presumably in response to downward brine flushing. Brine migration is the agent coupling the atmosphere and ocean in the presence of an ice cover. Observed and predicted reductions in the Arctic sea ice perennial cover point to the conclusion that an increasing proportion of the sea ice will be FYI. Thus, one may expect the surface heat and gas fluxes to be altered as the ocean's surface changes. Unique to the ice cover is the ice's ability to store high volumes of dissolved CO_2 in the brines and presumably deliver dissolved CO_2 to the seawater below. It has been observed that the sea ice colder than –8°C behaves differently that that warmer than –8°C. To account for the differences and changes in brine solute content spatially and temporally future sea ice brine CO_2 solubility modelling considerations include brine migration rates. Brine CO_2 solubility is dependent on temperature and depth within the sea ice at which the atmosphere has free influence over the sea ice. In other words, it will be meaningful to determine a slope for the pCO_2 gradient from the atmosphere to the 20cm depth within the sea ice.

Models of future sea ice coverage indicate a decrease in sea ice surface coverage in the near future. The possibility that FYI coverage may decrease will decrease the proportion of seawater that becomes brine, resulting in less liquid draining into the surface seawater under FYI. The high salinity/alkalinity brine has the potential to carry large volumes of $CO_{2(g)}$ and dominates FYI export to seawater by volume during growth and early melt. This high saline water is very dense and sinks, carrying dissolved CO_2 down with it (Rudels and Quadfasel, 1991; Rudels et al., 1996). As demonstrated in this experiment, this contributed brine has the potential to be $CO_{2(g)}$ rich. With its coolness and high density there is potential for removal from the surface seawater to deeper waters (Anderson et al., 1990). As forecasts predict, sea ice is becoming thinner. Thinner ice, under exhibits steeper temperature gradients under cold atmospheric temperatures (over the relatively warm seawater). Though the gradient does not contribute to elevated pCO_2

in sea ice, this condition will result in less ice thickness to attain the high levels of pCO_2 observed in the colder sea ice in this experiment.

5.5 Conclusion

These experiments were designed to build on the work completed previously on the geochemistry of FYI. Based on the theories developed in the earlier work of such researchers as Cox, Eicken, Gosink and Kelly, Kammann, Kier, Papadimitriou, Papakyriakou, Miller, Semiletov, and Weeks, a discussion with our results was possible. The methods described in Chapter 3 lead to results that indicate:

- One would expect solubility of $CO_{2(g)}$ in FYI brine to be related to temperature, as is the case in seawater. Evidence that this is in part true was shown in the results.
- Mobility of salinity, and more importantly in this report, carbonate constituents of ice brine varies within the ice pack. This may explain in part the variability of absorbed gas content within the ice at various depths.
- FYI has the capacity to hold $CO_{2(g)}$ in concentrations about 20 times those measured in the atmosphere and the seawater (throughout the experiment, DT sea ice pCO_2 was 10 to 60 times that of atmospheric pCO_2 ; followed by NT FYI pCO_2 about 3 times atmosphere pCO_2 , with a range of 2 to 9times atmosphere).
- Differences in diurnal capacity of FYI $CO_{2(g)}$ exist.

Chapter 6: Conclusion

Our understanding of sea ice brine characteristics, such as the high capacity of seawater to hold CO_2 and brine migration patterns in FYI, no longer allow for the assumption that ice is a barrier to ocean - atmosphere gas exchange. On the contrary, the conclusion that ice brine channels provide access between the atmosphere and seawater can be drawn based on the following:

- Gossink et al. (1976) and Kelley (1979) demonstrated in lab conditions that the rate of gas movement through sea ice can be high.
- In 2004, Papakyriakou et al. measured short periods of high downward flux and longer periods of low downward flux of CO_2.
- Semiletov et al., in 2006, measured upward and downward fluxes over open seawater in the Arctic and downward fluxes of carbon during the melt season.
- Semiletov et al. (2006) confirmed ice uptake of CO_2 using the chamber method.
- Meanwhile in Anarctica, Zemmelink et al. (2006) measured downward CO_2 exchange over Antarctic sea ice in 2004.
- A recent tank experiment performed by Rysgaard's group (2007) showed that greater than 99.99% of CO_2 transport out of growing ice was downwards.

These studies indicate gas exchange exists between the atmosphere and ocean. The following studies indicate the ability for sea ice brine to absorb large amounts of CO_2:

- Papadimitriou et al. (2003), and Semiletov et al. (2008), have shown Arctic seawater and sea ice brine to have a high capacity to absorb and carry CO_2 and carbonates.
- Papadimitriou et al. (2003) found CO_2 degassing as a result of carbonate mineral precipitation in brine inclusions during cooling of the ice sheet.

Papadimitriou's team measured total carbon concentrations in the sea ice that were approximately 50% greater than those in seawater below.

- Delille et al. (2006) measured elevated dissolved inorganic carbon and total alkalinity in Antarctic sea ice using a sack-hole. From these results, the group computed carbon fluxes over the ice surface and acknowledged other strategies are needed to assess the role sea ice plays in carbon exchange between the atmosphere and the ocean.

Besides these, there is a notable lack of literature in climate modeling and regional oceanography in the second half of the last century, leading us to believe that carbon exchange over sea ice in the Arctic was ignored for a long time. Zubov (1945), for instance, did not make the observation that sea ice has a role in this exchange. He did notice that, compared to the atmosphere, sea ice had a decreased dissolved oxygen, increased dissolved carbon dioxide and similar nitrogen content, but he attributed these differences to biological activity alone. Studies since the mid seventies indicate that:

a) a gas flux over the ice surface is possible and that

b) sea ice has the potential to be chemically active in the transfer.

However, none of them measured pCO_2 in sea ice *in situ*, presenting an opportunity to improve accuracy through a new methodology. In response, my objective was to add to the study of the role of sea ice in the exchange of CO_2 between the atmosphere and the ocean. To implement a methodology for measuring sea ice CO_2 concentrations *in situ,* a procedure was adapted that had proven effective in soils. Further, supporting data was analyzed for determining the role of sea ice in the exchange of CO_2 between the atmosphere and the ocean to gage the method's potential as a tool for better understanding the role of sea ice in CO_2 exchange. Finally, I report on the space/time variation in sea ice gas content over first-year sea ice.

This experiment exploited the process of passive diffusion in order to collect $CO_{2(g)}$ samples from defined depths within sea ice. As opposed to having to rely on destructive or bulk ice studies, the new non-destructive technique described here provides a starting point from which a more accurate methodology can be developed for measuring carbon dioxide gas concentrations in sea ice. The method enabled the collection of $CO_{2(g)}$ samples directly from sea ice via implanted Silicone membrane chambers providing reproducible gas samples from known locations within the sea ice.

Overall, the results show that sea ice can play an active role in gas exchange between the sea and the atmosphere and has the capacity to carry high concentrations of CO_2 compared to seawater. This conclusion is based on the high measured values of ice pCO_2 coupled with the understanding of the CO_3^{2-} equations as presented by Papadimitriou et al. (2003) and others. Considering the ice pCO_2 data, the CO_3^{-} equations and ice temperature together, CO_2 off-gassing is certainly possible in the ice. Recall that ice pCO_2 increased during ice cooling and ice pCO_2 decreased during ice warming. The conversion of carbon between various species under these conditions can be explained in the carbonate precipitation/dissolution formula described earlier.

Further research is needed to determine the origin of CO_2 gas in the ice: what fraction of the high ice pCO_2 is the result of carbonate off-gassing, and what fraction is the result of other influences on sea ice carbon balances, such as carbon fluxes and biology? Further examination of the time-rate of change of brine constituents is needed.

Evidence shows that sea ice extent is diminishing, ice is becoming thinner, and average air temperature is becoming warmer. The rapid changes are influenced by such forces as altered global energy balance due to surface albedo changes and changes to atmospheric chemistry. The short time scale on which

these measurements have been recorded show that the changes are occurring rapidly. But this work and other sea and atmosphere surface work are beginning to show that the sea ice contributes to global air-sea carbon exchanges. The question here becomes how the thinning and receding ice is going to change carbon gas exchange dynamics in the region.

In light of rapid changes in the Arctic environment, these results have several implications. Predicted bulk warming of sea ice will reduce the volume of off-gassed CO_2 from the ice brines during cooling. Also, as noted earlier, how much of the high ice pCO_2 originates from carbonate off-gassing, and how much originates from surface fluxes is currently unknown. The downward flux of carbon during the rapid increase of sea ice pCO_2 in early February would indicate that the brine may be able to absorb and transport further CO_2. There is however the issue of ice's low permeability when cold. Missing is the mechanism whereby CO2, taken in at the surface or liberated via carbonate precipitation, is transported down and made available to in ice biological communities or the oceans inorganic carbon stock. I suspect we do not know the limit of absorption in the ice. The thinning ice cover will naturally shorten the distance between potential atmospheric, or seawater CO_2 removal. If brine was truly the vehicle through which CO_2 was removed from the atmosphere, the period of gas exchange may shorten.

The results from this work are part of a growing body of literature supporting the theory that FYI does not cap the seawater it covers. This work is showing that FYI has a capacity to store and move large volumes of $CO_{2(g)}$ as part of the sea ice brine system. Further developing our understanding of the sea ice brine solubility and transport mechanisms will assist modeling of the atmosphere's response to the observed shrinking of the Arctic sea ice cover.

Appendix A

A.1 Products required to build the sea ice pCO_2 samplers

Table A.1: List of products required for construction of pCO_2 samplers and their purpose in the construction of the Si chambers and the array assembly.

Item	Description
Disposable Syringe	60 mL; w/ luer lock, used to collect pCO_2 samples from Si chambers, inject sample into Exetainer™, and into GC for analysis.
Great Stuff™ foam	Foam used to prevent vertical flow
Luer Lock	2 way locks inserted in C-Flex® (1.6 mm ID) on one end and screwed to syringe on the other.
Needles	Used for injecting pCO_2 samples into Exetainers™
Non-diffuse tubing	C-Flex®, 7.6 m x 1.6 mm; Used to take pCO_2 surface samples
PVC tubing	5.0 cm diameter, white tubing, used for supporting array of Si chambers.
Rubber stoppers	36-43 mm stoppers used to plug top and bottom of PVC tube, to prevent vertical flow.
Si membrane	Cole-Parmer Si tubing, OD 12.8 mm, ID 12.4 mm, used to act as chamber.
Si stoppers	Used to plug Si membrane tubes at the top and bottom, to contain sample within chamber. The top stopper had a hole in the middle with the C-Flex® tubing to provide access to the chamber from the surface.
Silicone sealant	Clear sealant, used as a gluing and sealing agent, with stoppers, C-Flex® tubing, and luer locks.

A.2 Ice Chemistry Sampling Schedule

Table A.2: Date that sea ice pCO_2 and sea ice chemistry (including alkalinity, salinity and temperature) parameters were collected.

Date (2004)	Location	Ice Sampling Parameter			
		Salinity (psu)	Temperature (°C)	Alkalinity (umol/kg)	pCO_2 (ppmv)
November 30, 2003	A random pan	X	X	X	
December 10, 2003	E[1]	X	X	X	
January 23,2004	F, C1 and C2[1]		X*		X
January 24	F, C1 and C2	X	X*	X	
January 26	F, C1 and C2	X	X*	X	X
January 27	F, C1 and C2		X*		X
January 29	F, C1 and C2		X*		X
January 30	F, C1 and C2		X*		X
January 31	F, C1 and C2		X*		X
February 02	F, C1 and C2		X*		X
February 03	F, C1 and C2		X*		X
February 04	F, C1 and C2		X*		X
February 05	F, C1 and C2	X	X*	X	X
February 06	F, C1 and C2		X*		X
February 07	F, C1 and C2	X	X*	X	
February 08	F, C1 and C2		X*		X
February 09	F, C1 and C2	X	X*	X	
February 10	Angaguk[2]	X	X*	X	
February 11	F, C1 and C2	X	X*	X	X
February 12	F, C1 and C2	X	X*	X	
February 14	F, C1 and C2		X*		X
February 16	F, C1 and C2		X*		X
February 22	F, C1 and C2	X	X*	X	
February 29	F, C1 and C2	X	X*	X	
March 07	F, C1 and C2	X	X*	X	
March 14	F, C1 and C2	X	X*	X	
March 17	F, C1 and C2		X*		X

Date (2004)	Location	Ice Sampling Parameter			
		Salinity (psu)	Temperature (°C)	Alkalinity (umol/kg)	pCO_2 (ppmv)
March 18	F, C1 and C2		X*		X
March 21	F, C1 and C2	X	X*	X	
March 23	F, C1 and C2		X*		X
March 24	F, C1 and C2		X*		X
March 27	F, C1 and C2		X*		X
March 31	F, C1 and C2		X*		X
April 06	F, C1 and C2		X*		X
April 10	F, C1 and C2		X*		X
April 15	F, C1 and C2		X*		X
April 18	F, C1 and C2		X*		X
April 21	F, C1 and C2		X*		X
April 24	F, C1 and C2		X*		X
April 29	F, C1 and C2		X*		X
May 02	F, C1 and C2		X*		X
May 04	F, C1 and C2		X*		X
May 05	F, C1 and C2		X*		X
May 06	F, C1 and C2		X*		X
May 08	F, C1 and C2		X*		X
May 10	F, C1 and C2		X*		X
May 16	F, C1 and C2	X	X*	X	
May 18	F, C1 and C2		X*		X
May 26	HR transect[3]	X		X	
May 28	F, C1 and C2				X
May 30	F, C1 and C2	X		X	

***** Measured continuously via thermocouples in the ice connected to the MET tower. Data provided in hourly averages in °C. Detailed in section 3.2.2.

[1] Location detailed in Section 3.1 and Table 3.1.

[2] Remote sampling site, close to the mouth of the Horton River. Used primarily by biologists.

[3] Route from Angaguk to the mouth of the Horton River.

A.3 Components of GC for pCO_2 analysis from Si chambers

Table A.3: Instrumentation required for GC set up and operation.

Item	Description
ComputerH2O	Used to host PeakSimple 3D program to run GC and to collect and manipulate resulting gas printouts.
H_2O scrubber	To prevent water from samples contaminating GC at injection.
Helium gas tank	Used for He carrier gas.
Loops	3 sizes of loops used for different sample concentrations and GC calibration.
Needles	22 gauge attached to the syringe for extraction of gas sample from Exetainer™.
PeakSimple 3D	Program used to operate GC and interpret and manpulate data output graphs.
SRI 8610B GC	Gas chromatograph (GC) with TCD, used for sample analysis.
Standard gas tank	CO_2 gas standard; 412 +/-8.25 ppm.
Syringe	60-100 mL syringe, used to extract sample from Exetainer™ and inject into GC.

A.4 Vial preparation components

Table A.4: Items required for sample vial preparation. Set up as in Figure 3.15.

Item	Description
Exetainers™	12 mL vials used for sample collection.
Flow meter	Used to indicate flow of He to Exetainers™.
Hard tubing	15.2 m x 1.6 mm tubing, used for Exetainer™ evacuator.
Helium gas	Used for flushing Exetainers™, and providing a neutral headspace.
Luer Manifold	5 x 360° luer, used to allow multiple Exetainer™ evacuation.
Needles	22 gauge, 1" in length, turquoise hub colour, used for evacuating Exetainers™.
Silicone	Used to cover Exetainer™ septum after evacuation.
Vacuum pump	Fisher Scientific Maxima Plus M2C used for drawing gas from Exetainer™.
Vacuum pump gauge	Pump used to ensure complete evacuation.

A.5 Materials used for alkalinity analysis for both sea ice and seawater

Table A.5: Equipment required for sea ice and seawater alkalinity analysis.

Item	Description
180 ml beaker	Used as a sample receptacle during titration.
Balance	Reads to 5 decimal points.
Computer	Used to host TitraMaster85 and operate TitraLab 865.
Electrode	1) $HgSO_4$ reference electrode (ref. 201 no. 237-12-017), and 2) platinum electrode (M241Pt no. 243-11-005).
Stir bar	To stir titrating solution.
Storage solution	0.6 M KCL solution used for electrode storage.
Thermometer	Used to collect lab temperature for titration calibration.
TitraLab 865 Potentiometric Titration Workstation	TIM865 pH/EP/IP Titrator, bi-burette; resolution = 0.1 mV.
TitraMaster85	Radiometer Analytical software used for running TitraLab 865.
Titrant	Target titrant concentrations were: 0.1 M HCl for seawater; 0.03 N HCl for ice core A_T analysis up to March 30; and 0.005 N HCl for ice cores from March 31 to June.
Water jacketed pipettes	Calibrated, used for measuring known volumes of water titration during mobile phase.

Appendix B: Data Validation

The GC produced data from the analysis of gas samples collected from the atmosphere, sea ice, seawater, and a standard. Calibration were performed with analysis of a $CO_{2(g)}$ CRM (certified reference material) of 412 +/- 2% ppmv. During calibration the GC was subject to the range of CO_2 injections from 7.0% above atmospheric CO_2 concentration to all but one sea ice sample injection. The procedure used for calibrating the GC is outlined in the Methods Chapter (3.3.1). To determine the robustness of the calibration process, the quality of the results were investigated. The calibration process enabled the investigation of results produced by the three different loop volumes (Appendix B.1), determination of drift in the instrument during an analysis period by producing calibration data the beginning and end of each analysis series (Appendix B.2).

To obtain a linear calibration curve, results from the three different loop sizes were required. An average peak area (PA) of CO_2 from minimum three standard analyses of each loop was plotted against the number of moles to produce a linear calibration curve. The slope was forced through the origin (0, 0) in the calculation of slope. Theoretically, a zero PA should result from a zero pCO_2 injection.

The slopes experienced zero drift during this experiment the experiment. The calibration increased in precision during the experiment, presumably as the method of analysis was improved. The R^2 of greater than 95% of the calibration curves were between $R^2 = 1.00$ and $R^2 = 1.00$. The worst R^2 values belonging to two outliers with $R^2 = 1.00$ and 1.00.

B.1. Analysis of GC Multiple Loop Volumes

Table B.1 lists the mean, standard deviation (StDev) from the mean, median and percentage of error of standard analysis with respect to the gas standard. Table B.1 summarizes and compares all results from post integration analysis performed on the data to the value expected from the standard rating. Since the GC data from analysis of the standard differs from the standard "true" value, verification is required to determine if the difference is based on chance or truly incorrect data.

Table B.1: Statistics from GC analysis by loop volumes, and the CO_2 standard. Mean, StDev, root mean square error (RMSE), and the mean bias error (MBE) are listed.

Statistic	0.25 mL	1.0 mL	5.0 mL	All Volumes	Standard
Count (n)	163	57	64	284	
Mean (x_{AVG}) (ppmv)	413.31	378.14	413.46	406.29	412.0
StDev. (ppmv)	41.30	39.40	11.50	40.10	
Median (ppmv)	411.40	366	416	409.5	412.0
MBE (ppmv)	-1.31	33.86	-1.46	5.71	
RMSE (ppmv)	75.27	53.46	11.59	63.58	2% or 8.24

Figure B.1 represent the centre of the data, the spread, and the overall range of distribution using the box and whisker method. The box plot displays skewness in the data based on a five number summary, which includes median, upper and lower quartiles, and outliers. The segment inside the rectangle is within the lower and upper lower quartile or the population median. The lower quartile is found by determining the median of all values smaller than the population median; the upper quartile is performed using the same method for all values larger than the median. This range of the data makes up the lower and upper portion of the box respectively and is known as the interquartile range *(*IQR*)*. The "whiskers" above and below the box show the locations of maximum values up to 1.5×IQR. This dataset has displayed some outliers, usually high maximums. The circles are suspected outliers: 1.5×IQR or more outside the IQR up to 3xIQR. Outliers outside the 3xIQR are shown as large black dots.

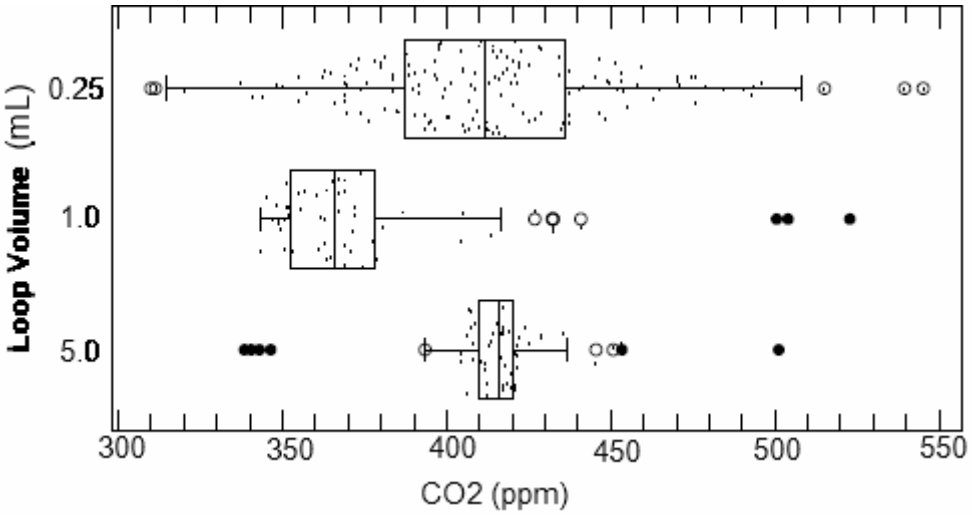

Figure B.1: New 412 ppm CO_2 standard calibration. Results from all CO_2 gas standard analysis, categorized by the loop volume they were injected with; 0.25, 1 and 5 mL. The box (□) provides the data within inner interquartile range, with the median marked by a line within. The whiskers (┤) provide the range of 1.5 x IQR. The specks (·) represent all data used. The circles (¤) signify outliers from 1.5 x IQR to 3 x IQR and the dots (•) those greater than 3 x IQR.

ANOVA (analysis of a variance) is used for analyzing experimental data by testing the statistical significance of the differences among the means of two or more groups on one or more variables. ANOVA was used with the data presented in Figure B.1 as described in Section 3.3.3.3. The box and whisker plots of loop volume data indicate that the 1.0 mL loop was different from the 0.25 and 5.0 mL loops because the 1.0 mL loop IQR is less than both the 0.25 and 5.0 mL loop's IQRs. But ANOVA analysis did not indicate significant difference. This may be because the overall range of data by the 1.0mL loop is smaller than the range from the 0.25 and 5.0 mL loops. Also, the extreme upper range of the 1.0mL and small sample set will have contributed to the result.

Second, ANOVA predicts (Table B.2) small probability of a difference between the measured CO_2 concentration in the GC and the gas standard value published by the gas producer. The null hypothesis is that in fact such differences are due to chance. To report the variety of possible outcomes from means not significantly different to means in fact significantly different, the probability (p) that the difference is due to chance is reported in Table B.2.

Table B.2: Results of the 412 ppmv CO_2 standard analysis vs. 412 ppmv CO_2 standard reported value ANOVA f-test. Sum of squares, degrees of freedom (d. f.) and the F statistic.

Source of Variation	Sum of Squares	d. f.	Mean of the Squares	F
Between	32.49	1	32.49	0.02
Error	4.55E+05	283	1.61E+03	p = 0.887
Total	4.55E+05	284		

Based on a 95% confidence interval, the calculated p-value of 0.887 means our measurements of the CRM are consistent with the null hypothesis, that the observed calibration standard analysis result of 406.29 ppmv CO_2 can be ascribed to chance alone. Although the GC standard analysis data is 1.39% below the rated value of the standard gas, the deviation from expected outcome is just small enough to be reported as being "not statistically significant at the 5% level".

B.2. Analysis of GC Calibration Standard Data

Changes in calibration points at the start and end of analysis were determined and their results are shown in Figure B.2. This information is used to determine the strength of a calibration used in a particular analysis run. Drift from the start to end calibration would indicate such factors as:

- GC detector or column ageing, and/or
- Barometric pressure changes during analysis.

Once a calibration is deemed unacceptable, the decision is made to utilize a previous good calibration or ignore that particular set of the data. The choice may be made to utilize a previous calibration curve because of the frequency of calibration required versus the frequency of calibration practiced allows this to occur. The instrument calibration was prescribed for every 2 weeks, while in practice, the instrument was calibrated 77% of analysis periods.

To calculate instrument drift, the values of standard analysis run through the smallest loop volume, 0.25 mL, at both the beginning calibration and end calibration on analysis periods that had both were compared. The difference was found by the following:

$$CO_{2(ppm,C,0.25mL,S)} - CO_{2(ppm,C,0.25mL,E)} = CO_{2(ppm,Diff,0.25mL)} \qquad \text{(Eq. B.1)}$$

Where, the subscripts 'ppm' is the units that are compared; 'C' indicates a calibration value; '0.25 mL' is the loop volume; 'S' represents a start calibration and 'E' represents an end calibration; and 'Diff' represents the difference. The StDev and RMSE were calculated for the above (Equation B.1) calculation. Multiple factors of these values are also shown in the figure (Figure B.2). The factors shown for both StDev and RMSE are +1, -1, +2, and –2. The values for StDev and RMSE happened to be very similar for this representation and therefore do not show well as separate values on this graph. Standard deviation values are shown on the graph.

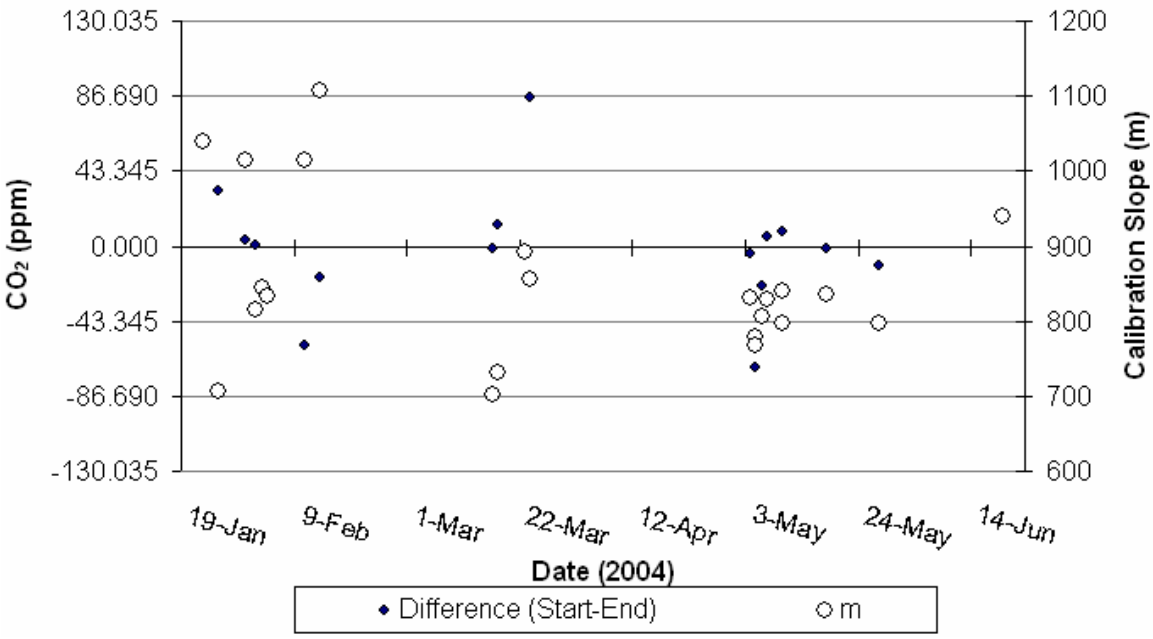

Figure B.2: Difference between start and end GC calibration analysis and calibration slopes. Difference is represented as a closed circle (●), left hand y-axis labels first, second and third standard deviations from zero of the differences between start and end standard analysis. The right hand y-axis and open circles shows the slope of the calibration curve for each calibration.

A second analysis for determining data drift was to compare slopes produced by calibration curves. These are shown in Figure B.2 as open circles. The difference between the average of all calibration slopes and the average of May calibration slopes resulted in a StDev of 26.4 from the mean. Meanwhile the remaining calibration slopes (produced January to April and June) resulted in a StDev of 131.72 from the mean. Early calibration runs had a high degree of variability, while calibrations performed in May where consistent, indicating increased reliability in GC data produced during this time.

Five calibration dates were selected for extrapolation: meaning, each date had drift greater than one StDev from the mean, therefore the calibration slope was extrapolated throughout the analysis period. The date and time stamp for each analysis was used to ensure the extrapolation was applied linearly throughout the inter-calibration

period. This method was applied to the following dates: February 4 and 11, March 23 and 24, and May 5.

B.3. Preparing the GC calibration curves: y-intercepts

Theoretically, if CO_2 is not injected into the GC during sample injection, there should be a zero response by the GC to CO_2. In reality this may not happen. Firstly, a low response may be falsely identified within the noise of the detector output. For this reason a low threshold was set in PeakSimple 3D for data acquisition to prevent recording false positive responses. Second, a false response to a zero sample may occur because a zero response may be outside the calibration range, as in this experiment. Figure B.3 shows the y-intercepts for calibration curves not forced through the zero y-intercept. The slope of the linear regression of these curves is $5x10^{-06}$ over 6 months. Table B.3 lists basic statistics for the slopes and y-intercepts of the calibration curves that have not been forced to a zero y-intercept and curves that have been forced to a zero y-intercept.

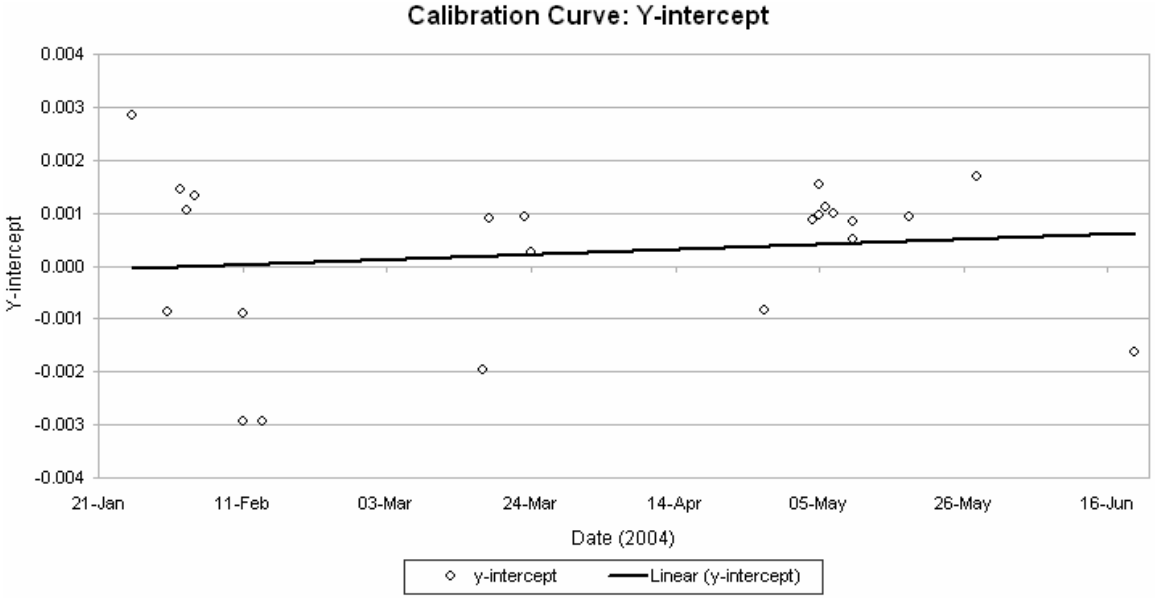

Figure B.3: Y-intercepts for calibration curves not forced through the zero y-intercept.

Table B.3: Comparison of slope and y-intercept for calibrations equations produced during calibration for forced and non-forced y-intercepts: Average and StDev, and the interquartile range.

Statistic	Y-intercept		Forced Zero Y-Intercept
	m	y-intercept	m
Mean	$9.00E^{-03}$	$2.65E^{-04}$	$9.02E^{-03}$
St Dev (of mean)	$1.40E^{-03}$	$1.51E^{-03}$	$1.24E^{-03}$
Q1 (25%)	$8.15E^{-03}$	$-8.40E^{-04}$	$8.32E^{-03}$
Median (50%)	$8.54E^{-03}$	$8.84E^{-04}$	$8.67E^{-03}$
Q3 (75%)	$9.64E^{-03}$	$1.08E^{-03}$	$9.49E^{-03}$
Interquartile Range (25% to 75%)	$1.49E^{-03}$	$1.92E^{-03}$	$1.17E^{-03}$

The mean and standard deviation for non zero and forced zero y-intercepts are shown in Table B.3 to illustrate that the forced zero y-intercept showed less deviation about the mean than the non forced equation slope. Comparing the interquartile range of the slopes in both situations shows that the slopes from the forced zero y-intercept curves were within a tighter range than the non-forced slopes. For these reasons, the decision was made to force the calibration curves through the zero y-intercept.

B.4 Testing for significance.

The significance of some data sets was determined by comparing the range of the standard deviation one piece of data against another. For example,

Statitical significance was investigated in several cases to determine the likelehood that an observation was due to chance.

Simple cases, it is defined as the probability of making a decision to reject the null hypothesis when the null hypothesis is actually true (a decision known as a Type I error, or "false positive determination"). The decision is often made using the p-value: if the p-value is less than the significance level, then the null hypothesis is rejected. The smaller the p-value, the more significant the result is said to be.

"A statistically significant difference" simply means there is statistical evidence that there is a difference; it does not mean the difference is necessarily large, important, or significant in the common meaning of the word.

Appendix C: Atmospheric Gas Sample Collection for GC Analysis

Figure C.1 graphically presents a monthly breakdown of wind directions and speeds at the sampling site. Winds typically occurred in east-west directions. January and March had the highest proportion of days in which the ship's exhaust passed over the gas sampling sites. Table C.1 lists the dates of the experiment where wind passed over the ship and sea ice pCO_2 sampling sites in coincidence with atmospheric CO_2 sampling dates. An examination of atmospheric samples analyzed in the GC (Figure C.2) and wind data (Figure C.1) showed that contamination of the air samples was possible. Five of the nine atmosphere samples with extremely high pCO_2 coincide with days when the ship smoke was traveling in the direction of the pCO_2 sampling locations.

Table C.1: Wind speed, direction, and corresponding atmosphere pCO_2 measured by the GC. Wind speed (m/s) and direction (º), and the pCO_2 of the atmosphere at that time, including sample collector and notes on the GC analysis calibration.

Date	Time	Wind speed (m/s)	Wind direction (º)	Measured Atm. pCO_2 by GC (ppm)	Measurements made by:
February 12	9am	0.15	287	568	Owen
February 14	6pm	2.90	242	577	Owen
February 16	9am	7.90	251	649	Owen
	6pm	5.60	260	630	Owen
March 10	9am	2.50	153	577	Leg 5
March 20	9am	4.0	274	635	Leg 5
April 20	6pm	3.20	90	575	Leg 6
April 29	6pm	2.60	70	584	Leg 6
May 28	9am	No data available		578	Owen

Dates highlighted as having wind that allowed for ship smoke to travel over the pCO_2 sampling sites.

These elevated pCO_2 values picked up by the GC were not detected by the IRGA installed at the MET tower. Possible explanation for this observation may relate to the difference in sampling heights between the two measurements. Westerly winds that brought the exhaust over the sampling sites appeared to contaminate the point atmosphere samples analyzed by the GC and were screened from the data. Meanwhile it was found that high atmospheric pCO_2 was measured when the conditions allowed pooling of stack exhaust at the sampling sites.

The steps taken include collecting the sample with the worker facing into the wind, and drawing the sample away from the ground. Facing into the wind during sample collection allowed exhaled breath to not travel over the syringe during drawing. Effectiveness of this method decreased as the wind speed decreased. The assumption

being that the workers breath was more efficiently transported away from the site during periods of high winds. In Table C.2, shading in the left hand side of the column marks low wind speed during sampling, and shading on the right hand side of the column marks anomalously high pCO_2 measured. An advantage of the cold environment was that it was possible for workers to see their breath when collecting samples allowing appropriate caution to be taken during sampling.

Next page: **Figure C.1**: **Wind roses indicating direction wind by origin and the proportion of wind speeds from each direction.**

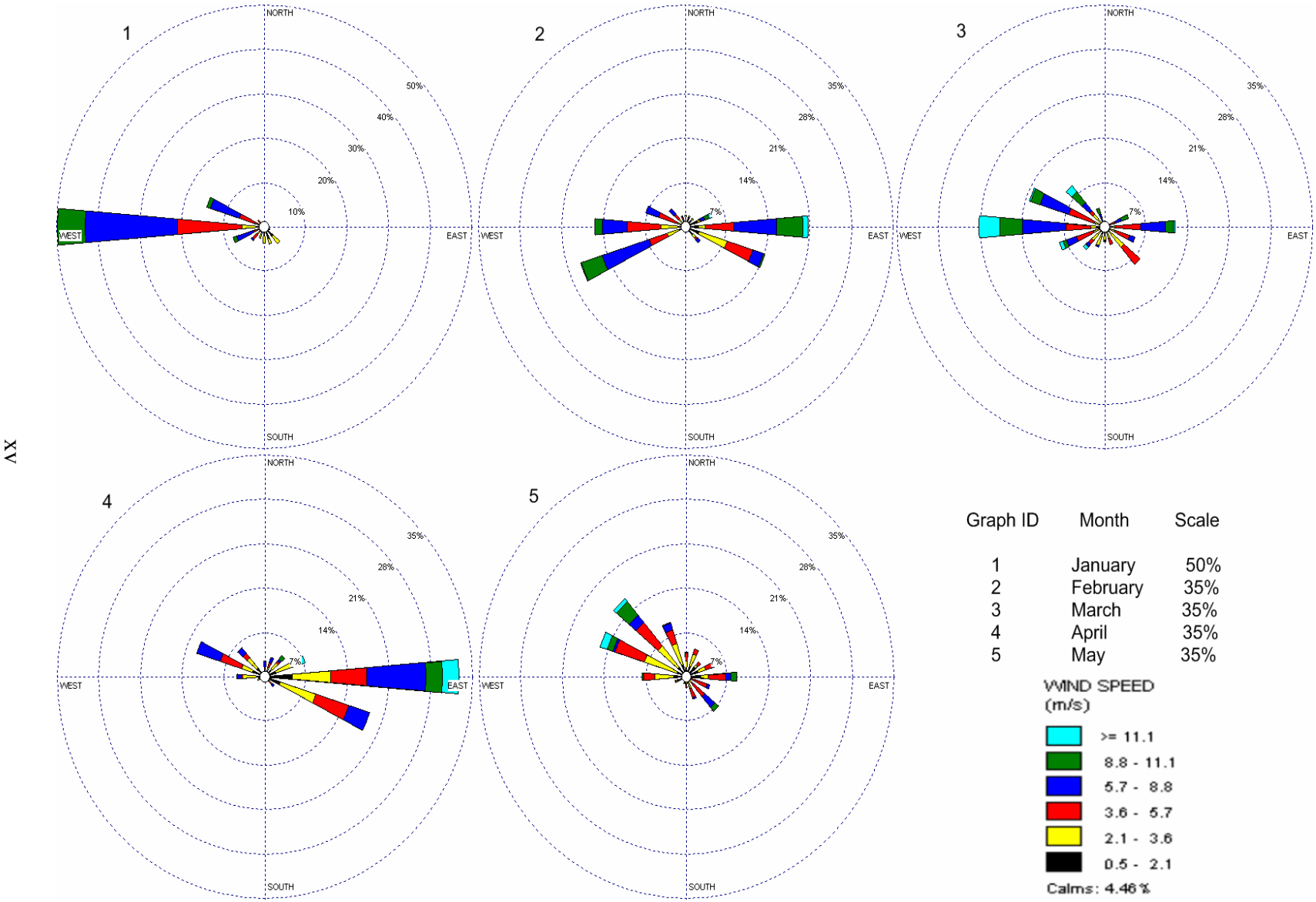
1
NORTH
50%
40%
30%
20%
10%
WEST
EAST
SOUTH
2
NORTH
35%
28%
21%
14%
7%
WEST
EAST
SOUTH
3
NORTH
35%
28%
21%
14%
7%
WEST
EAST
SOUTH
4
NORTH
35%
28%
21%
14%
7%
WEST
EAST
SOUTH
5
NORTH
35%
28%
21%
14%
7%
WEST
EAST
SOUTH
Graph ID
Month
Scale
1
January
50%
2
February
35%
3
March
35%
4
April
35%
5
May
35%
WIND SPEED
(m/s)
>= 11.1
8.8 - 11.1
5.7 - 8.8
3.6 - 5.7
2.1 - 3.6
0.5 - 2.1
Calms: 4.46 %

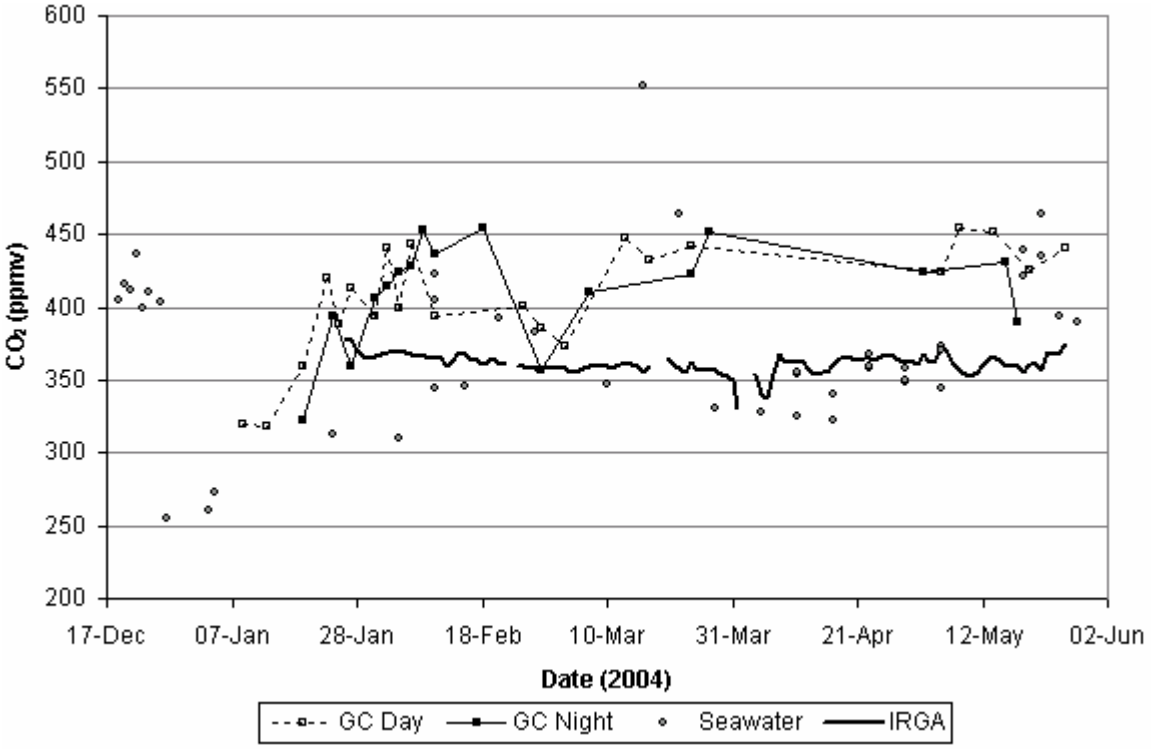

Figure C.2: Air and seawater CO_2 (ppm) measurements. Li-750 IRGA (▬▬) and GC measured DT (---▫---) and NT (—▪—) atmospheric pCO_2. Calculated seawater pCO_2 (○) is included.

Table C.2: Dates where low wind speed coincided with high atmospheric $pCO_{2(atm)}$ measured by the GC.

Date	Low wind speed	High DT $pCO_{2(atm)}$	High NT $pCO_{2(atm)}$
February 16	√	√	√
March 10	√		√
March 13	√	√	√
April 6	√	√	
April 18	√		√
April 21	√	√	√
April 24	√	√	√
April 29	√	√	√
May 8	√	√	√
May14	√	√	√
May 18	√	√	

References

Aagaard, K and E.C. Carmack. 1989. The Role of Sea Ice and Other Fresh Water in the Arctic Circulation, *J. Geophys. Res. -C*, **94**: 14485 - 14498. DOI: 10.1191/0959683603hl626rp

Aagaard, K., E. Fahrbach, J. Meincke and J.H. Swift. 1991. Saline outflow from the Arctic Ocean: Its contribution to the deep waters of the Greenland, Norwegian, and Iceland seas. *J. Geophys. Res. -C*, **96**: 20,433-20,441. doi:10.1016/S0924-7963(99)00069-X

Aagaard, K., J.D. Schumacher, and A.T. Roach. 1985. On the wind-driven flow through Bering Strait. *J. Geophys. Res.* **90**: 7213–7221.

Aagard, K and E.C. Carmack. 1994. The Arctic Ocean and Climate: A Perspective. In: J. Johannessen et al. (eds.), The Polar Oceans and their role in shaping the global environment. *Geophysical Monograph* **85**, American Geophysical Union.

Almgren, T., D. Dyrssen & S. Fonselius. 1983. Determination of alkalinity and total carbonate. In: Methods of Seawater analysis, K. Grasshoff, M. Ehrhardt and K. Kremling, editor, Verlag Chemie, Weinheim: 99-123.

Andersen L., E. Falck, E. P. Jones, S. Jutterström, and J. H. Swift. 2004. Enhanced uptake of atmospheric CO_2 during freezing of seawater: A field study in Storfjorden, Svalbard. *J. Geophys. Res.* **109:** C06004. doi:10.1029/2003JC002120

Anderson, L.G. and E.P. Jones. 1985. Measurements of total alkalinity, calcium and sulphate in natural sea ice. *J. Geophys. Res.,* 90: 9194–9198.

Anderson, L.G., D. Dyrssen, and E.P. Jones (1990), An assessment of the transport of atmospheric CO2 into the Arctic Ocean, J. Geophys. Res., **95** (C2): 1703–1711.

Anderson, L.G., S. Jutterström, S. Kaltin, E. P. Jones, and G. Björk, 2004. Variability in river runoff distribution in the Eurasian Basin of the Arctic Ocean, *J. Geophys. Res.,* **109:** C01016. doi:10.1029/2003JC001773

Andreas, E.L., P.S. Guest, P.O.G. Persson, C.W. Fairall, T.W. Horst, R.E. Moritz, S.R. Semmer. 2002. Near-surface water vapor over polar sea ice is always near ice saturation. *J. Geophys. Res. –C*, **107**: 8033. doi:10.1029/2000JC000411

Aok, T.N., T. Michida, S. Sugawara, S. Morimoto, G. Hashida, T. Yamanouchi, K. Kawamura, H. Honda. 2003. Carbon dioxide variations in the stratosphere over Japan, Scandinavia, and Antarctica. *Tellus **55B***: 178-186. DOI**:** 10.1034/j.1600-0560.2003.00059.x

Armstrong, T., G. Rogers, G. Rowley. 1978. The Circumpolar North. Methuen & Co. Ltd., London: 9.

Arrhenius, S. 1896. The London, Edinburgh, and Dublin Physiological Magazine and *J. of Science* [**5**th Series], **41**: 237-275.

Arrigo, K.R. and D.N. Thomas. 2004. Large scale importance of sea ice biology in the Southern Ocean. Antarctic Science, 16: 471-486. doi:10.1017/S0954102004002263

Assur, A. 1960. Composition of sea ice and its tensile strength, *SIPRE Res. Rep*., 44.

Bacastow, R.B., C.D. Keeling, and T.P. Whorf. 1985. Seasonal amplitude increase in atmospheric CO_2 concentration at Mauna Loa, Hawaii, 1959-1982. *Journal of Geophysical Research* 90(D6): 10529-40.

Backhaus J.O., H. Fohrmann, J. Kampf, and A. Rubino. 1997. Formation and export of water masses produced in arctic shelf polynyas – process studies of oceanic convection. *ICES J. of Marine Science*, **54**: 366-382.

Barber, D.G., J.Y. Yackel, and J.M. Hanesiak. 2001. Sea ice, RADAR-SAT-1 and arctic climate processes: a review and update. *Canadian J. of Remote Sensing,* **27**: No 1.

Barnola, J., P. Pimienta, D. Raynaud, and Y. Korotkevich. 1991. CO_2-climate relationship as deduced from the Vostok ice core - A reexamination based on new measurements and on a reevaluation of the air dating. *Tellus B-Chemical and Physical Meteorology*, **43**(2): 83 - 90.

Belanger, S., H. Xie, N. Krotkov, P. Larouche, W.F. Vincent, and M. Babin. 2006. Photomineralization of terrigenous dissolved organic matter in Arctic coastal waters from 1979 to 2003: Interannual variability and implications of climate change. *Global Biogeochemical Cycles*, **20**: GB4005. doi:10.1029/2006GB002708

Belzile, C., Johannessen, S.C., Gosselin, M., Demers, S., Miller, W.L. 2000. Ultraviolet Attenuation by Dissolved and Particulate Constituents of First-Year Ice during Late Spring in an Arctic Polynya. *Limnology and Oceanography*, **45 (**6): 1265-1273.

Bigg, G. R. 2001. The Oceans and Climate. Cambridge, United Kingdon, Cambridge University Press.

Bollin, B. 1960. *Tellus*, **12**: 274.

Boyd, T.J., and E.A. D'Asaro. 1994. Cooling of the West Spitsbergen Current - wintertime observations west of Svalbard. *J. Geophys. Res.*, **99**: 22597-22618.

Brewer, P. G., A. L. Bradshaw, and R.T. Williams. 1986. Measurements of total carbon dioxide and alkalinity in the North Atlantic Ocean in 1981. In: *The changing carbon cycle. A global analysis*. J. R. Trabalka and D. E. Reichle, editors, Springer-Verlag, New York, 348-370.

Brewer, P.G., E.T. Peltzer, G. Friederich, I. Aya, and K. Yamane. 2000. Experiments on the ocean sequestration of fossil fuel CO_2: pH measurements and hydrate formation. *Marine Chemistry,* **72**: 83-93.

Broecker, W. S., and T. Takahashi, 1978. Neutralization of fossil fuel CO_2 by marine calcium carbonate, in The Fate of Fossil Fuel CO_2 in the Oceans, edited by N. R. Andersen, and A. Malahoff, Plenum Press, New York.

Broecker, W.S. 1974. Chemical Oceanography. Harcourt Brace Jovanovich, New York.

Bufflap, W.E. and H.E. Allen. 1995. Sediment pore water collection methods: A review. *Water Research* **29**: 165-177.

Campbell, G. S. and J. M. Norman. 1998. An Introduction to Environmental Biophysics, 2nd edition, Springer.

Fortier, Martin; A. Langlois, T. Fisico, R. Galley and D.G. Barber. 2004. CASES Data Report; Sub-Group 2.2; Ice-Atmosphere Interactions and Biological Linkages.

Carpenter, E. J., S. Lin, and D. G. Capone. 2000. Bacterial activity in South Pole snow. Appl. Environ. Microbiology **66**: 4514-4517.

Carr, R.S. and D.C. Chapman. 1995. Comparison of methods for conducting marine and estuarine sediment porewater toxicity tests – Extraction, storage, and handling techniques. *Environmental Contamination and Toxicity,* **28**: 69-77.

Cavalieri, D.J., C.L. Parkinson, and K.Y. Vinnikov. 2003. 30-year satellite record reveals contrasting Arctic and Antarctic decadal sea ice variability. *Geophys. Res. Lett.,* **30**: 18. doi:10.1029/2003GL018031

Chapman, W.L. and J.E. Walsh. 1993. Recent variations of sea ice and air temperatures in high latitudes, *Bulletin of the American Meteorological Society* **74**: 33-47. DOI: 10.1175/1520-0477(1993)074

Chung, S. N., K. Lee, R. A. Feely, C. L. Sabine, F. J. Millero, R. Wanninkhof, J. L. Bullister, R. M. Key, and T.-H. Peng. 2003. Calcium carbonate budget in the Atlantic Ocean based on water column inorganic carbon chemistry. *Global Biogeochemical Cycles*, **17** (4): 1093. doi: 10.1029/2002GB002001

Clarke, C. H. 2003. Polar Marine ecosystems: major threats and future changes *Environmental Conservation* **30**(1): 1-25. doi:10.1017/S0376892903000018

Coale, K. H., K. S. Johnson, S. E. Fitzwater, S. P. G. Blain, T. P. Stanton, T. L. Coley. 1998. IronEx-I, an in situ iron-enrichment experiment: Experimental design, implementation and results. *Deep-Sea Research Part II,* **45**: 919-945. DOI: 10.1016/S0967-0645(98)00019-8

Cobb, AE. 1963. *Science*, **141**: 733.

Coble, C. R, E. G.Murray; Rice, Dole R. 1987. Earth Science. Englewood Cliffs, NJ: Prentice-Hall, pp 102.

Espie, G. S. And B. Colman. 1986. Inorganic Carbon Uptake during Photosynthesis. Plant Physiology. **80**: 863-869.

Comiso, J.C. 2003. Large scale characteristics and variability of the global se ice cover. In Se-Ice – An Introduction to its Physics, Chemistry, Biology and Geology (ed. D.N. Thomas and G.S. Deickmann), pp. 112-142. Blackwell Science.

Cox, G.F.N. and Weeks W.F. 1975. Brine drainage and initial salt entrapment in sodium chloride ice. *CRREL Res. Rep*., 345.

Cox, G.F.N., and W.F. Weeks. 1983. Equations for determining the gas and brine volumes in sea-ice samples. *J. Glaciol.*, **29**: 306–316.

Crowley, T.J. 2000. Causes of Climate Change Over the Past 1000 Years. *Science*, **289**: 270-277. DOI: 10.1126/science.289.5477.270

Curry, R. and M. S. McCartney. 2001. Ocean gyre circulation changes associated with the North Atlantic Oscillation. *J. Physical Oceanography*, **31**: 3374–3400. DOI: 10.1175/1520-0485(2001)031

Davis, Tiganis, Burn. 2004. The effect of photo-oxidative degradation on fracture in ABS pipe resins. *Polymer Degradation and Stability*, **84**: 233-242. doi:10.1016/j.polymdegradstab.2003.10.017

De Abreu, R., D.G. Barber, K. Misurak and E.F. LeDrew. 1994. Spectral albedo of snow-covered first year and multi year sea ice during spring melt. *Annals of Glaciology*. **21**: 337-342.

Defant, A. 1961. Physical Oceanography, Pergamon Press, New York, Vol 1, Chap 8.

Delille, B., B. Jourdain, A. Vieira Borges A.V., J.-L. Tison, and D. Delille. 2007. Biogas (CO_2, O_2, dimethylsulfide) dynamics in Spring Antarctic fast ice. *Limnology and Oceanography,* **52(4)**: 1367-1379.

Delworth, T. L. and K.W. Dixon. 2000. Implications of the recent trend in the Arctic/North Atlantic Oscillation for the North Atlantic thermohaline circulation. *J. of Climatology,* **13**: 3721–3727. DOI: 10.1175/1520-0442(2000)013

Dickson, A. and C. Goyet, DOE. 1994. Handbook of methods for the analysis of the various parameters of the carbon dioxide system in seawater, version 2.0 (A. Dickson and C. Goyet, Eds.).

Dickson, A. G. 1993. The analytical chemistry of the oceanic carbon dioxide system. In Proceedings of the International Symposium on Global Change (IGBP), Tokyo, Japan, March 27-29, 1992. Secretariat of International Symposium on Global Change. pp. 183-192.

Dickson, A. G. 1981. An exact definition of total alkalinity and a procedure for the estimation of alkalinity and total inorganic carbon from titration data. *Deep Sea Research*, **28A**: 609-623.

Dickson, A. G., J. D. Afghan, and G. C. Anderson. 2002. Reference materials for oceanic CO_2 analysis: a method for the certification of total alkalinity. *Marine Chemistry*, **32:** 185–197. doi:10.1016/S0304-4203(02)00133-0

Dieckmann, G.S., Nehrke, G., Papadimitriou, S., Göttlicher, J., Steininger, R., Kennedy, H., Wolf-Gladrow, D., Thomas, D.N. 2008. Calcium carbonate as ikaite crystals in Antarctic sea ice. *Geophysical Research Letters*, 35, L08501, doi:10.1029/2008GL033540

DOE, Version 2.1. 1996. SOP2: Determination of total dissolved inorganic carbon in sea water; SOP3: Determination of total alkalinity in sea water.

Duffy, P. B., M. Eby, A. J. Weaver. 2001. Climate Model Simulations of Effects of Increased Atmospheric CO_2 and Loss of Sea Ice on Ocean Salinity and Tracer Uptake. *J. of Climatology,* **14** (4): 520-532. DOI: 10.1175/1520-0442(2001)014

Eicken, H. 1992. Salinity profiles of Antarctic sea ice: field data and model results. *J. Geophys. Res.,* **97(C10)**: 15,545-15,557.

Eicken, H.; Lensu, M.; Leppäranta, M.; Tucker, W. B.; Gow, A. J.; Salmela, O. 1995. Thickness, structure, and properties of level summer multiyear ice in the Eurasian sector of the Arctic Ocean. *J. Geophys. Res*., **100**, C11: 22697-22710.

Eicken, H. 1998. Factors determining microstructure, salinity and stable-isotope composition of Antarctic sea ice: Deriving modes and rates of ice growth in the Weddell Sea. *AGU Antarct. Res. Ser.* (Antarctic Sea Ice Physical Processes, Interactions and Variability, edited by M. O. Jeffries), **74**: 89-122.

Eicken, H., Bock C., Wittig R., Miller H. & Poertner H.-O. 2000. Nuclear magnetic resonance imaging of sea ice pore fluids: Methods and thermal evolution of pore microstructure. *Cold Reg. Sci. Technol.,* **31**: 207-225. **DOI:** 10.1016/S0165-232X(00)00016-1

Eicken, H. and P. Lemke. 2001. The response of polar sea ice to climate variability and change. In: Lozán et al., Climate of the 21st century: Changes and risks. GEO, Hamburg/Germany, pp. 206-211.

Eicken, H. 2003. Contribution to Thomas D. & G. S. Dieckmann (eds.): Sea Ice – An Introduction to its Physics, Biology, Chemistry and Geology. Blackwell Science, London, 2003: 22-81. From the microscopic to the macroscopic to the regional scale: Growth, microstructure and properties of sea ice.

Eide, L. I. and S. Martin. 1975. The formation of brine drainage features in young sea ice. *J. Glaciol.,* **14**: 137-154.

Etheridges, D.M., L.P. Steele, R.L. Langenfelds, R.J. Francey, J.-M Barnola, V.I. Morgan. 1996. Natural and anthropogenic changes in atmospheric CO2 over the last 1000 years from air in Antarctic ice and firn. *J. Geophys. Res. -D,* **101:** 4115-4128.

Fairall et al. 2000. Parameterization and micrometeorological measurement of air sea gas transfer. *Boundary Layer Meteorol*., **96**: 63-105.

Feely, R. A., C. L. Sabine, T. Takahashi, and R. Wanninkhof. 2001. Uptake and Storage of CO_2 in the Ocean: The Global CO_2 Survey. *Oceanography*, **14(4)**: 18–32.

Fetterer, F., and K. Knowles. 2004. Sea ice index monitors polar ice extent. Eos, Trans. Am. Geophysics Union, **85**: 163.

Fofonoff, P. and R. C. Millard Jr. 1983. Algorithms for computation of fundamental properties of seawater. *Unesco Technical Papers in Marine Sciences*, **44**: 53.

Folland, C.K, N.A. Rayner, S.J. Brown, T.M. Smith, S.S. Shen, D.E. Parker, I. Macadam, P.D. Jones, R.N. Jones, N. Nicholls and D.M.H. Sexton. 2001. A comprehensive analysis of global temperature change and its major uncertainties since 1861. *GeophysicalResearch Letters* **28**: 2621-2624.

Folland, C.K, T.R. Karl, J.R. Christy, R.A. Clarke, G.V. Gruza, J. Jouzel, M.E. Mann, J. Oerlemans, M.J. Salinger and S.-W. Wang. 2001. Observed Climate Variability and Change. In: *Climate Change 2001: The Scientific Basis*. Contribution of Working Group I to the Third Assessment Report of the Intergovernmental Panel on Climate Change [Houghton, J.T., Y. Ding, D.J. Griggs, M. Noguer, P.J. van der Linden, X. Dai, K. Maskell, and C.A. Johnson (eds.)]. Cambridge, United Kingdom and New York, NY, USA, pp. 881.

Forchhammer, E. P. 2004. Using large scale climate indices in climate change ecology studies. *Population Ecology* **46**: 1-12.

Frere, M.H. 1975. Integrating chemical factors with water and sediment transport from a watershed. *J. Environ. Qual.,* **11(3)**: 497-505.

Fung, I. 2001. Modelling carbon climate interactions. Present and Future of Modeling Global Environmental Change: Toward Integrated Modeling Terra Scientific Publishing Co.: 187-194.

Garrels, R.M., and M.E. Thompson. 1962. A chemical model for sea water at 25 degrees C and one atmosphere total pressure. *American J. of Science*, **260**: 57-66.

Gavrilo, V. P., and B. Y. Gaitskhoki. 1970. The statistics of air inclusions in ice, in The Physics of Ice, edited by V. V. Bogorodskii, translated from Russian, pp. 125–128, Isr. Program for Sci. Transl., Jerusalem.

Gibson, J.A.E. and Trull, T.W. 1999. Annual cycle of fCO_2 under sea-ice and in open water in Prydz Bay, East Antarctica. *Marine Chemistry*, **66(3-4)**: 187-200. DOI: 10.1016/S0304-4203(99)00040-7

Gitterman K.E. 1937. Thermal analysis of seawater. *CRREL TL.,* **287**. USACRREL.

Gleitz, M., v.D. Rutgers, M. Loeff, D.N. Thomas, G.S. Dieckmann and F.J. Millero. 1995. Comparison of summer and winter inorganic carbon, oxygen and nutrient concentrations in Antarctic sea ice brine. Marine. *Mar. Chem.*, **51**: 81–91.

Gloersen, P, WJ Cambell, DJ Cavalieri, JC Comiso, CL Parkinson, HJ Wally. 1992. Arctic and Antarctic Sea Ice, 1978-1987: satellite passive microwave observations and analysis, NASA SP-511.

Gloersen, P., and W.J. Campbell. 1991. Recent variations in Arctic and Anarctic sea ice covers. *Nature*, **352**: 33-36.

Golden, K. M., Ackley, S. F., and Lytle, V. I. 1998. The percolation phase transition in sea ice. *Science*, **282**: 2238-2241. DOI: 10.1126/science.282.5397.2238

Gosink, T. A. J. G. P., John J. Kelley. 1976. Gas movement through sea ice. *Nature*, **263**: 41-42.

Gosselin, M., Levasseur, M., Wheeler, P.A., Horner, R.A., Booth, B.C. 1997. New measurements of phytoplankton and ice algal production in the Arctic Ocean. *Deep-Sea Research II,* **44**: 1623-1644. **DOI:** 10.1016/S0967-0645(97)00054-4

Goto S.; Fukuhara A.; Miyasaka H.; Krembs C.; Gradinger R.; Spindler M. 2000. Implications of brine channel geometry and surface area for the interaction of sympagic organisms in Arctic Sea ice. *J. of Experimental Marine Biology and Ecology,* **243**: 55-80. DOI: 10.1016/S0022-0981(99)00111-2

Goyet, C. and Hacker, S.D. 1992. Procedure for calibration of a coulometric system used for total inorganic carbon measurements in seawater. *Marine Chemistry*, **38**, 37.

Granskog, M. 1999. Baltic Sea ice as a medium for storage of particulate matter and elements. *J. of Marine Science,* **56**(supplement): 172-175.

Granskog, M.A., H. Kaartokallio, K Shirasawa. 2003. Nutrient status of the Baltic Sea: evidence for control by snow-ice formation, ice permeability, and ice algae. *J. Geophys. Res.* **108** (C8): 3253. doi:10.1029/2002JC001386

Grenfell, T.C. and D.K. Perovich. 2004. Seasonal and spatial evolution of albedo in a snow-ice-land-ocean environment. *J. Geophys. Res. -C,* **109**: 1029-1039. doi:10.1029/2003JC001866

Grenfell, T. C., and G. A. Maykut. 1977. The optical properties of ice and snow in the Arctic Basin. *J. Glaciol*., **18**: 445–463.

Grenfell, T. C., D. G. Barber, A. K. Fung, A. J. Gow, K. C. Jezek, E. J. Knapp, S. V. Nghiem, R. G. Onstott, D. K. Perovich, C. S. Roesler, C. T. Swift, and F. Tanis. 1998 Evolution of Electromagnetic Signatures of Sea Ice from Initial Formation to the Establishment of Thick First-Year Ice, IEEE Trans. *Geosci. Remote Sens*., **36(5)**: 1642-1654.

Grenfell, T. C., S. G. Warren, and P. C. Mullen. 1994 Reflection of solar radiation by the Antarctic snow surface at ultraviolet, visible, and near-infrared wavelengths. *J. Geophys. Res*., **99**: 18,669– 18,684.

Grenfell, T.C. 1986. Surface based passive microwave observations of sea ice in the Bering and Greenland Seas. *IEEE Transactions on Geoscience and Remote Sensing*, GE-**24**: 378-382. DOI: 10.1109/TGRS.1986.289595

Grenfell, T.C., and D.K. Perovich. 1984. Spectral albedos of sea ice and incident solar irradiance in the southern Beaufort Sea. *J. Geophys. Res.* **89**: 3573-3580.

Gross, Wolfgang G. 1965. The Workman-Reynolds Effect and ionic transfer processes at the ice-solution interface. *J. of Geophys. Res*., **70:** 2291.

Hanesiak J.M., D.G. Barber, R. DeAbreu, and J.J. Yackel. 2001. Local and regional albedo. Observations of arctic first year sea ice during melt ponding. *J. Geophys. Res. – C Oceans*, **106**: 1005-1016.

Hansen, B., W.R. Turrell, and S. Østerhus. 2001. Decreasing overflow from the Nordic seas into the Atlantic Ocean through the Faroe-Shetland Channel since 1950. *Nature,* **411**: 927–930. doi:10.1038/35082034

Harries, J.E., H. E. B., Pretty J. Sagoo, Richard J. Bantges. 2001. Increases in greenhouse forcing inferred from the outgoing longwave radiation spectra of the Earth in 1970 and 1997. *Nature,* **410**: 355 - 357. doi:10.1038/35066553

Harris, D. C. 2003. Quantitative Chemical Analysis 6th ed. pp. 91-92, 555-572, 579-590, 598-600.

Harrison, J.D. 1965. Measurement of Brine Droplet Migration in Ice. *J. of Applied Physics*, **36**: 3811. DOI:10.1063/1.1713953

Haugan, P.M. 1999. Structure and heat content of the West Spitsbergen Current. *Polar Research*, **18**: 183-188.

Hesslein, R. 1976. An in situ sampler for close interval pore water studies. *Limnology and Oceanography*, **21** (6): 912-914.

Hibler, W.D. 1989. Arctic Ice-Ocean Dynamics, in The Arctic Seas, Van Nostrand Reinhold Co., New York.

Hoekstra, P., Osterkamp, T.E. and Weeks, W.F. 1965. The migration of liquid inclusions in single ice crystals. *J. Geophys. Res.*, **20**: 5035-5041.

Hooper, R. 2005. Marine crisis looms over acidifying oceans. *NewScientist.com news service*. http://www.newscientist.com/article.ns?id=dn7609 (Accessed 28 June 2005).

Horne, RA. 1969. Marine Chemistry: the structure of water and the chemistry of the hydrosphere. John Wiley and Sons, Inc. USA.

IPCC, A. I. A. 2001. Intergovernmental Panel on Climate Change; Synthesis Report. Cambridge University Press, Cambridge, UK.

IPCC, J. T. H., Y.Ding, D.J. Griggs, M. Noguer, P.J. van der Linden, X. Dai, K. Maskell, and C.A. Johnson, (eds). 2001. IPCC. Intergovernmental Panel on Climate Change, Climate Change 2001: The Scientific Basis. Cambridge University Press, Cambridge, UK.

Jacinthe, P. -A. and Dick W. A. 1996. Use of silicone tubing to sample nitrous oxide in the soil atmosphere. *Soil Biology and Biochemistry*, **28(6)**: 721-726. doi:10.1016/0038-0717(95)00176-X

Jezek, K. C., D.K. Perovich, K.M. Golden, C. Luther, D.G. Barber, P. Gogineni, T.C. Grenfell, A.K. Jordan, C.D. Mobley, S.V. Nghiem and R.G. Onstott. 1998. A broad spectral, interdisciplinary investigation of the electromagnetic properties of sea ice. *Geoscience and Remote Sensing*, **36 (5)**. Part II. IEEE Periodicals. N.J.

Johannessen Ola M., Elena V. Shalina, Martin W. Miles. 1999. Satellite Evidence for an Arctic: Sea Ice Cover in Transformation. *Science*, **286** (3): 1937-1939.

Johannessen, M. M., E Bjorgo. 1995. The Arctic's shrinking sea ice. *Nature,* **376**: 126-127.

Johnson, M. A., I. Polyakov. 2001. The Laptev Sea as a source for recent Arctic Ocean salinity change. *Geophys. Res. Lett*., **28** (10): 2017-2020.

Johnson, K.M., Wills, K.D., Butler, D.B., Johnson, W.K., and Wong, C.S. 1993. Coulometric total carbon dioxide analysis for marine studies: maximizing the performance of an automated gas extraction system and coulometric detector. *Marine Chemistry*, **44**, 167.

Johnston, C. G., and J. R. Vestal. 1991. Photosynthetic carbon incorporation and turnover in Antarctic cryptoendolithic microbial communities – are they the slowest growing communities on earth? Appl. Environ. Microbiol. **57**: 2308-2311.

Jones, D.R.H. 1973. The temperature gradient migration of liquid droplets through ice, *J. Cryst. Growth*, **20**: 145-151.

Kammann, C., L. Grunhage, and H.-J Jager. 2001. A new sampling technique to monitor concentrations of CH_4, N_2O and CO_2 in air at well-defined depths in soils with varied water potential. *Eur. J. Soil Sci*., **52**: 297-303. DOI: 10.1046/j.1365-2389.2001.00380.x

Kann, Billingham. 2004. Chemiluminescence is shedding light on degradation and stabilization of plasticized poly(vinyl chloride). *Polymer Degradation and Stability*, **85**: 957-966.

Kanwisher, I. 1960. pCO_2 in the sea-water and its effects on the movement of CO_2 in nature. *Tellus*, **12**: 209-215.

Karl, T. R., and K. E. Trenberth. 2003. Modern global climate change. *Science,* **302**: 1719-1723. DOI: 10.1126/science.1090228

Kasai, T. and N. Ono. 1984. An experimental study of brine upward migration in thin sea ice. *Low Temp. Sci*., **43(A)**: 149-155.

Kattenberg, A., F. Giorgi, H. Grassl, G. A. Meehl, J. F. B. Mitchell, R. J. Stouffer, T. Tokioka, A. J. Weaver & T. M. L. Wigley. 1996. Climate models - projections of future climate. In: Houghton, J. T., L. G. Meira Filho, B. A. Callander, N. Harris, A. Kattenberg and K. Maskell (Hrsg.). *Climate change* 1995. The science of climate change. Cambridge University Press, Cambridge, 285-357.

Keeling, C. D. 1973. The carbon dioxide cycle: reservoir models to depict the exchange of atmospheric carbon dioxide with the oceans and land plants. In: Rasool, S. J. (ed.), Chemistry of the Lower Atmosphere, 251-329. Plenum Press, New York, London.

Keeling, C.D., J.F.S. Chin, and T.P. Whorf. 1996. Increased activity of northern vegetation inferred from atmospheric CO_2 measurements. *Nature* 382: (6587) 146-49.

Keeling, C.D., T. P. W., and the Carbon Dioxide Research Group. 2004. Atmospheric CO_2 concentrations (ppmv) derived from in situ air samples collected at Mauna Loa Observatory, Hawaii, Scripps Institution of Oceanography (SIO), University of California, La Jolla, California USA 92093-0444.

Kelley, J.J. 1968. Carbon dioxide in the seawater under the Arctic sea ice. *Nature*, **218**: 862.

Kelley, J.J., and T.A. Gosink, 1979. Gases in the sea ice, Rep. N000 14-760331, 107pp., Inst. of Mar. Sci., Uni. of Alaska Fairbanks, Fairbanks.

Kier, R. S. 1993. Cold surface ocean ventilation and its effects on atmospheric CO_2. *J. Geophys. Res. –C,* **98**: 849 - 856.

Killawee, J. A., I. J. Fairchild, J.-L. Tison, L. Janssens, and R. Lorrain. 1998. Segregation of solutes and gases in experimental freezing of dilute solutions: Implications for natural glacial systems. *Geochim. Cosmochim. Acta,* **62**: 3637–3655. DOI: 10.1016/S0016-7037(98)00268-3

King, Cuchlaine. A. M. 1962. Oceanography for Geographers. Edward Arnold, London.

Kingery, W. D. and W. H. Goodnow. 1963. Brine migration in sea ice. In Ice and Snow, Properties, Processes and Applications, W.D. Kingery (ed), Proceedings of a conference held at MIT, 1962, Chapter 19, 237-247.

Kingery, W. D., and W. H. Goodnow. 1963. In WD Kingery, ed., Ice and Snow Properties, Technology Press, Cambridge, Mass.

Kowalik, Z and A.Y. Proshutinsky. 1994. The Arctic Ocean Tides, in The Polar Oceans and their role in shaping the global environment, *Geophysical Monograph, American Geophysical Union,* **85**: 137-158.

Krabill, W., and Coauthors. 1999. Rapid thinning of parts of the southern Greenland Ice Sheet. *Science*, **283**: 1522–1524.

Krembs, C., H. Eicken, K. Junge, J.W. Deming. 2002. High concentrations of exopolymeric substances in Arctic winter sea ice: Implications for the polar ocean carbon cycle and cryoprotection of diatoms. *Deep Sea Research*, **49**: 2163-2181.

Kühl, M., R.N. Glud, J. Borum, R. Roberts, and S. Rysgaard. 2001. Photosynthetic performance of surface-associated algae below seaice as measured with a pulse-amplitude-modulated (PAM) fluorometer and O_2 microsensors. *Marine Ecology Progress Series,* **223**: 1–14.

Lake, R.A. and E.L. Lewis. 1970. Salt rejection by sea ice during growth. *J. Geophys. Res.* **75(3)**: 583–597.

Lammers, R.B, A.I. Shiklomanov, C. J. Vörösmarty, and B. J. Peterson. 2000. An assessment of the contemporary gauged river discharge and runoff in the pan-Arctic region. *J. Geophysical Research,* **106**(D4): 3321-3334.

Lazar, A. S., A Katz, E Sass, S Ben-Yaakov. 1983. The carbonate system in hypersaline solutions: alkalinity and $CaCO_3$ solubility of evaporated seawater. *Limnology and Oceanography,* **28(5)**: 978-986.

LeDrew, E.F., D.G. Barber, T. Agnew and D. Dunlop. 1992. Canadian Sea Ice Atlas from Microwave Remotely Sensed Imagery: July 1987 to June 1990. *Climatological Studies,* **44**: 80.

Lee, K. 2001. Global net community production estimated from the annual cycle of surface water total dissolved inorganic carbon. *Limnol. Oceanogr*., **46(6)**: 1287–1297.

Lefevre, A. W., A. Olsen, A.F. Rios, F.F. Perez, T. Johannessen. 2004. A decrease in the sink for atmospheric CO_2 in the North Atlantic. *Geophys. Res. Lett.,* **31**: 7306. doi: 10.1029/2003GL018957

Lepparanta, M. 1993. A review of analytical models of sea-ice growth. *Atmosphere-Ocean*, **31(1)**: 123-138.

Lindsay, R.W. 2001. Arctic sea ice albedo derived from RGPS-based ice thickness estimates. Polar Science Center, Applied Physics Laboratory. *Annals of Glaciology*, **33**.

Longhurst, A.R., 1991. Role of the marine biosphere in the global carbon cycle. *Limnology and Oceanography*, **36**: 1507–1526.

Machta, L. 1972. The role of the oceans and the biosphere in the carbon dioxide cycle. In: Dyrssen, D. and Jagner, D. (eds), The Changing Chemistry of the Oceans. Nobel Symposium **20**: 121-145. Almqvist and Wiksell, Stockholm.

Maier-Reimer, E., and K. Hasselmann, 1987. Transport and storage of CO_2 in the ocean - an inorganic ocean-circulation carbon cycle model. *Climate Dynamics,* **2**: 63-90.

Malmgren, F. 1927. On the properties of sea ice. Norweg. North Pole expedition. "Maud". 1918-1925. **1(5)**: 1-67.

Manabe, R. S., M.J. Spelman, K. Bryan. 1991. Transient responses of a coupled ocean-atmosphere model to gradual changes in atmospheric CO_2. Part I: Annual mean response. *J. of Climatology,* **4**: 785-818.

Marion, G.M. and R.E. Farren. 1999. Mineral solubilities in the Na-K-Mg-Ca-Cl-SO4-H_2O system: A re-evaluation of the sulfate chemistry in the Spencer-Moller-Weare model. *Geochim. Cosmochim. Acta.,* **63**: 1305–1318. DOI: 10.1016/S0016-7037(99)00102-7

Martin, E. M., R Drucker. 1997. Recent observations of a spring-summer surface warming over the Arctic Ocean. *Geophys. Res. Lett.,* **24**: 1259-1262.

Maslanik, M. S., M.C. Serreze and RG Barry. 1996. Recent decreases in summer Arctic ice cover and linkages to atmospheric circulation anomalies. *Geophys. Res. Lett.,* **23**: 1677-1680.

Massman, W.J.; Lee, X. 2002. Eddy covariance flux corrections and uncertainties in long-term studies of carbon and energy exchanges. *Agricultural and Forest Meteorology*, **113**: 121-144. DOI: 10.1016/S0168-1923(02)00105-3

Matsuo, S. and Y. Miyake. 1966. *J. Geophys. Res.,* **71**: 5235.

Melnichenko N. A., V. I. Mikhaylov, and V. I. Chizhik. 1979. Study of the temperature-dependence of the brine content in sea ice by the pulsed NMR method. *Oceanology,* **19:** 535-537.

Miller, W. L., and R. G. Zepp (1995), Photochemical production of dissolved inorganic carbon from terrestrial organic matter: Significance to the oceanic organic carbon cycle. *Geophys. Res. Lett.*, **22**(4): 417–420.

Millero, F.J., F Huang, A.L. Laferiere. 2002. Solubility of oxygen in the major sea salts as a function of concentration and temperature. *Marine Chemistry,* **78**: 217-230.

Mills R. and V.M.M. Lobo. 1989. Self-Diffusion in Electrolyte Solutions, Elsevier.

Mock, T., G.S. Dieckmann, C. Haas, A. Krell, J.-L. Tison, A.L. Belem, S. Papadimitriou and D.N. Thomas. 2002. Micro-optodes in sea ice: A new approach to investigate oxygen dynamics during sea ice formation. *Aquat. Microbial Ecol.*, **29**: 297–306.

Nesje, A., Ø. Lie, S. O. Dahl. 2000. Is the North Atlantic Oscillation reflected in Scandinavian glacier mass balance records? *J. of Quaternary Science*, **15(6)**: 587 - 601. doi: 10.1002/1099-1417(200009)15:6

Niedrauer, T. M., and Martin, S. 1979. An experimental study of brine drainage and convection in young sea ice. *J. Geophys. Res.* **84**: 1176-1186.

Oke, T. 1996. Boundary Layer Climatology. cambridge, Great Britain, Routledge.

Ono, N. and T. Kasai. 1985. Surface layer salinity of young sea ice. *Ann. Glaciol.*, **6**: 298-299.

Papadimitriou, S., H. Kennedy, G. Kattner, G. S. Dieckmann, and D. N. Thomas. 2003. Experimental evidence for carbonate precipitation and CO_2 degassing during sea ice formation. *Geochimica et Cosmochimica Acta*, **68(8)**: 1749–1761.

Papakyriakou, T.N. 1999. An examination of relationships among the energy balance, surface properties and climate over snow-covered sea ice during the spring season. PhD. Thesis, Geography Department. University of Waterloo.

Papakyriakou, T.N., Miller, L. A., Langlois, A., Mundy, C., and Owens, O. 2004. CO_2 Exchange Over Sea Ice in the Canadian Arctic. Presented at the SOLAS Science Conference, October 13-16, Halifax, Nova Scotia.

Parkinson, C.L., J.C. Comiso, H.J. Zwally, P. Gloersen, W.J. Cambell, D.J. Cavalieri. 1987. Arctic Sea Ice, 1973-1976, NASA SP-489, National Aeronautics and Space Administration.

Parkinson, D.C., P. Gloersen, H.J. Zwally, J.C. Comiso. 1999. Arctic sea ice extents, areas and trends, 1978-1996. *J. Geophys. Res.,* **104**: 20837-20856.

Perkin, R.G., and E.L. Lewis. 1984. Mixing in the West Spitsbergen Current. *J. of Physical Oceanography*, **14**: 1315-1325.

Perovich, D. K., C. S. Roesler, and W. S. Pegau. 1998. Variability in Arctic sea ice optical properties. *J. Geophys. Res.*, **103**: 1193–1208.

Perovich, D.K. 1996. The optical properties of sea ice. Monograph 96-1. US Army Corps of Engineers. Cold Regions Research and Engineering Laboratory (CRREL). 25.

Perovich, D.K. and B.C. Elder. 2001. Temporal evolution of Arctic sea -ice temperature. *Ann. Glaciol*., **33**: 207–211.

Perovich, D.K., T.C. Grenfell, B. Light, and P.V. Hobbs. 2002. The seasonal evolution of Arctic sea-ice albedo. *J. Geophys. Res.,* **107**. doi:10.1029/2000JC000438

Petit, J. R. et al. 1999. Climate and atmospheric history of the past 420,000 years from the Vostok ice core, Antarctica. *Nature,* **399**: 429. doi:10.1038/20859

Petrenko, V. F., Whitworth, R. W. 2002. Physics of ice. P xiii + 373. New York: Oxford University Press.

Price, P. B. 2000. A habitat for psychrophiles in deep Antarctic ice. Proc. Natl. Acad. Sci. USA 97:1247-1251.

Le Quere, O. A., L. Bopp, P. Bousquet, P. Ciais, R. Francey, M. Heimann, C.D. Keeling, R.F. Keeling, H. Kheshgi, P. Peylin, S.C. Piper, I.C. Prentice, P.J. Rayner. 2003. Two decades of ocean CO_2 sink and variability. *Tellus* **55B**: 649.

Ramanathan, V., B.R. Barkstrom, and E.F. Harrison. 1989. Climate and the Earth's radiation budget. *Physics Today,* **42**: 22-32.

Raven JA, Falkowski PG. 1999. Oceanic sinks for CO_2. *Plant, Cell and Environment* **22**: 275–278.

Redfield**,** A.C., B.H. Ketchum, and F.A. Richards. 1963. The influence of organisms on the composition of seawater. In: *The Sea* [Hill, M.N. (ed.)]. Wiley, New York, NY, 26-77.

Reeburgh, W.S., 1984. Fluxes associated with brine motion in growing sea ice. Polar Biology, **3** (1): 29 - 33.

Revell, R. and H.E. Seuss. 1957. *Tellus*, **9**: 18.

Richardson C., and E. E. Keller (1966) The brine content of sea ice measured with a nuclear magnetic resonance spectrometer. *J. Glaciol.,* **6**.

Richardson C. 1976. Phase relationships in sea ice as a function of temperature. *J. Glaciol.,* **17:** 507-519.

Richardson, S.M. and H.Y. McSween. 1989. Geochemistry; Pathways and Processes. Prentice Hall, Englewood Cliffs, New Jersey, USA.

Rigor, I. G., J. M. Wallace, and R. L. Colony. 2002. Responses of sea ice to the Arctic Oscillation. *J. of Climatology,* **15**: 2648–2663.

Rivkin, R. B. and L. Legendre. 2001. Biogenic Carbon Cycling in the Upper Ocean: Effects of Microbial Respiration. *Science*, **291(5512)**: 2398-2400. DOI: 10.1126/science.291.5512.2398

Rothrock, D.A., Y. Yu and G.A. Mayhut. 1999. Thinning of the Arctic sea ice cover. *Geophys. Res. Lett*., **26**: 3469-3472.

Rudels, B., H.J. Friedrich, and D. Quadfasel. 1999. The Arctic circumpolar boundary current. *Deep Sea Res. II*, **46**: 1023-1062.

Rudels, B., and D. Quadfasel. 1991. Convection and deep water formation in the Arctic Ocean - Greenland Sea system. *J. of Marine Systems*, **2**: 435-450.

Rudels, B., L. G. Anderson and E. P. Jones. 1996. Formation and evolution of the surface mixed layer and halocline of the Arctic Ocean. *J. of Geophys. Res*, **101**: 8807-8821.

Rysgaard, S., R. N. Glud, M. K. Sejr, J. Bendtsen, P. B. Christensen, 2007. Inorganic carbon transport during sea ice growth and decay: A carbon pump in polar seas. *J. of Geophys. Res*, 112: C03016. doi:10.1029/2006JC003572

Saloranta, T.M., and P.M. Haugan. 2001. Interannual variability in the hydrography of Atlantic water northwest of Svalbard. *J. Geophys. Res.*, **106**: 13931-13943.

Sarmiento, J. L., and N. Gruber, 2006. Ocean Biogeochemical Dynamics, Princeton University Press, Princeton. 503.

Sarmiento, J.L., Orr, J.C. 1991. Three-dimensional simulations of the impact of Southern Ocean nutrient depletion on atmospheric CO_2 and ocean chemistry. *Limnology and Oceanography*, **36**: 1928–1950.

Schlesinger, W. H. 1997. Biogeochemistry, An Analysis of Gobal Change, 2nd ed. Academic Press, San Diego California.

Schneider, S.H. 1989. The greenhouse effect: science and policy. *Science*, **243**: 771-781.

Semiletov, I., A. Makshtas, E. Andreas. 2005. Air-Sea Ice-Water CO_2 Balance: the Arctic Ocean. 37th International Liège Colloquium on Ocean Dynamics, Gas Transfer at Water Surfaces.

Semiletov, I.P., A.P. Makshtas, S. Akasofu, and E. Andreas. 2004. Atmospheric CO_2 balance: The role of Arctic sea ice. *Geophys. Res. Lett.*, **31**: 5121. DOI:10.1029/2003GL017996

Semiletov, I.P., I.I. Pipko, I.Repina and N.E. Shakhova. 2006. Carbonate chemistry dynamics and carbon dioxide fluxes across the atmosphere–ice–water interfaces in the Arctic Ocean: Pacific sector of the Arctic. Journal of Marine Systems, **66** (1-4): 204-226. doi:10.1016/j.jmarsys.2006.05.012

Serreze, M. C., J. C. Rogers, F.D. Carsey and R.G. Barry. 1997. Icelandic Low cyclone activity: climatological features, linkages with the NAO and relationships with recent changes in the N. H. circulation, *J. of Climatology,* **10**: 453-464.

Serreze, M. C., J. E. Walsh, F. S. Chapin III, T. Osterkamp, M. Dyurgerov, V. Romanovsky, W. C. Oechel, J. Morison, T. Zhang1 and R. G. Barry. July 2000. Observational Evidence of Recent Change in the Northern High-Latitude Environment. Climatic Change, **46** (1-2): 159-207.

Serreze, M.C., J.A. Maslanik, T.A. Scambos, F. Fetterer, J. Stroeve, K. Knowles, C. Fowler, S. Drobot, R.G. Barry, and T.M. Haran. 2003. A record minimum arctic sea ice extent and area in 2002. *Geophys. Res. Lett.*, **30(3)**: 1110 doi:10.1029/2002GL016406

Serreze, M.C., JE Walsh, FS Chapin III, T Osterkamp, M. Dyurgerov, V.Romanovsky, W.C. Oechel, J. Morison, T. Zhang and R.G. Barry. 2000. Observational evidence of recent change in the northern high-latitude environment. *Climatic Change*, **46**: 159-207.

SETAC. 2001. Porewater Toxicity Testing: Biological, Chemical, and Ecological Considerations with a Review of Methods and Applications, and Recommendations for Future areas of Research. SETAC Technical Workshop. Society for Environmental Toxicology and Chemistry, Pensacola, FL.

Shcherbina, Andrey Y. ; Lynne D. Talley; Daniel L. Rudnick. 2003. Direct Observations of North Pacific Ventilation: Brine Rejection in the Okhotsk Sea. Science, **302**, *5652*, 1952 – 1955. DOI: 10.1126/science.1088692

Shiklomanov, I. A., A. I. Shiklomanov, R. B. Lammers, C. J. Vörösmarty, B. J. Peterson, and B. Fekete. 1999. The dynamics of river water inflow to the Arctic Ocean. The Freshwater Budget of the Arctic Ocean. NATO Advanced Study Institute Series. E. L. Lewis, Kluwer Academic Press.

Skirrow, G. 1965. The dissolved gasses-CO_2. in JP Riley and G Skirrow, eds., *Chemical Oceanography*. Academic Press, London, **1**, Chp 7.

Smethie, W.M., Jr., D.W. Chipman, J.H. Swift, and K.P. Koltermann. 1988. Chlorofluoromethanes in the arctic mediterranean seas: Evidence for formation of bottom water in the Eurasian Basin and deep-water exchange through Fram Strait. *Deep Sea Res*., **35**: 347-369.

Snyder, K.A. 2001. The relationship between the formation factor and the diffusion coefficient of porous materials saturated with concentrated electrolytes: Theoretical and experimental considerations. *Concr. Sci. Engin*., **3**: 216-224.

Stiller, M., J. S. Rounick, and S. Shasha. 1985. Extreme carbon-isotope enrichment in evaporating brines. *Nature,* **316**: 434–435.

Stoll, M.H.C., H.M. van Aken, H.J.W. de Baar, M. Kraak. 1996. Carbon dioxide characteristics of water masses in the northern North Atlantic Ocean. *Marine Chemistry,* **55**: 217-232.

Stouffer, S. M., K Bryan. 1989. Interhemispheric asymetry in climate response to a gradual increase in atmospheric CO_2. *Nature,* **342**: 660-662.

Stroeve J. C., Serreze M. C., Fetterer F., Arbetter T., Meier W., Maslanik J., Knowles K. 2005. Tracking the Arctic's shrinking ice cover: Another extreme September minimum in 2004. *Geophys. res. lett*., **32** (4). doi:10.1029/2004GL021810

Stroeve, J.C., M.C. Serreze, F. Fetterer, T. Arbetter, W. Meier, J. Maslanik, and K. Knowles. 2005. Tracking the Arctic's shrinking ice cover: another extreme minimum in 2004. *Geophys. Res. Lett*. doi:10.1029/2004GL021810

Stumm, W. and Morgan, J.J., 1981, *Aquatic chemistry*, 2nd ed.: New York, John Wiley & Sons, 780.

Takahashi, T. 1961. Carbon dioxide in the atmosphere and in the Atlantic Ocean water. *J. Geophys. Res.*, **66**: 477-494.

Takahashi, T. et al. 2002. Global air-sea CO_2 flux based on climatological surface ocean pCO_2, and seasonal biological and temperature effects. *Deep Sea Res., Part II,* **49**: 1601-1622.

Tans, P.P., I.Y. Fung, T. Takahashi. 1990. Observational constraints on the global atmospheric CO_2 budget. *Science,* **247**: 1431-1438.

Thomas, D. N. and G. S. Dieckmann. 2002a. Antarctic sea ice –a habitat for extremophiles. *Science*, **295**: 641–644.

Thomas, D. N. and G. S. Dieckmann. 2002b. Biogeochemistry of Antarctic sea ice. Oceanogr. *Mar. Biol. Annu. Rev*., **40**: 143–169.

Thomas, D. N. and Papadimitriou S. 2003. Biogeochemistry of sea ice. In Sea Ice—An Introduction to Its Physics, Chemistry, Biology and Geology (eds. D. N. Thomas and G. S. Dieckmann), pp. 267–302. Blackwell Science. DOI: 10.1002/9780470757161

Toggweiler, J. R., A. Gnanadesikan, and S. Carson, R. Murnane, J. L. Sarmiento, 2003. Representation of the carbon cycle in box models and GCMs: 1. Solubility pump. *Global Biogeochemical Cycles*, **17(1)**: 1026. doi:10.1029/2001GB001401

Toggweiler, J.R. and B. Samuels. 1995. Effect of sea ice on the salinity of Antarctic bottom waters. *J. of Physical Oceanography*, **25(9)**: 1980-1997.

Tréguer, P., and P. Pondaven. 2002. Climatic changes and the carbon cycle in the southern ocean: A step forward. *Deep Sea Res., Part II*, **49**: 1597-1600.

Unesco. 1981a. The Practical Salinity Scale 1978 and the International Equation of State of Seawater 1980. *Tech. Pap. Mar. Sci.*, 36: 25 pp.

Unesco. 1981b. Background papers and supporting data on the Practical Salinity Scale 1978. *Tech. Pap. Mar. Sci.*, **37**: 144 pp.

Untersteiner, N. 1968. Natural desalination and equilibrium salinity profile of perennial sea ice. *J. Geophys. Res.*, **73**: 1251-1257.

Urban, O. 2003. Physiological impacts of elevated CO_2 concentration ranging from molecular to whole plant responses. *Photosynthetica*, **41(1)**: 9-20.

Usdowski E., J. Hoefs, and G. Menschel. 1979. Relationship between ^{13}C and ^{18}O fractionation and changes in major element composition in a recent calcite-depositing spring –a model of chemical variations with inorganic $CaCO_3$ precipitation. *Earth Planet. Sci. Lett*., **42**: 267–276.

Vant, M.R., R.O. Ramseier and V. Makios. 1986. The complex dielectric constant of sea ice at frequencies in the range 0.1 to 40 GHz. *J. of Applied Physics*., **49(3)**: 1264-1280.

Vodacek, Anthony; N. V. Blough, M. D. DeGrandpre, E. T. Peltzer, R. K. Nelson, 1995. Seasonal Variation of CDOM and DOC in the Middle Atlantic Bight: Terrestrial Inputs and Photooxidation. *Limnology and Oceanography*, **42** (4): 674-686.

Volk, T. 1989. Sensitivity of climate and atmospheric CO_2 to deep-ocean and shallow-ocean carbonate burial. Nature, **337**: 637–640. doi:10.1038/337637a0

Volk, T. and M. I. Hoffert. 1985. Ocean carbon pumps: Analysis of relative strengths and efficiencies in ocean-driven atmospheric CO_2 changes. In: E.T. Sundquist and W.S. Broecker (eds) *The Carbon Cycle and Atmospheric CO_2: Natural Variations Archean to Present. AGU, Washington, D.C: Geophys. Monogr,.* **32**: 99-110.

Wadhams, P. 2000. Ice in the Ocean. Gordon and Breach Science, London.

Wadhams, P. L. M., J.C. Gascard. 1999. The European Subpolar Ocean Prgramme - an introduction. *Deep-Sea Research II,* **46**: 1011-1021.

Wadhams, P. N. D. 2000. Further evidence of ice thinning in the Arctic Ocean. *Geophys. Res. Lett.,* **27**: 3973.

Wagenet, R.J. 1984. Principals of salt movement in soils. In Nelson, D.W. et al. (ed.) Chemical mobility and reactivity in soil systems. SSSA Spec. Publ. 11. ASA and SSSA, Madison, WI. pp.123-140.

Wagenet, R.J., and Hutson, J.L. 1989. LEACHM: Leaching Estimation and Chemistry Model - A process based model of water and solute movement, transformation, plant uptake, and chemical reactions in the unsaturated zone. Ithaca: Water Resources Institute, Cornell University.

Wakatsuchi, M. and T. Kawamura 1987: Formation processes of brine drainage channels in sea ice. *J. Geophys. Res.*, **92**: 7195-7197.

Walker, J. Q., M. T. Jackson, J. B. Maynard. 1977. Chromatographic Systems, maintenance and troubleshooting, 2nd edition, pp195. Academic Press Inc., New York, NY.

Wanninkhof, R. 1992. Relationship between wind speed and gas exchange over the ocean. *J. Geophys. Res.,* **97(C5)**: 7373 - 7382.

Warren, S. G. 1982. Optical properties of snow. *Reviews of Geophysics and Space Physics*, **20**: 67-89.

Watson, A. J., P. S. Liss and R. Duce. 1991. Design of a small-scale in situ iron fertilization experiment. *Limnology and Oceanography*, **36**: 1960-1965.

Watson, AJ, C. Robinson, J.E. Robinson, P.J. le B. Williams, M.J.R. Fasham. 1991. Spatial variability in the sink for atmospheric carbon dioxide in the North Atlantic. *Nature*, **350**: 50-53. doi:10.1038/350050a0

Weeks, W. F. and S. Ackley. 1982. The Growth, Structure and Properties of Sea Ice, CRREL Monograph 82-1 (Cold Regions Research and Engineering Laboratory, Hanover, NH).

Weeks, W. F., and G. Lofgren. 1967. The effective solute distribution coefficient during the freezing of NaCl solutions. In: Physics of snow and ice: international conference on low temperature science. Proceedings, **1(1)**, Oura H., editor, Inst. *Low Temp. Sci*., Hokkaido, 579-597.

Weeks, W.F. and S. Ackley. 1986. The growth structure and properties of sea ice. In: the Geophysics of Sea Ice, N. Untersteiner, Ed. NATO ASI Series. Martinus Nijhoff Publ., Dordrecht, pp. 9-164.

Wegener, A. Institute. 1997. Sea Ice-An Antarctic Habitat, http://www.awi-bremerhaven.de/Eistour/index-e.html (Last accessed October 01, 2005)

Whorf, T., and C. D. Keeling. 1998. Rising carbon. *New Scientist*. **157**: 54.

Wigley, T. M. L. 1983. The pre-industrial carbon dioxide level. *Climatic Change*, **5(4)**: 315 – 320.

Wiscombe, W. J. and S. G. Warren. 1980. A Model for the spectral albedo of snow. In: Pure snow. *J. of Atmospheric Science*, **37(12)**: 2712-2733.

Xie, H., and M.Gosselin. (2005). Photoproduction of carbon monoxide in first-year sea ice in Franklin Bay, southeastern Beaufort Sea. *Geophys. Res. Lett.,* **32**: L12606, doi:10.1029/2005GL022803. doi:10.1029/2005GL022803

Young, S. B. 1989. To the Arctic. John Wiley & Sons, Inc., New York.

Yukimoto, S. and K. Kodera. 2005. Interdecadal Arctic Oscillation in twentieth century climate simulations viewed as internal variability and response of external forcing. *Geophys. Res. Lett.,* **32**: 3707. doi:10.1029/2004GL021870

Zemmelink, H.J., B. Delille, J.L. Tison, E.J. Hinsta, L. Houghton, and J.W.H. Dacey. 2006. CO_2 deposition over the multi year ice of the western Weddell Sea. *Geophys. Res. Lett*., **33**: L13606. doi:10.1029/2006GL026320

Zubov, N.N. 1945. L’dy Arktiki (Arctic Ice). Izdatel'stvo Glavsevmorputi. Moscow, 360 (U.S Navy Hydrographic Office, Translation 217, 1963; available as AD426972 from NTIS, Springfield, VA.).

Appendix C
The role of First Year Sea Ice in the Exchange of CO_2 between the Atmosphere and the Ocean

Data Summary
November 30, 2003 to May 31, 2004

1 Data collected at 9:00 (+/- 1hr) (local) to represent sea ice PCO2 from the previous **night** conditions
2 Data collected at 18:00 (+/- 1hr) (local) to represent sea ice PCO2 from the previous **day** conditions
3 Each sample collected over a 20cm depth range: depth indicated by **mid point** of sampler
4 **Average** of hourly measurements over 24 hours; midnight to midnight
5 **Maximum** hourly measurement measured in 24 hour period; midnight to midnight
Data exceeding 1 standard deviation, therefore **questionable, but acceptable**

											Sea ice		
Parameter	**Date**	**Depth**		**A.M.**[1,3]	*p* CO_2			**P.M.**[2,3]	*p* CO_2		**Thickness**	**Alkalinity**	**Salinity**
Location/Time		**Midpoint**	[1]**Atmosphe**	**30 cm**[1,3]	**70cm**[1,3]	**110cm**[1,3]	[2]**Atmosphe**	**30 cm**[2,3]	**70cm**[2,3]	**110cm**[2,3]			
Units	mm/dd/yy	cm	ppmv	ppmv	ppmv	ppmv	ppmv	ppmv	ppmv	ppmv	cm	µmol/kg	psu
	11/30/03	2.50										441.91	9.60
		7.50											4.20
		12.50										253.33	3.20
		17.50											3.80
		22.50										422.56	5.90
		27.50											5.90
		32.50										338.73	4.80
		37.50											4.30
		42.50										467.28	4.30
		47.50											4.60
		52.50											12.00
	12/10/03	2.50									55.33	523.98	9.00
		7.50											6.20
		12.50										409.31	5.30
		17.50											5.20
		22.50										364.64	5.00
		27.50											4.40
		32.50										388.34	4.60
		37.50											5.40
		42.50										308.45	3.50
		47.50											4.50
		52.50										343.56	4.80
	12/16/03										65.88		

					Atmosphere				Seawater				
Temperature				PAR[5]	Temperature		Day length	[4]pCO2	Time	Depth	DIC	A_t	Date
Point Meas	30 cm[4]	70cm[4]	100cm[4]	Under Sno	Min	Max				From H_2O Surface			
°C	°C	°C	°C	mmol/m²s¹	°C	°C	hours	ppm		m	µmol/kg	µmol/kg	mm/dd/yy
							0.00				1719.36		**11/30/03**
							0.00						
							0.00						**12/10/03**
							0.00			0.5	2046.33		**12/16/03**

Parameter / Location/Time / Units	Date	Depth Midpoint	[1]Atmosphe	A.M.[1,3] 30 cm[1,3]	pCO_2 70cm[1,3]	110cm[1,3]	[2]Atmosphe	P.M.[2,3] 30 cm[2,3]	pCO_2 70cm[2,3]	110cm[2,3]	Sea ice Thickness	Alkalinity	Salinity
		cm	ppmv	ppmv	ppmv	ppmv	ppmv	ppmv	ppmv	ppmv	cm	µmol/kg	psu
	12/18/03												
	12/19/03												
	12/20/03												
	12/21/03												
	12/22/03												
	12/23/03												
	12/24/03												
	12/26/03												
	12/27/03												
	12/28/03												
	12/30/03												
	01/03/04												
	01/04/04												
	01/06/04												
	01/09/04						324.20	1278.05	1762.67	459.86			
	01/10/04										92.00		
	01/11/04										89.50		
	01/12/04												
	01/13/04						312.70	1960.06	1700.77	469.76	95.75		
	01/14/04												
	01/15/04												
	01/16/04										101.00		
	01/17/04										99.75		
	01/18/04										99.83		
	01/19/04		326.15	1063.33	1110.91	352.85	343.48	1741.45	1336.07	563.86			
	01/20/04										101.00		
	01/21/04												
	01/22/04										112.00		
	01/23/04						662.90	1770.10	1534.51	1171.58	106.89		
	01/24/04	5	406.44421	982.68	1509.04	889.30					106.50	500.14	5.8
		15										355.16	5.9
		25										366.17	4.8
		35										375.98	4.6
		45										310.39	4.9

					Atmosphere				Seawater			
Temperature				PAR[5]	Temperature		Day length	[4]pCO2	Time	Depth	DIC	A_t	Date
Point Meas	30 cm[4]	70cm[4]	100cm[4]	Under Sno	Min	Max				From H_2O Surface			
°C	°C	°C	°C	mmol/m²s¹	°C	°C	hours	ppm		m	µmol/kg	µmol/kg	mm/dd/yy
										0.5	X		**12/18/03**
										0.5	2075.58	2157.15	**12/19/03**
										0.5	2082.69	2163.94	**12/20/03**
										0.5	2096.83	2173.36	**12/21/03**
										0.5	2095.90	2177.26	**12/22/03**
										0.5	2103.15	2179.64	**12/23/03**
										0.5	2098.38	2178.02	**12/24/03**
										0.5	2097.12	2174.13	**12/26/03**
										0.5	2078.27	2161.94	**12/27/03**
										0.5	2097.49		**12/28/03**
										0.5	2288.12	2117.64	**12/30/03**
										0.5	2105.37	2183.23	**01/03/04**
										0.5	2145.04	2178.19	**01/04/04**
										0.5	X	2186.18	**01/06/04**
													01/09/04
							0.00						**01/10/04**
							0.00						**01/11/04**
							0.00						**01/12/04**
							0.00						**01/13/04**
							0.00						**01/14/04**
							0.00						**01/15/04**
							0.00						**01/16/04**
							0.98			2.5	2107.20	2192.49	**01/17/04**
							1.52						**01/18/04**
							1.90						**01/19/04**
							2.23						**01/20/04**
							2.53						**01/21/04**
	-18.09	-9.64	-3.44	13.56	-32.61	-29.70	2.80	380.86					**01/22/04**
	-18.60	-9.98	-3.65	15.23	-33.98	-32.59	3.07	379.20					**01/23/04**
-21.2	-19.23	-10.38	-3.80	16.77	-34.24	-31.57	3.30	376.44		2.5	2123.13	2208.90	**01/24/04**
-21.8													
-17.9													
-15.6													
-15.7													

											Sea ice		
Parameter	**Date**	**Depth**		**A.M.**[1,3]	*p* CO_2			**P.M.**[2,3]	*p* CO_2		**Thickness**	**Alkalinity**	**Salinity**
Location/Time		**Midpoint**	**[1]Atmosphe**	**30 cm**[1,3]	**70cm**[1,3]	**110cm**[1,3]	**[2]Atmosphe**	**30 cm**[2,3]	**70cm**[2,3]	**110cm**[2,3]			
Units	mm/dd/yy	cm	ppmv	ppmv	ppmv	ppmv	ppmv	ppmv	ppmv	ppmv	cm	µmol/kg	psu
		55										340.55	5.9
		65										385.42	5.0
		75										359.71	4.2
		85										309.16	4.3
		95										329.34	5.5
		102.5										285.94	9.8
		108.5										373.74	
	01/25/04						436.07	1976.68	1662.21	535.56			
	01/26/04	2.5									109.00	472.97	8.60
		7.5											6.30
		12.5										474.97	5.70
		17.5											6.20
		22.5										478.99	6.10
		27.5											6.10
		32.5										491.32	6.10
		37.5											6.70
		42.5											6.00
		47.5											4.90
		52.5										414.17	5.40
		57.5											5.30
		62.5										364.57	5.00
		67.5											4.50
		72.5										322.69	4.30
		77.5											4.10
		82.5										280.45	3.80
		87.5											3.50
		92.5										268.15	4.30
		97.5											4.20
		102.5										318.17	3.60
		107.5											3.20
		112.5											4.60
	01/27/04		376.55	1325.10	1704.31	702.17	401.14	1929.28	1437.77	1086.15	113.33		
	01/28/04												
	01/29/04						513.09	2854.74	2969.44	1163.47	115.00		

					Atmosphere				Seawater				
	Temperature			PAR[5]	Temperature		Day length	[4]pCO2	Time	Depth	DIC	A_t	Date
Point Meas	30 cm[4]	70cm[4]	100cm[4]	Under Sno	Min	Max				From H_2O Surface			
°C	°C	°C	°C	mmol/m²s¹	°C	°C	hours	ppm		m	µmol/kg	µmol/kg	mm/dd/yy
-13.8													
-12.2													
-10.9													
-9.4													
-7.1													
-0.8													
	-20.09	-10.87	-4.10	18.27	-35.22	-33.49	3.53	379.14					**01/25/04**
	-20.30	-11.34	-4.42	15.52	-33.55	-27.67	3.77	377.47					**01/26/04**
	-18.84	-11.37	-5.26	23.04	-27.05	-22.74	3.97	370.86					**01/27/04**
	-17.18	-10.89	-6.74	25.94	-22.89	-18.06	4.18	366.11					**01/28/04**
	-15.61	-10.09	-4.68	28.67	-22.42	-16.86	4.38	364.46		2.5	2115.98		**01/29/04**

										Sea ice			
Parameter	**Date**	**Depth**		**A.M.**[1,3]	***p*** CO_2			**P.M.**[2,3]	***p*** CO_2		**Thickness**	**Alkalinity**	**Salinity**
Location/Time		**Midpoint**	[1]**Atmosphe**	**30 cm**[1,3]	**70cm**[1,3]	**110cm**[1,3]	[2]**Atmosphe**	**30 cm**[2,3]	**70cm**[2,3]	**110cm**[2,3]			
Units	mm/dd/yy	cm	ppmv	ppmv	ppmv	ppmv	ppmv	ppmv	ppmv	ppmv	cm	µmol/kg	psu
	01/30/04										115.50		
	01/31/04		405.56	1711.59	1716.48	730.74	394.13	2490.88	2799.33	572.03	116.57		
	02/01/04												
	02/02/04		414.13	2025.34	1776.19	722.17	440.65	2913.17	3369.32	1885.81	118.00		
	02/03/04												
	02/04/04		418.38	1771.28	1884.58	853.01	394.77	3584.76	5514.34	2377.53	118.88		
	02/05/04	25									119.00	391.33	5.00
		35										321.70	4.20
		65										310.67	4.10
		75										309.88	4.10
		85										341.75	4.50
		95										345.25	4.70
		105										304.75	4.10
		115										287.42	3.90
	02/06/04		422.41	2183.68	2283.66	999.92	437.96	3781.94	5307.72	2358.65			
	02/07/04	5									125.00	468.99	7.40
		15										381.13	4.80
		25										343.97	4.30
		35										332.95	4.20
		45										329.96	4.30
		55										329.76	4.30
		65										336.23	4.50
		75										346.51	4.40
		85										333.14	5.00
		95										379.38	4.70
		105										349.38	4.00
		115										302.73	4.30
	02/08/04		447.40	2058.99	1929.57	967.01	516.27	3725.29	4792.55	3313.85			
	02/09/04										121.17		
	02/10/04		524.43	2725.08	2499.05	1415.71	496.02	6759.71	6640.52	2621.11			

					Atmosphere				Seawater				
	Temperature			PAR[5]	Temperature		Day length	[4]pCO2	Time	Depth	DIC	A_t	Date
Point Meas	30 cm[4]	70cm[4]	100cm[4]	Under Sno	Min	Max			From H_2O Surface				
°C	°C	°C	°C	mmol/m²s¹	°C	°C	hours	ppm		m	µmol/kg	µmol/kg	mm/dd/yy
	-15.98	-9.78	-4.73	35.48	-28.59	-23.46	4.58	366.28					**01/30/04**
	-17.47	-10.05	-4.84	36.81	-32.16	-28.60	4.78	368.29					**01/31/04**
	-18.93	-10.69	-5.06	39.97	-32.70	-31.84	4.97	368.80					**02/01/04**
	-19.91	-11.35	-5.39	44.64	-33.01	-29.36	5.15	368.98					**02/02/04**
	-19.06	-11.68	-5.62	32.43	-28.43	-23.87	5.33	368.98					**02/03/04**
	-17.22	-11.33	-5.78	34.45	-27.85	-24.25	5.52	368.71		2.5	2120.53	2220.52	**02/04/04**
	-16.16	-10.81	-5.75	61.27	-26.49	-21.69	5.70	367.84					**02/05/04**
	-15.45	-10.40	-5.66	40.96	-26.14	-21.29	5.87	366.46		2.5	2116.52	2214.51	**02/06/04**
	-14.62	-10.01	-5.59	38.50	-28.23	-22.24	6.05	367.42					**02/07/04**
	-15.11	-9.84	-5.81	43.49	-30.09	-25.66	6.22	364.69					**02/08/04**
	-15.11	-9.86	-5.84	52.31	-33.19	-28.64	6.38	364.38					**02/09/04**
	-16.15	-10.05	-5.96	85.84	-35.63	-25.71	6.55	364.93		2.5	2124.63	2224.14	**02/10/04**
									8:30		2147.41	2220.37	
									11:30		2125.63	2254.64	
									15:30		2394.31	2092.40	
									19:30		2149.12	2222.44	

											Sea ice		
Parameter	**Date**	**Depth**		**A.M.**[1,3]	***p*** CO_2			**P.M.**[2,3]	***p*** CO_2		**Thickness**	**Alkalinity**	**Salinity**
Location/Time		**Midpoint**	[1]**Atmosphe**	**30 cm**[1,3]	**70cm**[1,3]	**110cm**[1,3]	[2]**Atmosphe**	**30 cm**[2,3]	**70cm**[2,3]	**110cm**[2,3]			
Units	mm/dd/yy	cm	ppmv	ppmv	ppmv	ppmv	ppmv	ppmv	ppmv	ppmv	cm	µmol/kg	psu
	02/11/04	5										549.78	5.80
		15										385.22	4.30
		25										382.06	4.30
		35										425.74	4.70
		45										401.26	4.10
		55										398.67	4.20
		65											4.10
		75										367.57	4.60
		85										452.77	4.70
		95										378.79	4.70
		105										321.06	4.40
		115										320.51	4.20
		120											
	02/12/04		568.10	3375.77	3506.44	1816.16	570.13	6669.96	6705.39	5120.68	124.00		
	02/13/04												
	02/14/04		627.53	3426.34	2977.47	2245.10	577.33	5797.68	6523.59	4856.01	127.33		
	02/15/04												
	02/16/04		649.31	3698.21	2873.00	2019.00	630.49	6508.46	7531.89	6408.61			
	02/17/04												
	02/18/04		453.92	2206.50	2452.32	1482.72							
	02/19/04												
	02/20/04												
	02/21/04												
	02/22/04	7.5										807.25	
		22.5										330.68	
		37.5										320.46	
		52.5										372.11	
		66.5										327.08	
	02/23/04												
	02/24/04												
	02/25/04						469.52		7154.61	5283.81	135.00		
	02/26/04												
	02/27/04												
	02/28/04		356.14		1180.82		384.94	7428.40	6498.48	3660.99			

					Atmosphere				Seawater				
	Temperature			PAR[5]	Temperature		Day length	[4]pCO2	Time	Depth	DIC	A_t	Date
Point Meas	30 cm[4]	70cm[4]	100cm[4]	Under Sno	Min	Max				From H_2O Surface			
°C	°C	°C	°C	mmol/m²s¹	°C	°C	hours	ppm		m	µmol/kg	µmol/kg	mm/dd/yy
-22.30	-16.13	-10.29	-5.97	52.59	-25.85	-24.01	6.72	359.02					**02/11/04**
-20.70													
-18.50													
-16.60													
-15.10													
-12.10													
-10.40													
-10.20													
-8.50													
	-15.74	-10.28	-6.14	75.81	-32.10	-26.32	6.88	363.12					**02/12/04**
	-17.05	-10.53	-5.79	72.20	-35.28	-32.61	7.05	369.28					**02/13/04**
	-18.25	-11.11	-5.66	76.79	-35.15	-32.52	7.22	367.30					**02/14/04**
	-18.93	-11.65	-6.42	61.99	-34.42	-30.58	7.38	363.65		2.5	2129.42	2225.29	**02/15/04**
	-18.87	-12.01	-6.45	36.52	-33.50	-32.45	7.53	363.09					**02/16/04**
	-18.98	-12.24	-6.84	96.65	-35.21	-34.53	7.70	361.31					**02/17/04**
	-19.72	-12.54	-7.59	97.66	-37.94	-35.68	7.85	362.50					**02/18/04**
	-20.74	-13.07	-7.88	105.23	-38.12	-35.41	8.02	364.27					**02/19/04**
	-21.05	-13.53	-8.19	75.85	-35.92	-31.26	8.17	361.12					**02/20/04**
	-20.21	-13.63	-8.41	81.19	-32.93	-30.42	8.32	360.72		3	2128.53	2232.85	**02/21/04**
	-20.06	-13.55	-8.57	113.39	-34.90	-32.72	8.47	360.37		10			**02/22/04**
	-20.53	-13.66	-8.68	129.35	-34.38	-32.33	8.63	358.93					**02/23/04**
	-20.89	-13.90	-8.82	135.96	-36.03	-33.18	8.78	359.55					**02/24/04**
	-21.23	-14.16	-9.01	101.11	-35.15	-28.76	8.93	358.69					**02/25/04**
	-20.14	-14.14	-9.14	102.09	-29.26	-27.46	9.08	357.49					**02/26/04**
	-19.06	-13.75	-9.14	145.16	-37.85	-28.03	9.23	357.00		3	2145.24	2239.26	**02/27/04**
	-20.32	-13.70	-9.10	154.20	-38.72	-35.92	9.38	358.97					**02/28/04**

		Sea ice										
Parameter	**Date**	**Depth**		**A.M.[1,3]**	***p*CO$_2$**			**P.M.[2,3]**	***p*CO$_2$**		**Thickness**	**Alkalinity**	**Salinity**
Location/Time		**Midpoint**	**[1]Atmosphe**	**30 cm[1,3]**	**70cm[1,3]**	**110cm[1,3]**	**[2]Atmosphe**	**30 cm[2,3]**	**70cm[2,3]**	**110cm[2,3]**			
Units	mm/dd/yy	cm	ppmv	ppmv	ppmv	ppmv	ppmv	ppmv	ppmv	ppmv	cm	µmol/kg	psu
	02/29/04	5									137.00	551.22	5.70
		15.5										496.61	3.30
		25.5										370.15	2.80
		35.5										452.32	2.70
		45.5										381.02	3.30
		55										388.53	3.20
		65										377.20	3.40
		75.5										414.15	3.30
		85.5										343.46	4.40
		95.5										440.36	3.20
		105.5										361.31	3.60
		115											3.50
		125.5										506.78	3.30
		134										531.77	6.30
	03/01/04												
	03/02/04										137.00		
	03/03/04						435.89		7180.74	3548.60			
	03/04/04												
	03/05/04												
	03/06/04												
	03/07/04	5	480.08692		2692.03	1996.32		5008.35	2512.10	2613.51	154.00	490.36	9.20
		15										345.26	4.30
		25										334.05	4.10
		35										351.21	4.30
		45										317.35	4.00
		55										322.32	4.00
		65										370.46	4.70
		75										530.71	6.70
		85										443.19	5.80
		95										438.75	5.80
		105										448.54	5.80
		115										350.20	4.50
		125										360.80	4.70
		135										340.13	4.20

					Atmosphere				Seawater				
	Temperature			PAR[5]	Temperature		Day length	[4]pCO2	Time	Depth	DIC	A_t	Date
Point Meas	30 cm[4]	70cm[4]	100cm[4]	Under Sno	Min	Max				From H_2O Surface			
°C	°C	°C	°C	mmol/m²s¹	°C	°C	hours	ppm		m	µmol/kg	µmol/kg	mm/dd/yy
-25.27	-21.37	-14.15	-9.24	155.78	-36.43	-33.50	9.53	357.48					**02/29/04**
-24.00													
-23.89													
-22.99													
-21.57													
-21.40													
-16.20													
-14.55													
-14.32													
-14.13													
-9.30													
-5.34													
-3.91													
-2.32													
	-21.70	-14.57	-9.50	147.87	-36.60	-34.20	9.68	357.80					**03/01/04**
	-21.74	-14.87	-9.76	168.87	-34.92	-30.23	9.83	358.73					**03/02/04**
	-21.40	-14.89	-9.94	176.69	-32.68	-29.44	9.98	354.99					**03/03/04**
	-21.94	-15.04	-10.08	183.57	-33.90	-30.29	10.13	355.70		3	2139.40	2239.64	**03/04/04**
	-22.18	-15.29	-10.25	206.54	-33.35	-29.79	10.27	357.65					**03/05/04**
	-23.05	-15.59	-10.51	195.55	-38.83	-32.84	10.42	359.06					**03/06/04**
-28.71	-24.89	-16.34	-10.90	211.20	-39.59	-34.31	10.57	360.70					**03/07/04**
-30.53													
-28.11													
-25.50													
-22.80													
-20.50													
-19.24													
-14.21													
-12.59													
-11.95													
-9.70													
-7.90													
-6.33													
-4.75													

Parameter	Date	Depth		A.M.[1,3]	pCO_2			P.M.[2,3]	pCO_2		Sea ice Thickness	Alkalinity	Salinity
Location/Time		Midpoint	[1]Atmosphe	30 cm[1,3]	70cm[1,3]	110cm[1,3]	[2]Atmosphe	30 cm[2,3]	70cm[2,3]	110cm[2,3]			
Units	mm/dd/yy	cm	ppmv	ppmv	ppmv	ppmv	ppmv	ppmv	ppmv	ppmv	cm	µmol/kg	psu
		145										297.98	3.90
		152.5											7.60
	03/08/04												
	03/09/04												
	03/10/04		577.44	2124.58	3123.46	2703.44	533.54	6387.73	7916.47	3621.70			
	03/11/04												
	03/12/04												
	03/13/04		471.38	2464.77	2280.59	1929.68	446.84	3612.57	4561.67	1779.56			
	03/14/04	5									163.00	414.95	8.00
		15										407.21	5.50
		25										345.53	4.30
		35										355.18	4.50
		45										374.68	4.60
		55										356.51	4.50
		65										324.70	4.00
		75										337.39	4.30
		85										344.72	4.40
		95										398.90	5.20
		105										397.17	5.20
		115										411.10	5.30
		125										389.01	5.10
		135										390.37	5.00
		145										349.83	
		155										283.05	3.70
	03/15/04												
	03/16/04												
	03/17/04		655.14	3002.04	2955.51	1976.28	682.94	3143.86	3806.88	6263.34			
	03/18/04												
	03/19/04												
	03/20/04		710.00		2397.59								
	03/21/04	5					724.87	4866.83	8367.92	3060.76	163.00	424.04	6.70
		15										350.16	4.20
		25										323.83	4.10
		35										348.95	4.30

					Atmosphere				Seawater				
	Temperature			PAR[5]	Temperature		Day length	[4]pCO2	Time	Depth	DIC	A_t	Date
Point Meas	30 cm[4]	70cm[4]	100cm[4]	Under Sno	Min	Max				From H_2O Surface			
°C	°C	°C	°C	mmol/m²s¹	°C	°C	hours	ppm		m	µmol/kg	µmol/kg	mm/dd/yy
-2.35													
-1.75													
	-25.17	-17.04	-11.34	220.45	-36.60	-30.42	10.72	359.18					**03/08/04**
	-24.65	-17.21	-11.68	225.56	-34.97	-27.97	10.87	359.97					**03/09/04**
	-24.18	-17.19	-11.85	228.69	-34.01	-26.83	11.00	358.34		3	2143.48	2252.33	**03/10/04**
	-23.80	-17.10	-11.93	229.51	-34.00	-27.50	11.15	360.26					**03/11/04**
	-23.40	-16.98	-11.97	247.80	-35.09	-28.32	11.30	360.40					**03/12/04**
	-24.07	-17.03	-12.01	243.23	-36.76	-31.99	11.43	361.44					**03/13/04**
	-24.14	-17.23	-12.12	252.36	-34.42	-22.98	11.58	358.82					**03/14/04**
	-22.12	-16.95	-12.16	226.73	-25.90	-20.91	11.73	355.55					**03/15/04**
	-20.35	-16.09	-11.89	229.15	-29.66	-22.17	11.87	359.60		3	2144.34	2243.58	**03/16/04**
	-20.02	-15.42	-11.53	246.40			12.02						**03/17/04**
	-19.54	-15.05	-11.20	251.31			12.17						**03/18/04**
	-19.52	-14.74	-11.00	277.75	-35.45	-27.63	12.32	364.72					**03/19/04**
	-20.51	-14.81	-10.90	266.30	-37.21	-21.13	12.45	360.37					**03/20/04**
-22.55	-19.28	-14.80	-10.85	318.11	-29.96	-15.96	12.60	358.66					**03/21/04**
-21.77													
-23.35													
-21.25													

		Sea ice										
Parameter	**Date**	**Depth**		**A.M.[1,3]**	***p*CO$_2$**			**P.M.[2,3]**	***p*CO$_2$**		**Thickness**	**Alkalinity**	**Salinity**
Location/Time		**Midpoint**	**[1]Atmosphe**	**30 cm[1,3]**	**70cm[1,3]**	**110cm[1,3]**	**[2]Atmosphe**	**30 cm[2,3]**	**70cm[2,3]**	**110cm[2,3]**			
Units	mm/dd/yy	cm	ppmv	ppmv	ppmv	ppmv	ppmv	ppmv	ppmv	ppmv	cm	µmol/kg	psu
		45										347.05	4.30
		55										316.33	4.00
		65										303.15	3.80
		75										407.75	2.30
		85										361.75	2.60
		95										347.62	4.40
		105										424.82	5.40
		115										364.70	4.70
		125										356.78	4.50
		135										319.70	4.10
		145										297.25	3.80
												268.97	3.80
		155										269.91	3.60
		161.5											8.80
	03/22/04												
	03/23/04												
	03/24/04		591.18		1595.34		517.71	1400.63	5516.43	3502.55			
	03/25/04												
	03/26/04												
	03/27/04		451.80	2399.92	1972.92	1661.74	475.49	4146.45	6898.83	2546.22			
	03/28/04	5										455.40	8.10
		15										391.79	4.70
		25										367.22	4.60
		35										360.13	4.60
		45										313.90	4.00
		55										318.59	4.00
		65										323.16	4.10
		75										313.41	4.00
		85										344.54	4.50
		95										357.53	4.70
		105										463.54	5.80
		115										369.94	4.80
		125										395.46	5.20
		135										424.65	4.70

					Atmosphere				Seawater				
	Temperature			PAR[5]	Temperature		Day length	[4]pCO2	Time	Depth	DIC	A_t	Date
Point Meas	30 cm[4]	70cm[4]	100cm[4]	Under Sno	Min	Max				From H_2O Surface			
°C	°C	°C	°C	mmol/m²s¹	°C	°C	hours	ppm		m	µmol/kg	µmol/kg	mm/dd/yy
-18.95													
-18.19													
-17.51													
-16.43													
-15.53													
-12.54													
-8.66													
-8.01													
-6.24													
-4.96													
-3.52													
-1.80													
-1.67													
	-18.93	-14.46	-10.79	169.50	-31.40	-11.58	12.75	355.52		3	2121.81	2241.86	**03/22/04**
	-18.15	-14.25	-10.74	314.20	-32.59	-21.61	12.88	362.50					**03/23/04**
	-19.12	-14.19	-10.65	328.23	-33.99	-30.86	13.03	357.11					**03/24/04**
	-19.77	-14.49	-10.69	332.21	-35.26	-26.86	13.18	356.69					**03/25/04**
	-20.00	-14.71	-10.83	352.31	-34.68	-27.03	13.33	356.08					**03/26/04**
	-20.25	-14.91	-11.00	360.41	-36.26	-28.04	13.47	356.38					**03/27/04**
-22.46	-20.18	-15.04	-11.14	368.89	-32.24	-26.29	13.62	354.59		3	2129.09	2244.40	**03/28/04**
-21.54													
-20.52													
-19.98													
-17.56													
-16.93													
-15.68													
-14.37													
-13.69													
-11.18													
-12.52													
-9.19													
-7.77													
-6.26													

		Sea ice										
Parameter	**Date**	**Depth**		**A.M.[1,3]**	***p*CO$_2$**			**P.M.[2,3]**	***p*CO$_2$**		**Thickness**	**Alkalinity**	**Salinity**
Location/Time		**Midpoint**	**[1]Atmosphe**	**30 cm[1,3]**	**70cm[1,3]**	**110cm[1,3]**	**[2]Atmosphe**	**30 cm[2,3]**	**70cm[2,3]**	**110cm[2,3]**			
Units	mm/dd/yy	cm	ppmv	ppmv	ppmv	ppmv	ppmv	ppmv	ppmv	ppmv	cm	µmol/kg	psu
		145										352.53	4.70
		155										342.90	4.50
		165										411.44	5.50
	03/29/04												
	03/30/04										163.00		
	03/31/04		481.11		1391.99	1247.34	627.07	8248.01	10673.28	3536.28			
	04/01/04												
	04/02/04												
	04/03/04												
	04/04/04										171.00		
	04/05/04	5									172.00	382.25	7.20
		15										343.31	4.53
		25										312.98	4.24
		35										349.85	4.63
		45										336.57	4.37
		55										341.96	4.42
		65										361.11	4.73
		75										374.51	4.96
		85											
		95										452.31	6.11
		105										380.09	5.01
		115										381.96	5.08
		125										348.42	4.62
		135										360.35	4.75
		145										349.55	4.67
	04/06/04	155	465.95	1299.17	1454.01	1209.94	480.87		2655.26			294.53	3.92
	04/07/04												
	04/08/04												
	04/09/04												
	04/10/04		490.46	1298.91	1409.92	1105.81	517.05	3478.88	2429.62	2068.19			
	04/11/04	5									179.00		6.85
		15										362.59	4.23
		25										341.61	4.24
		35											3.73

					Atmosphere				Seawater				
	Temperature			PAR[5]	Temperature		Day length	[4]pCO2	Time	Depth	DIC	A_t	Date
Point Meas	30 cm[4]	70cm[4]	100cm[4]	Under Sno	Min	Max				From H_2O Surface			
°C	°C	°C	°C	mmol/m²s¹	°C	°C	hours	ppm		m	µmol/kg	µmol/kg	mm/dd/yy
-4.83													
-3.43													
-1.83													
	-19.08	-14.85	-11.17	335.08	-27.39	-19.67	13.77	352.97					**03/29/04**
	-17.63	-14.31	-11.00	282.23	-23.33	-19.65	13.92	350.18					**03/30/04**
	-16.33	-13.57	-10.65	1073.83	-19.70	-18.36	14.07	330.95					**03/31/04**
	-15.39	-12.92	-10.27	812.33			14.20						**04/01/04**
	-14.88	-12.36	-9.87	105.24			14.35						**04/02/04**
	-14.88	-12.00	-9.43	106.51	-26.40	-20.98	14.50	353.61					**04/03/04**
	-14.65	-11.77	-9.32	80.29	-22.70	-18.90	14.65	340.36					**04/04/04**
-14.45	-13.91	-11.45	-9.11	36.01	-18.54	-15.27	14.80	337.24		3	2133.87	2252.03	**04/05/04**
-14.21													
-13.87													
-13.67													
-12.65													
-12.33													
-11.68													
-10.96													
-10.58													
-9.05													
-9.05													
-6.98													
-5.84													
-5.03													
-3.69													
-2.60	-13.13	-11.11	-8.96	37.02	-28.92	-15.07	14.95	354.58					**04/06/04**
	-12.54	-10.62	-8.63	47.27			15.10	367.89					**04/07/04**
	-11.97	-10.23	-8.36	64.48	-18.70	-10.67	15.27	362.47					**04/08/04**
	-11.45	-9.84	-8.08	61.38	-16.29	-6.69	15.42	362.09					**04/09/04**
	-10.98	-9.48	-7.79	61.81	-17.46	-8.09	15.57	363.45					**04/10/04**
-11.27	-10.61	-9.19	-7.57	65.62	-21.98	-10.13	15.72	361.78		3	2140.12	2238.72	**04/11/04**
-10.91										4.5	2140.61	2242.41	
-10.67										10	2143.54	2247.94	
-10.52													

		Sea ice										
Parameter	**Date**	**Depth**		**A.M.**[1,3]	pCO_2			**P.M.**[2,3]	pCO_2		**Thickness**	**Alkalinity**	**Salinity**
Location/Time		**Midpoint**	[1]**Atmosphe**	**30 cm**[1,3]	**70cm**[1,3]	**110cm**[1,3]	[2]**Atmosphe**	**30 cm**[2,3]	**70cm**[2,3]	**110cm**[2,3]			
Units	mm/dd/yy	cm	ppmv	ppmv	ppmv	ppmv	ppmv	ppmv	ppmv	ppmv	cm	µmol/kg	psu
		45											4.36
		55											4.25
		65											4.11
		75											4.55
		85											3.93
		95										327.25	4.19
		105										321.88	2.95
		115										395.42	3.35
		125											3.39
		135										384.91	2.99
		145											3.01
		155										318.36	2.72
		165											3.16
		174.5										512.44	4.40
	04/12/04												
	04/13/04												
	04/14/04												
	04/15/04		502.88	1459.06	1462.84	1187.17	503.44	4160.76	4991.15	2492.84			
	04/16/04												
	04/17/04												
	04/18/04	5	506.53	1338.03	1175.82	791.94					176.00		6.37
		15										347.15	4.41
		25										327.74	4.18
		35										356.55	
		45										350.41	4.20
		55										347.17	4.03
		65										331.27	3.99
		75										325.21	4.26
		85										345.92	3.89
		95										341.21	3.91
		105										368.14	3.61
		115											3.51

					Atmosphere				Seawater				
	Temperature			PAR[5]	Temperature		Day length	[4]pCO2	Time	Depth	DIC	A_t	Date
Point Meas	30 cm[4]	70cm[4]	100cm[4]	Under Sno	Min	Max				From H_2O Surface			
°C	°C	°C	°C	mmol/m²s¹	°C	°C	hours	ppm		m	µmol/kg	µmol/kg	mm/dd/yy
-9.92													
-9.73													
-9.35													
-8.92													
-8.68													
-7.57													
-8.40													
-8.35													
-7.30													
-6.20													
-5.10													
-4.20													
-3.00													
-2.49													
	-10.51	-9.00	-7.45	65.89	-27.24	-18.74	15.88	357.37					**04/12/04**
	-10.56	-8.81	-7.23	66.36	-25.39	-17.81	16.03	354.48					**04/13/04**
	-10.53	-8.71	-6.83	67.77	-24.73	-15.44	16.18	355.49					**04/14/04**
	-10.42	-8.60	-7.02	67.63	-22.67	-15.90	16.35	355.33					**04/15/04**
	-10.34	-8.54	-6.97	67.44	-28.57	-16.94	16.52	361.10					**04/16/04**
	-10.44	-8.48	-6.89	70.61	-26.96	-17.46	16.67	364.65		3	2134.81	2245.45	**04/17/04**
										4.5	2133.60	2252.23	
										10	2132.52	2253.02	
-12.12	-10.48	-8.46	-6.84	69.20	-26.73	-15.48	16.83	365.56					**04/18/04**
-11.34													
-10.76													
-10.47													
-9.44													
-9.18													
-8.67													
-8.16													
-7.90													
-6.82													
-11.94													
-8.71													

Parameter	Date	Depth		A.M.[1,3]	pCO_2			P.M.[2,3]	pCO_2		Sea ice Thickness	Alkalinity	Salinity	
Location/Time		Midpoint	[1]Atmosphe	30 cm[1,3]	70cm[1,3]	110cm[1,3]	[2]Atmosphe	30 cm[2,3]	70cm[2,3]	110cm[2,3]				
Units	mm/dd/yy	cm	ppmv	ppmv	ppmv	ppmv	ppmv	ppmv	ppmv	ppmv	cm	µmol/kg	psu	
		125										337.52	3.36	
		135										336.14	3.23	
		145												
		155										309.86	2.64	
		165										307.58	2.96	
		175.5										524.37	5.71	
	04/19/04													
	04/20/04													
	04/21/04		315.88	1902.97	1483.86	1218.69	514.79	6254.80	5718.79	3476.20				
	04/22/04													
	04/23/04													
	04/24/04		495.60	1640.60	1484.28	1373.54	574.88	4576.38	5342.89	3117.10				
	04/25/04	5									188.00	366.28	6.25	
		15										348.48	4.18	
		25										347.77	4.36	
		35										400.15	5.26	
		45										361.78	4.84	
		55										360.30	4.72	
		65										348.67	3.84	
		75										352.62	3.93	
		85											4.17	
		95										380.53	4.51	
		105										398.84	4.32	
		115										368.36	4.20	
		125										355.12	3.81	
		135										380.04	X	
		145										389.22	3.66	
		155										435.87	4.21	
		165										408.45	3.53	
		175										352.26	3.35	
		185										621.39	4.80	
	04/26/04													

					Atmosphere				Seawater				
	Temperature			PAR[5]	Temperature		Day length	[4]pCO2	Time	Depth	DIC	A_t	Date
Point Meas	30 cm[4]	70cm[4]	100cm[4]	Under Sno	Min	Max				From H_2O Surface			
°C	°C	°C	°C	mmol/m²s¹	°C	°C	hours	ppm		m	µmol/kg	µmol/kg	mm/dd/yy
-6.32													
-5.95													
-4.83													
-4.15													
	-10.47	-8.44	-6.79	71.12	-26.26	-17.33	17.00	364.29					**04/19/04**
	-10.47	-8.44	-6.78	71.79	-27.50	-17.39	17.17	363.90					**04/20/04**
	-10.50	-8.43	-6.76	72.19	-28.07	-17.96	17.33	364.38					**04/21/04**
	-10.56	-8.42	-6.69	73.06	-26.91	-15.79	17.50	364.46					**04/22/04**
	-10.56	-8.43	-6.72	73.68	-26.73	-13.92	17.67	363.98		3	2139.49	2241.15	**04/23/04**
										4.5	2140.61	2247.04	
										10	2141.34	2242.79	
	-10.46	-8.42	-6.69	75.19	-25.59	-13.99	17.85	366.11					**04/24/04**
-11.97	-10.39	-8.39	-6.65	75.08	-26.10	-14.95	18.02	367.60					**04/25/04**
-11.23													
-10.66													
-10.38													
-9.38													
-9.12													
-8.61													
-8.12													
-7.87													
-6.43													
-10.43													
-8.65													
-7.90													
-7.40													
-5.70													
-5.80													
-5.10													
-4.40													
-3.82													
	-10.30	-8.34	-6.68	76.84	-22.70	-13.49	18.20	365.76					**04/26/04**

		Sea ice										
Parameter	**Date**	**Depth**		**A.M.[1,3]**	***p*CO$_2$**			**P.M.[2,3]**	***p*CO$_2$**		**Thickness**	**Alkalinity**	**Salinity**
Location/Time		**Midpoint**	**[1]Atmosphe**	**30 cm[1,3]**	**70cm[1,3]**	**110cm[1,3]**	**[2]Atmosphe**	**30 cm[2,3]**	**70cm[2,3]**	**110cm[2,3]**			
Units	mm/dd/yy	cm	ppmv	ppmv	ppmv	ppmv	ppmv	ppmv	ppmv	ppmv	cm	µmol/kg	psu
	04/27/04												
	04/28/04												
	04/29/04		446.85	1317.43	1385.72	1248.60	583.77	5892.12	6028.44	3134.80			
	04/30/04												
	05/01/04												
	05/02/04	CORE A	405.00	1092.45	1279.97	1694.90	446.63	4816.83	4241.23	2362.31	189.00		5.39
		5											5.39
		15										340.78	4.18
		25											4.24
		35										338.72	4.02
		45										325.79	4.23
		55										307.58	4.06
		65											3.57
		75										339.14	4.13
		85										340.61	4.12
		95										361.21	4.03
		105										367.03	4.23
		115										335.87	4.41
		125										326.40	4.56
		135										323.98	3.44
		145										298.53	3.08
		155										299.58	2.82
		165										318.86	3.47
		175										350.55	3.43
		184.75										626.40	5.86
		CORE B											
		5										377.16	5.39
		15											4.18
		25										372.52	4.24
		35										419.73	4.02
		45										441.29	4.23
		55											4.06

					Atmosphere				Seawater				
	Temperature			PAR[5]	Temperature		Day length	[4]pCO2	Time	Depth	DIC	A_t	Date
Point Meas	30 cm[4]	70cm[4]	100cm[4]	Under Sno	Min	Max				From H_2O Surface			
°C	°C	°C	°C	mmol/m²s¹	°C	°C	hours	ppm		m	µmol/kg	µmol/kg	mm/dd/yy
	-10.09	-8.27	-6.64	76.83	-21.13	-12.86	18.38	364.23					**04/27/04**
	-9.82	-8.16	-6.59	66.50	-16.87	-11.72	18.57	362.37					**04/28/04**
	-9.45	-7.99	-6.50	77.21	-16.33	-9.93	18.75	363.55		3	2148.55	2252.56	**04/29/04**
										4.5	2147.92	2251.30	
										10	2150.19	2250.84	
	-8.98	-7.78	-6.39	67.73			18.95	361.29					**04/30/04**
	-8.51	-7.57	-6.30	71.07	-16.69	-7.75	19.13	367.61					**05/01/04**
-7.93	-8.17	-7.33	-6.18	67.09	-16.11	-7.02	19.33	362.80					**05/02/04**
-7.93													
-7.47													
-7.17													
-7.03													
-6.61													
-6.50													
-6.29													
-6.06													
-5.94													
-5.39													
-6.15													
-5.90													
-4.80													
-4.70													
-4.50													
-4.00													
-3.80													
-2.80													
-2.50													
-7.93													
-7.47													
-7.17													
-7.03													
-6.61													
-6.50													

											Sea ice		
Parameter	**Date**	**Depth**		**A.M.[1,3]**	***p*CO$_2$**			**P.M.[2,3]**	***p*CO$_2$**		**Thickness**	**Alkalinity**	**Salinity**
Location/Time		**Midpoint**	**[1]Atmosphe**	**30 cm[1,3]**	**70cm[1,3]**	**110cm[1,3]**	**[2]Atmosphe**	**30 cm[2,3]**	**70cm[2,3]**	**110cm[2,3]**			
Units	mm/dd/yy	cm	ppmv	ppmv	ppmv	ppmv	ppmv	ppmv	ppmv	ppmv	cm	µmol/kg	psu
		65										408.29	3.57
		75										378.33	4.13
		85										354.26	4.12
		95											4.03
		105										381.04	4.23
		115										345.39	4.41
		125										357.24	4.56
		135											3.44
		145										329.56	3.08
		155											2.82
		165										329.42	3.47
		175											3.43
		184.75											5.86
	05/03/04												
	05/04/04												
	05/05/04		458.27	3251.24	1723.56		424.61	3611.78	3538.45	2429.32			
	05/06/04												
	05/07/04												
	05/08/04		476.55	1115.31	1243.90	968.23	454.91	9451.96	8919.10	3287.93			
	05/09/04	5									192.00		6.13
		15										366.47	4.31
		25										368.63	3.94
		35										432.05	4.03
		45											3.82
		55										459.61	3.63
		65										367.05	3.97
		75										382.68	3.88
		85										352.18	3.93
		95										364.87	4.36
		105										371.89	4.37
		115										330.64	3.84
		125										355.58	4.15

					Atmosphere				Seawater				
	Temperature			PAR[5]	Temperature		Day length	[4]pCO2	Time	Depth	DIC	A_t	Date
Point Meas	30 cm[4]	70cm[4]	100cm[4]	Under Sno	Min	Max				From H_2O Surface			
°C	°C	°C	°C	mmol/m²s¹	°C	°C	hours	ppm		m	µmol/kg	µmol/kg	mm/dd/yy
-6.29													
-6.06													
-5.94													
-5.39													
-6.15													
-5.90													
-4.80													
-4.70													
-4.50													
-4.00													
-3.80													
-2.80													
-2.50													
	-7.86	-7.08	-6.01	56.96	-13.73	-4.62	19.55	363.34					**05/03/04**
	-7.57	-6.88	-5.88	30.23	-10.06	-6.45	19.77	373.03					**05/04/04**
	-7.38	-6.71	-5.77	29.63	-12.35	-8.70	19.98	368.76		3	2153.03	2248.50	**05/05/04**
										4.5	2152.95	2255.74	
										10	2154.53	2255.33	
	-7.20	-6.56	-5.66	50.99	-16.32	-9.46	20.20	360.15					**05/06/04**
	-7.07	-6.45	-5.60	41.50	-23.39	-11.85	20.45	357.13					**05/07/04**
	-7.05	-6.31	-5.37	40.96	-21.67	-13.78	20.68	353.87					**05/08/04**
-7.93	-7.04	-6.23	-5.43	44.87	-24.11	-10.62	20.95	352.01					**05/09/04**
-7.47													
-7.17													
-7.03													
-6.61													
-6.50													
-6.29													
-6.06													
-5.94													
-5.39													
-5.45													
-5.58													
-5.60													

		Sea ice										
Parameter	**Date**	**Depth**		**A.M.**[1,3]	*p* CO_2			**P.M.**[2,3]	*p* CO_2		**Thickness**	**Alkalinity**	**Salinity**
Location/Time		**Midpoint**	[1]**Atmosphe**	**30 cm**[1,3]	**70cm**[1,3]	**110cm**[1,3]	[2]**Atmosphe**	**30 cm**[2,3]	**70cm**[2,3]	**110cm**[2,3]			
Units	mm/dd/yy	cm	ppmv	ppmv	ppmv	ppmv	ppmv	ppmv	ppmv	ppmv	cm	µmol/kg	psu
		135										346.19	3.45
		145										329.89	3.15
		155										342.19	2.57
		165										397.04	3.36
		175										347.94	3.23
		185										474.67	4.72
		191.25											
	05/10/04												
	05/11/04												
	05/12/04												
	05/13/04												
	05/14/04		475.00	1003.52	1756.16	1138.99	451.37	6752.43	7602.50	3573.37			
	05/15/04												
	05/16/04	5	431.23457	998.08	1330.92	1252.73					189.50	335.49	5.40
		15										364.01	4.50
		25										375.28	4.60
		35										367.45	4.60
		45										366.76	4.50
		55										333.47	4.10
		65										347.78	4.20
		75										340.52	4.10
		85										361.75	4.40
		95										363.35	4.50
		105										336.26	4.20
		115										334.68	4.10
		125										319.24	3.90
		135										325.21	3.90
		145										328.65	3.90
		155										291.32	3.50
		165										347.77	4.20
		175										435.82	5.60
		185										562.32	7.30

					Atmosphere				Seawater				
	Temperature			PAR[5]	Temperature		Day length	[4]pCO2	Time	Depth	DIC	A_t	Date
Point Meas	30 cm[4]	70cm[4]	100cm[4]	Under Sno	Min	Max				From H_2O Surface			
°C	°C	°C	°C	mmol/m²s¹	°C	°C	hours	ppm		m	µmol/kg	µmol/kg	mm/dd/yy
-5.00													
-5.30													
-4.40													
-4.20													
-3.90													
-3.60													
-3.00													
	-6.98	-6.12	-5.29	41.19	-19.88	-5.67	21.23	355.99		3	2138.60		**05/10/04**
										4.5	2136.57		
										10	2142.56		
	-6.78	-6.02	-5.18	42.22	-18.05	-5.25	21.55	360.92					**05/11/04**
	-6.57	-5.92	-5.11	43.45	-15.98	-6.10	21.88	363.44					**05/12/04**
	-6.39	-5.81	-5.05	43.81	-11.88	-9.61	22.28	365.96					**05/13/04**
	-6.20	-5.74	-5.02	45.48	-23.22	-10.69	22.82	363.79					**05/14/04**
	-6.11	-5.61	-4.95	45.45	-23.35	-10.29	24.00	359.89					**05/15/04**
-4.60	-6.03	-5.48	-4.84	44.44	-13.34	-11.24	24.00	358.95		3	2140.51	2251.42	**05/16/04**
-5.50										10	2140.60	2263.38	
-5.60													
-5.40													
-4.80													
-4.90													
-5.20													
-5.30													
-4.90													
-5.60													
-4.30													
-3.90													
-3.90													
-3.50													
-3.30													
-3.00													
-2.70													
-2.30													
-2.30													

Parameter / Location/Time / Units	Date	Depth Midpoint	[1]Atmosphe	A.M.[1,3] 30 cm[1,3]	pCO_2 70cm[1,3]	110cm[1,3]	[2]Atmosphe	P.M.[2,3] 30 cm[2,3]	pCO_2 70cm[2,3]	110cm[2,3]	Sea ice Thickness	Alkalinity	Salinity
	mm/dd/yy	cm	ppmv	ppmv	ppmv	ppmv	ppmv	ppmv	ppmv	ppmv	cm	µmol/kg	psu
	05/17/04												
	05/18/04		389.70	940.80	1705.15		460.78	9198.09	8214.64	3512.32			
	05/19/04												
	05/20/04						425.02	10899.68	8042.93	2844.60			
	05/21/04										202.00		
	05/22/04						510.98	23672.14	9985.17	3119.20			
	05/23/04		489.75		1550.44						180.00		
	05/24/04												
	05/25/04										199.00		
	05/26/04						440.94	11055.28	7425.50	3012.54			
	05/27/04						489.49	10141.96	8513.92	2850.97			
	05/28/04		577.84		1322.81		550.38	12399.58	4025.74	2620.16	198.00		
	05/29/04		372.49		1392.06								
	05/30/04	5									179.00	334.33	5.90
		15										349.77	4.60
		25										361.51	4.50
		35										345.57	4.30
		45										318.58	4.00
		55										335.76	4.20
		65										332.29	4.20
		75										327.20	4.10
		85										336.73	4.30
		95										318.35	4.00
		105										338.84	4.20
		115										318.75	4.10
		125										330.60	4.00
		135										338.83	4.20
		145										343.90	4.30
		155										330.38	4.20
		165										338.86	4.40

					Atmosphere				Seawater				
	Temperature			PAR[5]	Temperature		Day length	[4]pCO2	Time	Depth	DIC	A_t	Date
Point Meas	30 cm[4]	70cm[4]	100cm[4]	Under Sno	Min	Max				From H_2O Surface			
°C	°C	°C	°C	mmol/m²s¹	°C	°C	hours	ppm		m	µmol/kg	µmol/kg	mm/dd/yy
	-5.90	-5.42	-4.80	42.68	-21.59	-11.36	24.00	358.79					**05/17/04**
	-5.86	-5.35	-4.74	45.03	-23.43	-10.67	24.00	355.97					**05/18/04**
	-5.88	-5.26	-4.65	47.16	-19.22	-6.89	24.00	360.35		3	2139.55	2259.30	**05/19/04**
										10	2135.77	2254.30	
	-5.85	-5.17	-4.54	40.67	-16.94	-5.02	24.00	360.91					**05/20/04**
	-5.73	-5.13	-4.49	44.22	-13.07	-6.57	24.00	357.23					**05/21/04**
	-5.48	-5.00	-4.45	46.77	-6.42	-0.24	24.00	368.44		3	2151.81	2267.61	**05/22/04**
										10	2151.62	2260.83	
	-5.24	-4.92	-4.40	42.49	-11.02	-2.06	24.00	368.38					**05/23/04**
	-4.96	-4.74	-4.23	45.19	-1.65	4.28	24.00	368.90					**05/24/04**
	-4.62	-4.65	-4.18	25.09	-3.91	1.25	24.00	374.07		3	2138.64	2258.86	**05/25/04**
										10	2144.00	2262.60	
							24.00						**05/26/04**
							24.00						**05/27/04**
							24.00			3	2147.55	2270.30	**05/28/04**
										10		2266.86	
							24.00						**05/29/04**
							24.00						**05/30/04**

Parameter / Location/Time / Units	Date mm/dd/yy	Sea ice: Depth Midpoint cm	[1]Atmosphe ppmv	A.M.[1,3] 30 cm[1,3] ppmv	pCO_2 70cm[1,3] ppmv	110cm[1,3] ppmv	[2]Atmosphe ppmv	P.M.[2,3] 30 cm[2,3] ppmv	pCO_2 70cm[2,3] ppmv	110cm[2,3] ppmv	Thickness cm	Alkalinity µmol/kg	Salinity psu
	05/31/04	175										706.60	7.50

					Atmosphere				Seawater				
Temperature				PAR[5]	Temperature		Day length	[4]pCO2	Time	Depth	DIC	A_t	Date
Point Meas	30 cm[4]	70cm[4]	100cm[4]	Under Sno	Min	Max			From H_2O Surface				
°C	°C	°C	°C	mmol/m²s¹	°C	°C	hours	ppm		m	µmol/kg	µmol/kg	mm/dd/yy
							24.00						**05/31/04**